PEOPLE'S DEMOCRATIC REPUBLIC OF ALGERIA
MINISTRY OF HIGHER EDUCATION AND SCIENTIFIC RESEARCH

University of Mohamed Boudiaf - M'sila
Faculty of Technology
Department of civil engineering

THESIS

A dissertation submitted for the degree of
DOCTORAT

Field: Civil Engineering
Option: Structures

By: MAGHAGHI Bilal

THEME

Evaluation of the strength and the ductility of shear connectors in (steel-concrete) composite beams.

« Evaluation de la résistance et la ductilité des connecteurs dans les poutres mixtes (acier-béton) »

Presented and publicly defended on the 22 /11/2022

JURY MEMBERS:

KHEMISSA Mohamed	**Professor**	**Univ. of M'sila**	**Chairman**
TITOUM Messaoud	**Professor**	**Univ. of M'sila**	**Supervisor**
MAZOZ Aida	**MCB**	**Univ. of B.B. Arréridj**	**Co-supervisor**
MERDAS Abdelghani	**Professor**	**Univ. of Setif**	**Examiner**
BELAGRAA Larbi	**Professor**	**Univ. of M'sila**	**Examiner**

2021/2022

Acknowledgement

*First of all, the author would like to express his deepest gratitude to Almighty **ALLAH**, our Lord, the All-Knowing, the Most Merciful and the Most Compassionate, the Benevolent and the Kind, for His graciousness, Unlimited Kindness and Divine Blessings for allowing him to bring this effort to an end.*

The author would like to thank the light of his life, the source of his tenderness: his mother, father, wife and family members who have helped him with their advice and moral support, their encouragement, and their sacrifices during this study.

The author would like to express his heartfelt gratitude and sincere thanks to the supervisor Pr. Messaoud Titoum and the co supervisor Dr. Aida Mazoz for their constant supervision, continuous guidance, helpful criticism, continued encouragement and suggestions, generous help and unfailing enthusiasm at all the stages of this work.

The author would like to sincerely thank the jury members: KHEMISSA Mohamed, BELAGRAA Larbi, and MERDAS Abdelghani.

The author acknowledges the support of all the administrative staff of the University of M'sila and the various officials of our university.

The author would finally like to sincerely thank the Dr. Sid Mohammed Amin and Dr. Daas Abd elaziz from the department of electrical engineering of Setif university.

ملخص

يعتمد السلوك العام للرافدة المركبة من البلاطة الخرسانية والعتبة الفولاذية إلى حد كبير على نظام الربط المستخدم لنقل قوى القص على مستوى سطح التلامس بين العنصرين. ومع ذلك، تحدث اغلب حالات الانهيار في هذه المنطقة الحساسة. لذلك، من الضروري تحسين أداء أنظمه الربط في الروافد المركبة. من جهة اخرى، روابط القص الأكثر شيوعًا والمستخدمة في جميع أنحاء العالم هي روابط مسمار ذو الرأس وروابط القص ذو مقطع " U " نظرًا للعديد من المزايا.

كمرحلة أولى في هذه الأطروحة، تم اقتراح ودراسة خمسة أشكال جديدة لروابط القص ذو مقطع " U " وشكل جديد لرابط القص مسمار ذو الرأس. تم إجراء ما مجموعه عشرين اختبار <push-out> باستخدام إعداد جديد، وثلاثة اختبارات <pull-out>، تحت تحميل رتيب لتحديد الاشكال التي تعطي أفضل أداء. تمت دراسة أوضاع الانهيار، وتأثيرات الأشكال الجديدة لروابط القص على سلوك التحميل - الانزلاق، البلاطات الخرسانية، الانحناء، وغيرها من العوامل. أوضحت الدراسة أن تعديل كل من أشكال روابط القص ذو مقطع " U " وروابط مسمار ذو الرأس يعد طريقة واعدة ويؤثر بشكل إيجابي على العلاقة بين روابط القص والخرسانة، وكذلك قدرة التشوه لهذه الروابط. نتيجة لذلك، انخفاض كميه التشققات في الخرسانة، والزيادة في الليونة من 15 الى 31٪، مع تحسن القوة القصوى بشكل طفيف بين 0 و5.1٪ لروابط القص ذو مقطع" U ". أما بالنسبة لروابط القص مسمار ذو الرأس، فقد زادت ليونتها لتصل إلى حوالي 22٪، ولكن كان هناك انخفاض طفيف في قوتها القصوى (6٪).

في المرحلة الثانية، تم تطوير نموذج ثلاثي الأبعاد للعناصر المحدودة لمحاكاة عينة <push-out> لروابط القص التي قدمت أفضل أداء في المرحلة الأولى. تم التحقق من صحة النموذج المقترح من خلال مقارنة نتائج المحاكاة مع نتائج الاختبارات التجريبية. علاوة على ذلك، قدمت هذه المحاكاة التفاصيل السلوكية الكاملة للروابط وتأثير بعض العوامل الأخرى. بالإضافة إلى ذلك، تم أيضًا تطوير نموذج ثلاثي الأبعاد لرافدة مركبة بأربع نقاط انحناء. في الاخير، تم إجراء دراسة معيارية لتقييم تأثير عدة عوامل مختلفة. نتيجة لذلك ، تؤثر درجات الربط وقوة الخرسانة بشكل كبير على السلوك العام للروافد المركبة المصنوعة من الصلب والخرسانة. وفي الوقت نفسه، لا تؤثر نوعيه فولاذ الروابط على ادائها.

الكلمات المفتاحية:

الروافد المركبة حديد- خرسانه، الروابط، اختبار دفع باستخدام إعداد جديد، محاكاة باستخدام العناصر المحدودة.

Abstract

The overall behavior of steel-concrete composite beams largely depends on the connection used to transfer shear forces at the interface between steel and concrete members. Nevertheless, the majority of failure occurs in this sensitive area. Therefore, it is necessary to improve the connection performance in the steel-concrete composite beams. However, the most common shear connectors used worldwide are headed stud connectors and channel shear connectors due to many advantages.

In the first part of the present thesis, five new channel shear connector shapes, and a new stud connector shape, are proposed and studied experimentally. A total of twenty push-out tests using a new setup, and three pull-out tests, were carried out under monotonic loading to identify the shapes that give the best performance. The failure modes, the effects of new channel and stud connectors shapes on the load-slip behavior, the concrete slabs, the bending deformation, and other parameters were studied. The study showed that the modification of both channel and stud connector shapes is a promising way and positively influences the concrete-connector relationship and also the bending deformation capacity of these shear connectors. As a result, the concrete cracking decreased, the ductility increased in the range of 15-31%, and the ultimate strength improved slightly from 0 to 5.1% for channel connectors. As for the stud connectors, their ductility increased to reach around 22%, but a slight decrease was observed in its ultimate strength (6%).

As a second part, a three-dimensional (3D) finite element model was developed to simulate the push-out specimen of the shear connectors that carried the best performance in the first step. The proposed model was validated by comparing the numerical results with those of experimental tests. This simulation provided the full behavioral details of connectors and the effect of some other parameters. In addition, a 3D finite element model of a steel-concrete composite beam with four bending points was also developed. Finally, a parametric study was carried out to evaluate the influence of various parameters. As a result, the connection degrees and the concrete strength significantly affect the overall behavior of the steel-concrete composite beams. Meanwhile, the connectors ‘steel grade does not affect their performance.

Keywords:

Steel-concrete composite beams, connectors, new setup of push-out test, FEA.

Résumé :

Le comportement global des poutres mixtes acier-béton dépend largement de la connexion utilisée pour transférer les forces de cisaillement à l'interface entre les éléments en acier et en béton. Néanmoins, la majorité des défaillances se produisent dans cette zone sensible. Il est, donc, nécessaire d'améliorer la performance des connexions dans les poutres mixtes. D'autre part, les connecteurs de cisaillement les plus couramment utilisés dans le monde sont les connecteurs de goujons à tête et les connecteurs en « U », en raison de leurs nombreux avantages.

Dans la première étape de cette thèse, cinq nouvelles formes de connecteur de cisaillement en « U », et une nouvelle forme de connecteur de goujon à tête, sont proposées et étudiées expérimentalement. Au total, vingt essais appelés « push-out » utilisant une nouvelle configuration, et trois essais appelés « pull-out », ont été réalisés sous une charge monotone afin d'identifier les formes qui donnent la meilleure performance. Les modes de défaillance, les effets des nouvelles formes de connecteurs en « U » et de goujon à tête sur le comportement charge-glissement, les blocs de béton, la déformation par flexion et d'autres paramètres ont été étudiés. L'étude a montré que, la modification des formes de ces deux types de connecteurs est une solution prometteuse et influence positivement la relation béton-connecteur ainsi que la capacité de déformation de ces connecteurs. En conséquence, la fissuration du béton a diminué, la ductilité a augmenté d'environ 15 à 31% et la résistance ultime s'est légèrement améliorée (0-5,1%) pour les connecteurs en « U ». Pour les connecteurs de type goujon à tête, leur ductilité a augmenté pour atteindre environ 22%, mais sa résistance ultime a légèrement diminué (6%).

Dans la deuxième étape, un modèle d'éléments finis tridimensionnel (3D) a été développé pour simuler les spécimens de (push-out) des connecteurs qui présentaient les meilleures performances dans la première étape. Le modèle proposé a été validé en comparant les résultats numériques à ceux des essais expérimentaux. Cette simulation a fourni les détails complets du comportement des connecteurs et l'effet de certains autres paramètres. De plus, un modèle d'éléments finis 3D d'une poutre mixte acier-béton avec quatre points de flexion a été également développé. A la fin, une étude paramétrique a été réalisée pour évaluer l'influence de divers paramètres. Par conséquent, les degrés de connexion et la résistance du béton affectent le comportement global des poutres mixt acier-béton. En revanche, la nuance d'acier des connecteurs n'affecte pas leurs performances.

Mots clés :

Poutres mixtes acier-béton, connecteurs, nouvelle configuration de l'essai de push-out, MEF.

Table of contents

Experimental part

Numerical part

List of figures

List of tables

Notations

Capital letters

A_a ： cross-section area of steel beam;

A_c ：cross-section area of concrete slab;

A_s ： cross-section area of the reinforcing bars;

A_m: is the composite cross-section area ($A_m = A_a + {}^{A_c}/_{n}$);

E_a : longitudinal elasticity modulus of the steel;

E_c ： elasticity modulus of the concrete;

H_c ： shear channel height;

I_a ：the steel beam second moment of area.

I_m^+ ：second moment of area of the composite section;

L ： span length;

L_c ：length of the channel shear connector;

$M_{apl,Rd}$: plastic resistance moment of the steel beam alone;

$M_{pl.Rd}^{+(red)}$: reduced moment resistance;

N ：shear connectors number;

N_f ：number of shear connectors needed for a complete connection;

P_{Rd} : nominal strength of a headed stud shear connector;

P_u : nominal strength of a channel shear connector;

S : first moment of area of concrete slab about the elastic neutral axis;

T : applied vertical shear force at the point considered;

V_l : longitudinal shear force exerted on each critical length.

Lowercase letters

b_{eff} ：effective width of the concrete slab;

d ：stud shank diameter;

h : overall height of the stud;

f_y : yield strength of steel;

f_u : ultimate tensile strength of steel;

f_{ck} : compressive strength of concrete (MPa);

f_t : tensile strength of concrete;

n : equivalent coefficient;

t_f : flange thickness;

t_w : web thickness;

α : corrective factor:

ε_y : elastic relative strain;

ε_u : compressive ultimate strain;

ν : Poisson's ratio;

γ_a : Partial safety factor for steel beam;

γ_c : Partial safety factor for concrete slab;

γ_s : Partial safety factor for reinforcing bars;

γ_v : partial safety factor for connectors;

δ_u : the ultimate slip when the load reduced by 10% (0,9Pu) from the peak;

δ_m : the slip corresponds to the ultimate strength P_u;

δ_d : corresponding deflection;

η : degree of the shear connection.

Introduction

Introduction

I. 1-Generalities

The composite beam is a deflected load-bearing element composed of different material types, such as concrete slab, steel beam, and shear connectors.

Throughout the last decades, the steel-concrete composite beams have been increasingly used in bridges and buildings due to the many advantages of this type of structure such as small floor depth, high stiffness, speed of construction, and considerable span length.

The main role of shear connectors in a composite beam is to transfer the longitudinal shear forces at the steel-concrete interface to obtain the composite beam behavior. Nevertheless, the efficiency of the steel beam - concrete slab connection is a major issue [1]. Several mechanical shear connectors have been proposed to realize composite action such as headed stud shear connectors, channel shear connectors, angle shear connectors, perfobond ribs, I-shape shear connectors, T-shape shear connectors, and non-welded shear connectors.

I. 2-Motivation

The ultimate strength of composite beams depends not only on the strength of the shear connection but also on its ductility and slip capacity [2]. Moreover, the behavior of a composite beam is affected directly by the slip of the shear connection at the steel-concrete interface [3]. Furthermore, the flexibility of the shear connection affects the distribution of the shear flow in the connector in a composite beam and, hence, indirectly affects their flexural strength and fatigue life [4]. Therefore, ductile shear connector is imperative to allow the application of the plastic calculation method, and hence, provide better performance in case of high earthquake loads.

The most common types of shear connectors used worldwide are headed stud shear connectors and channel shear connectors. This is due to many advantages, such as:

(i) for headed stud; perfectly composite action can be achieved by this shear connector, easily installed by fast welding, good anchor in the concrete slab, as well as the standard dimensioned head, is a resistance factor for concrete slab uplift and they are practical to be used in steel deck slabs;

(ii) for channel shear connector; good economic advantage, easily manufactured by cutting UPN steel sections, higher load-carrying capacity, good resistance for concrete slab

uplift, and ease of fixing by standard welding. Thus, all these advantages motivated many previous researchers to study these two types of shear connectors and attempt to improve their performance by using different ways.

I. 3- Problematic and objective

This research work investigated experimentally and numerically the behavior of both channel shear connectors and headed stud shear connectors. At first, this section presents for each connector a literature review and then selects the problematic issue linked to our study objective.

I. 3.1-Channel shear connector

The first study of channel shear connectors was carried out at the University of Illinois (USA) by (Viest et al. 1951) [5], and they concluded that thick channel connectors' web affects lower slip and higher load capacity. Recently, (Maleki and Bagheri. 2008) [6] have evaluated the behavior of this shear connector embedded in reinforced concrete (RC), fiber reinforced concrete (FRC), and engineered cementitious composite (ECC). The results show that using polyvinyl alcohol fibers (ECC specimens) causes a considerable increase in ultimate strength and ductility. (Mahdi Shariati et al. 2011) [7] studied also the shear strength of channel shear connectors using regular, reinforced, and lightweight concrete, and they found that increasing the connector length leads to increased cracking of the concrete. Another experimental study (Mahdi Shariati et al. 2016) [8] compared the performance of channel and angle shear connectors embedded in high-strength concrete HSC. They also concluded that longer channel shear connectors resulted in greater cracking of the concrete.

The results mentioned earlier supported the conclusion that higher channel shear connector length has a negative effect on the concrete slab, and produces difficulties to position the longitudinal reinforcing bars. Especially, it is sometimes necessary to use a long channel shear connector, because bearing capacity increases linearly with length in a way that a channel shear connector with 150 mm length has almost 60% higher load carrying capacity in comparison to a 100 mm shear channel [9]. Furthermore, the shear strength and stiffness increase linearly with a longer shear connector length in which a 20 mm length of channel shear connector increment could contribute to a 32% increase of shear strength [10].

The main objective to investigate the channel shear connector is to overcome these failures and difficulties in the ordinary channel shear connector shape. For this purpose, five new channel shear connector shapes are proposed and studied in this thesis. These all-new shapes

were first studied experimentally, and then the shapes that gave the best performance were chosen to ender take numerical simulation study.

I. 3.2- Headed stud connector

The earliest research extends back to the 1950s. Since this time, the behavior of headed stud in the steel-concrete composite beam is the focus of lots of research. However, the behavior of headed stud connectors is categorized into three parts; strength, stiffness, and ductility. According to previous researchers, these three parts are influenced by several parameters, and the most important of them are; shank diameter, height and tensile strength of studs, compressive strength, elastic modulus of concrete, and reinforcement detailing [11-13].

In recent years, some research has focused on improving the ductility of the headed stud connector. (Han and al. 2015) [14] have studied through the push-out tests, the static behavior of headed stud connectors embedded in elastic concrete. The results show that the ductility of the stud improves significantly with the increasing rubber content. Especially, when the rubber content reaches 10%, the shear stud has a relatively high bearing capacity, better deformation, and better ductility. (Xing and al. 2016) [15] have investigated the static behavior of elastic concrete-steel composite beams, in the end, they concluded that elastic concrete could improve the ductility behavior of stud and composite beam, and reduce the width of concrete cracks efficiently. Another idea was proposed and studied by (Xu and al. 2014) [16] through the use of headed stud wrapped with a rubber sleeve, named ‘‘rubber-sleeve stud’’. The results show that; compared with ordinary stud, the variation of shear strength for rubber-sleeved stud is negligible, but the stiffness markedly decreases, and the shear mechanism changes.

On the other hand, the deformation behavior of headed studs is an important issue in the design of steel and concrete composite structures [17]. However, the stiffness of the headed stud is sometimes so large that it causes the non-uniform distribution of shear forces at the interface between steel and concrete members in composite structures. As a result, some headed studs suffer high shear forces, which affect the mechanical behavior of the structure [16]. Therefore, a new modified headed stud shape is proposed and studied experimentally and numerically in this thesis.

I. 4- Organization of thesis

The thesis is divided into 6 chapters, and the contents of each chapter are summarized in the following sections.

Introduction : Includes generalities about steel-concrete composite beams, the motivation, and the objective of this thesis.

Chapter 1: Constitutes a bibliographical study on the shear connection at the steel-concrete interface of composite beams to give an overview of some aspects that can be considered fundamental for the knowledge.

Chapter 2: Presents the properties of the materials used in the experimental program and the manufacturing details of the hydraulic test machine that was used to conduct the push and pull-out tests. In addition, a detailed description of a new push-out test setup was also presented.

Chapter 3: Is dedicated to the experimental push and pull-out tests on the ordinary channel shear connector and on the five new shapes of channel shear connector. Moreover, the description of the push and pull-out specimens is presented. Then, for the push-out test; the results concerning the failure modes, load-slip behavior, and the ductility factor, were revealed and discussed. As for the pull-out test, the effect of the new channel shapes on the concrete slab uplift was also revealed and discussed. In addition, an overall discussion was performed.

Chapter 4: Is dedicated to the experimental push-out test on headed stud shear connectors. A modified shape of headed stud sized 19 mm of diameter and 100 mm of length are proposed and studied. The performance of this shape was compared with those of two other ordinary-headed studs sized 19 mm,16 mm in diameter, and 100 mm in length. A total of eight experimental push-out specimens using a new setup were carried out under monotonic loading to evaluate the effect of some parameters on the ultimate load capacity, ductility, and also on the concrete slabs. Finally, the experimental results were also compared to the existing equations.

Chapter 5: Devoted to the development of a three-dimensional (3D) finite element model to simulate the non-linear push-out test using ABAQUS software version 6.14 [18] on both types of shear connectors channels and headed studs. The proposed model was validated by comparing the numerical results against those of some experimental push-out tests from chapters three and four. The results that were compared are load–slip curves, deformation patterns of shear connectors, and the failure modes. In addition, the distribution of stresses and strains was reviled to demonstrate the local phenomena that occur at the shear connectors. Afterward, a parametric study is carried out to discover the effect of some parameters.

Chapter 6: After investigating experimentally and numerically in previous chapters the behavior of shear connectors in push-out specimens, the nonlinear behavior of some shear connectors in the steel-concrete composite beams is numerically studied in this chapter. A 3D

finite element model of composite beam is developed using ABAQUS software version 6.14 [18]. The accuracy of the suggested modeling approach was validated against experimental results taken from the literature review. Finally, a parametric study was carried out to evaluate the influence of various parameters.

Conclusions: Summarizes the main results of the tests performed and the numerical analysis and also includes recommendations and suggestions.

Literature review on the shear connection in steel-concrete composite beams.

Chapter 1:

Literature review on the shear connection in steel-concrete composite beams.

1.1-Introduction

This chapter constitutes a bibliographical study on the connection in steel-concrete composite beams. The objective of this study is to give an overview of some aspects that can be considered fundamental for knowledge of the mechanical behavior of the connection at the steel-concrete interface of composite beams. First of all, we present the connection effect in the composite beams and some existing types of shear connectors. Then, the push-out test that was recommended by some design codes and commonly used to determine the load capacity of the shear connectors, the load−slip behavior, and the failure mode was explained. Furthermore, the ultimate load of certain types of connectors given by some design codes and previous research has also been specified. Finally, the elastic and plastic dimensioning of the shear connection have been treated in detail.

1.2- Effect of the shear connection

Steel and concrete are very different, but these two materials complement one another; concrete as a slab is efficient in compression, and steel as a beam is efficient in tension. In this case, the steel beam is subjected to tensile stresses and the concrete slab is primarily subjected to compressive stresses. Thus, utilizing the favorable attributes of each material in an efficient manner [19]. Moreover, if the concrete slab and the steel beam are freely superposed, the two elements deflect independently with free slipping at their interface (Fig. 1.1(a)). In contrast, creating connections at the steel-concrete interface increases the strength and stiffness of the beam [20] (Fig. 1.1(b)). In addition, the benefits of composite action are increased strength and stiffness with 1.5–2.5 times the moment resistance and stiffness of the steel beam, leading to the economy in the size of the steel beam used [21]. However, with different degrees of shear connection, composite beams can be divided into three types: no-shear connection beams, partial-shear-connection beams, and full-shear-connection beams.

1.2.1-No-shear connection beams

As mentioned earlier, the beam, in this case, is characterized by a free slip at the steel-concrete interface and the two elements deflect independently with a lower limit of strength.

1.2.2-Partial-interaction:

According to Rudolf. S [22] the first partial-interaction theory was developed in 1943 by Newmark Siess and Viest after the execution of a series of tests at the University of Illinois (USA).

In this case, the connection at the steel-concrete interface of the composite beams is achieved using ductile connectors, and the number of connectors is less than the total number of connectors ensuring the complete interaction.

1.2.3-Full-interaction

For a given beam, loading, and design method, 'full shear connection' is defined as the least number of connectors, such that the bending resistance of the beam would not be increased if more connectors were provided [23].

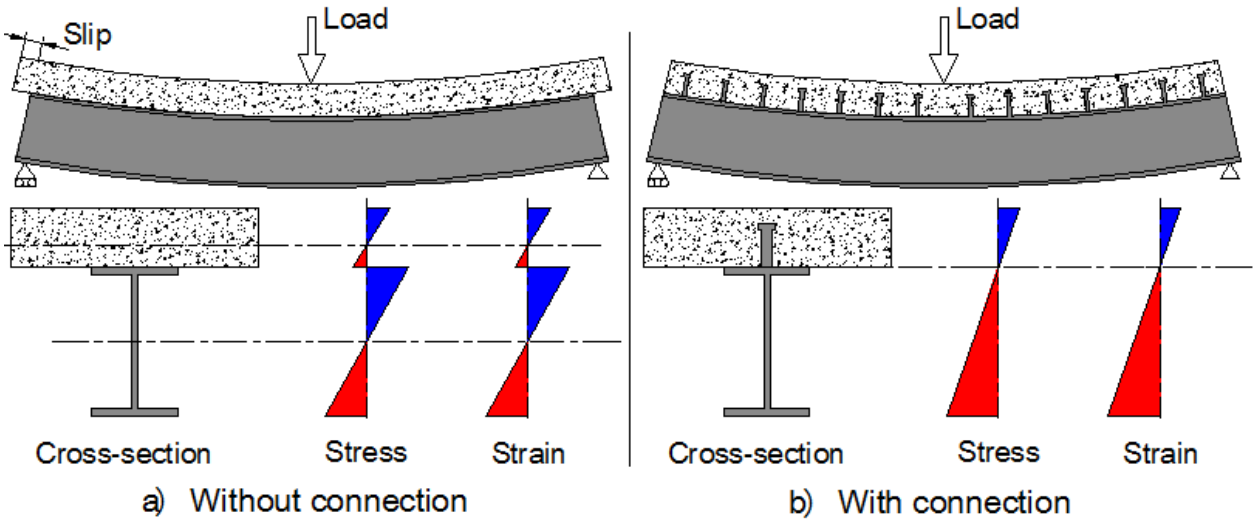

Figure 1.1: Effect of the steel-concrete connection.

1.3- Types of shear connectors

The shear connector is an essential element in the steel-concrete composite beam. As an important component of the steel-concrete beam, the shear connector transfers the longitudinal shear force at the interface between the steel and concrete. The presence of a shear connector limits the shear flow of the steel-concrete interface. The transfer of maximum shear force dictates chooses of suitable shear connectors in the composite structures.

The most commonly utilized type of shear connector is the headed stud shear connector (Fig 1.2 (a)). These connectors have good workability; they are suitable for fast welding and easy arrangement of reinforcement. However, due to the fatigue problems of stud shear connectors caused by moving loads in composite bridges Perfobond rib shear connectors were developed in Germany to mitigate the fatigue problems of stud shear connectors [24] (Fig 1.2 (b)).

Although headed stud and Perfobond rib connectors are quite appropriate as shear connectors, channel shear connectors have the advantage of being readily available and easily installable (Fig 1.2 (c)). The earliest study of channel shear connectors was carried out at the University of Illinois by Viest et al. in 1951 [6]. This connector has a higher load-carrying capacity as well. There are also alternative connectors such as welded angles equipped with anti-lift bars used particularly in Europe (Fig 1.2 (d)).

Recently, Aida M. et all, [25] proposed and investigated an I-shaped shear connector at the University of M'sila (Fig 1.2 (e)). The I-shaped connector is easier compared to the other connectors since, in most steel shops, commercial standard sizes for hot rolled steel profiles of I-shaped shear connectors are available. Moreover, by simply cutting in their long steel profiles, these types of connectors can be easily prepared.

On the other hand, the difficulty of welding the headed studs and the long time needed to weld the other shear connectors, especially in case of bad weather conditions, a connector called X-HVP developed in Germany [26] (Fig 1.2 (f)). These shear connectors are fixed by nails using a cartridge gun.

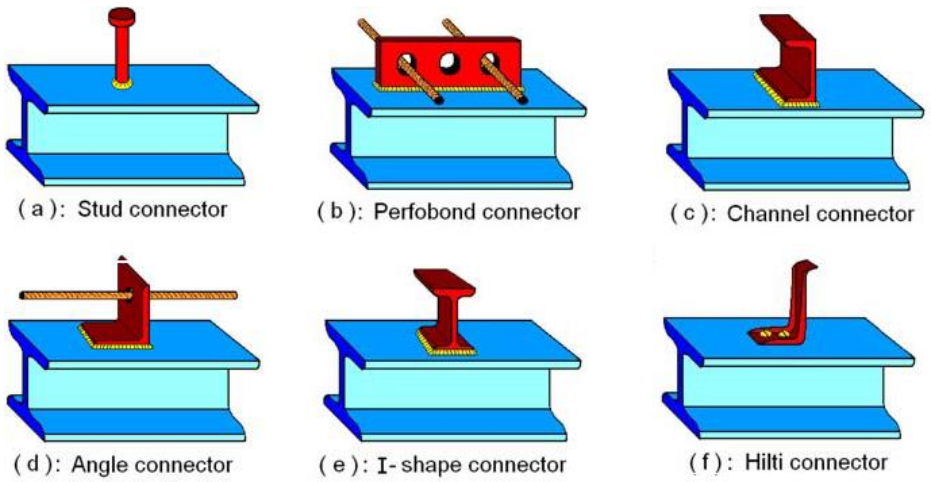

Figure 1.2 Types of shear connectors [25].

1.4-Push out test

The push-out test is commonly used to determine the capacity of the shear connectors, the load−slip behavior at the steel and concrete interface, and the failure mode. According to Rudolf. S [22] the first push-out tests were undertaken in Switzerland in the 1933s. When later, this test has been an important research topic. This type of test has been normalized in article 10-2 of

Eurocode 4 [27]. The test setup for the standard push test is shown in Figure 1.3. Each specimen consists of two concrete slabs and a metal profile section connected by two or four connectors. These connectors are attached to each flange of the profile section and are embedded in two concrete slabs.

This test aims to represent the functioning of the connection in the steel-concrete composite beam, and therefore the following conditions must be respected.

1. Both concrete slabs should be cast in the horizontal position, as is done for composite beams in practice.
2. The adhesion should be prevented at the interface between the flanges of the steel beam and the concrete by greasing the flanges.

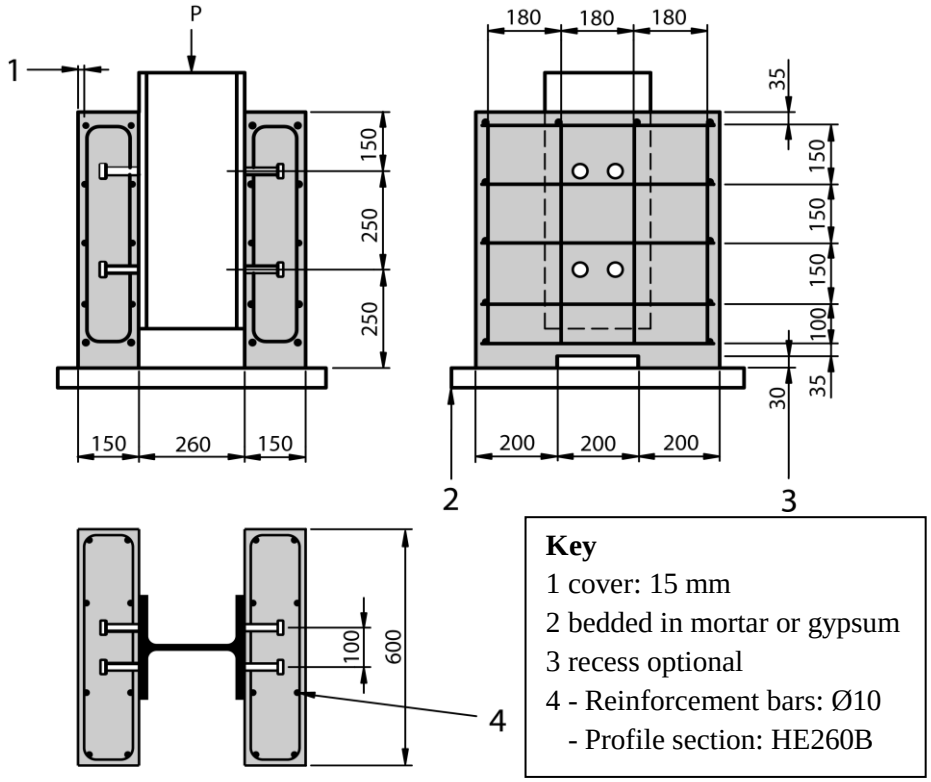

Figure 1.3: Test specimen for standard push test [27].

3. For each mix, a minimum of four concrete specimens (cylinders or cubes) for the determination of the cylinder strength should be prepared at the time of casting the push specimens. These concrete specimens should be cured alongside the push specimens. The concrete strength f_{cm} should be taken as the mean value.

4. The yield strength, the tensile strength, and the maximum elongation of a representative sample of the shear connector material should be determined.
5. If profiled steel sheeting is used for the slabs, the tensile strength and the yield strength of the profiled steel sheet should be obtained from coupon tests on specimens cut from the sheets as used in the push tests.
6. Subsequent load increments should then be imposed such that failure does not occur in less than 15 minutes.
7. The load should be applied to the profile section in increments up until the specimen fails.
8. The longitudinal slip between each concrete slab and the steel section should be measured continuously during loading or at each load increment. The slip should be measured at least until the load has dropped to 20% below the maximum load.
9. As close as possible to each group of connectors, the transverse separation between the steel section and each slab should be measured.

1.5- Shear strength capacity of shear connectors

1.5.1- Headed stud

After Eurocode 4 [27], for a plain concrete slab, the design shear resistance P_{Rd} of a welded stud with a normal weld collar (Fig. 1.4) should be determined from :

$$P_{Rd} = min\begin{cases} * P_{Rd}^{(1)} = 0.8 f_u \pi d^2/4 \times \dfrac{1}{\gamma_v} \\ * P_{Rd}^{(2)} = 0.29 \alpha d^2 \sqrt{f_c E_c}\ \dfrac{1}{\gamma_v} \end{cases} \qquad with\ P_{Rd} = 0{,}9 P_u \quad (1.1)$$

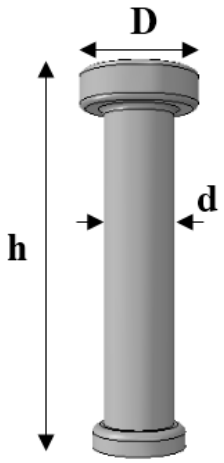

Figure 1.4 Stud shear connector

$P_{Rd}^{(1)}$, $P_{Rd}^{(2)}$ represent respectively the shear failure of the stud and the local concrete crushing around the shear connector, where:

d: is the diameter of the shank of the stud (mm);

f_u: is the specified ultimate tensile strength of the material of the stud but not greater than 500N/mm²;

f_c: is the characteristic cylinder strength of the concrete at the age considered;

E_c: elasticity modulus of the concrete;

α: is the corrective factor equal to:

$$1 \quad \text{if } {}^{h}/_{d} > 4$$
$$0.2[(h/d) + 1] \text{ if } 3 \leq {}^{h}/_{d} \leq 4 ;$$

h: is the overall height of the stud;

$\gamma_v = 1.25$: is a partial safety factor for connectors;

As provided in the Chinese code for design of steel structures GB50017—2003 [28], the stud shear bearing capacity is determined by:

$$P_u = 0.43A_s\sqrt{f_c E_c} \leq 0.7 f_u A_s \qquad (1.2)$$

The nominal strength of one stud shear connector embedded in solid concrete that proposed by Ollgaard et al [12] is adopted in the latest steel structure design code American Institute of Steel Construction regulations [29] as follows:

$$P_u = 0.5A_s\sqrt{f_c E_c} \leq f_u A_s \qquad (1.3)$$

1.5.2- Channel shear connector

The American Institute of Steel Construction regulations [29] recommend that the nominal strength of one channel shear connector (Fig. 1.5) embedded in a solid concrete slab shall be determined as:

$$P_u = 0.3(t_f + 0.5t_w)L_c\sqrt{(f_c\, E_c)} \qquad (1.4)$$

where,

P_u: strength of a channel shear connector embedded in a solid concrete slab (N);

t_f and t_w: are the thickness of the flange and the web, respectively (mm);

L_c: channel shear connector length (mm);

f_c : concrete compressive strength (MPa);

E_c: elasticity modulus of concrete (MPa);

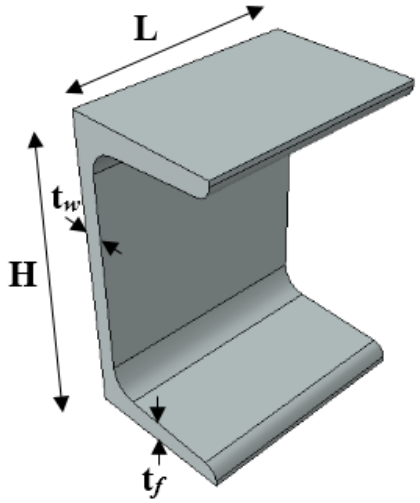

Figure 1.5: Channel shear connector.

The current Canadian standard [30] also suggests a similar equation to predict the ultimate load capacity of channel shear connectors:

$$P_u = 36.5(t_f + 0.5t_w)L_c\sqrt{f_c} \qquad (1.5)$$

concluded that the CSA [31] equation is too conservative. By including channel height H_c as a parameter, they developed the following empirical equation to evaluate the load capacity of channels having a height of 100 mm:

$$P_u = (336t_w^2 + 5.24L_cH_c)\sqrt{f_c} \qquad (1.6)$$

Based on the plastic deformation of channel shear connector, as well as the tensile strength of steel f_u (MPa) as a parameter, [32] established the following equation to evaluate the load capacity of shear channels:

$$P_u = 0.25 \times F_1 \times F_2 \times f_c \times L_c \times H + ((2 \times t_w^2 \times L_c \times f_u)/H) \qquad (1.7)$$

where, $F_1 = 7.2 - 0.023 \times L_c$ and $F_2 = 1.5 - 0.005 \times H$

F_1 is dedicated to representing the effect of channel length, and F_2 is dedicated to representing the channel height. The value 0.25 is the average of the term: $[(h_2 + (h_1 - h_2)/2)/H]$. Where: h_1, h_2 are the heights of the first and second plastic hinges respectively.

1.6- Classification of the shear connectors

Shear connectors can be classified as ductile or non-ductile. Ductile connectors are those with sufficient deformation capacity to justify the simplifying assumption of plastic behavior of the shear connection in the structure considered. Figure 1.6 shows examples of both ductile and non-ductile behavior of the shear-slip curves obtained by push-out tests.

.1.6.1- Ductile shear connectors

Ductile connectors are those which can provide sufficient slip at the steel-concrete interface, whilst maintaining their shear resistance. Eurocode 4 [27] considers that connectors having a characteristic slip capacity higher or equal to 6 mm can be assumed to be ductile, provided that the degree of shear connection is sufficient for the spans of the beam being considered.

According to the Eurocode 4 [27], headed studs may generally be considered ductile, subject to the following limitations:

- The overall length of the stud should be not less than four times its diameter.
- Stud diameter should be not less than 16 mm and not greater than 22 mm.

1.6.2- Non ductile shear connectors

Non-ductile (rigid) connectors are characterized by brittle failure just after reaching the ultimate shear strength. In practice, angle and Perfobond rib connectors are considered rigid connectors. In this case, the dimensioning of the cross-section and the connection must be carried out in elasticity.

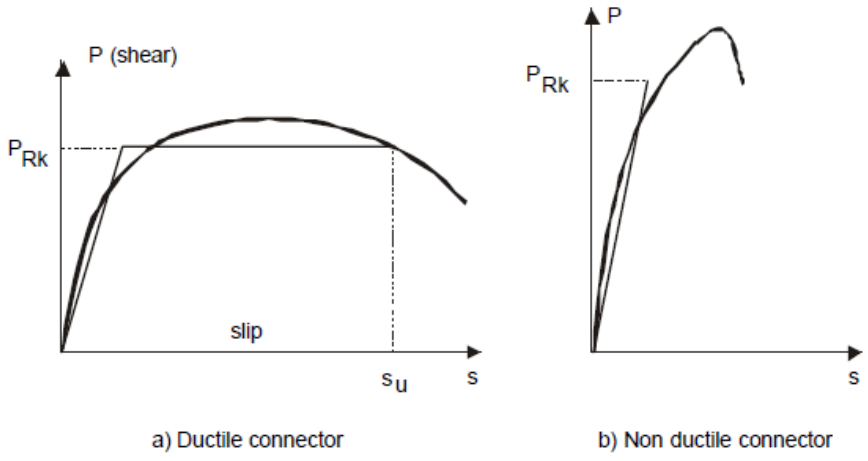

Figure 1.6: Classification of the connectors.

1.7- Geometrical characteristics of the composite beams cross-sections

1.7.1- Effective width of concrete slab (b_{eff})

In general, the ratio of the effective width to the real flange width depends on many factors including the type of loading, the support conditions, the cross-section considered, and the ratio of beam spacing to span. However, to treat a composite floor as an assembly of independent tee sections, the concept of an effective width b_{eff} of the concrete slab is introduced (Fig. 1.7). That is why in the domain of building, most of the design codes are satisfied with simple safe formulae. Eurocode 4 [27], proposes the following expression:

$$b_{eff} = b_{e1} + b_{e2} \qquad (1.8)$$

With

$$b_{ei} = \min(L_0/8\,, b_i) \qquad 1.9$$

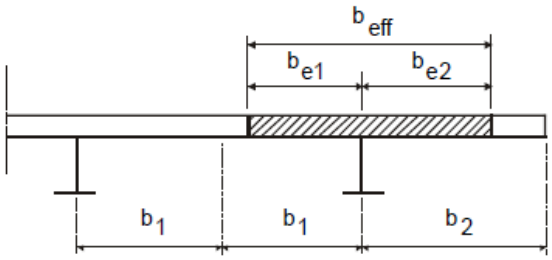

Figure 1.7: Effective width of concrete slab for composite beam.

Where L_0 is equal to the distance measured between consecutive points of contra flexure in the bending moments diagram. For an isostatic simply-supported composite beam, L_0 is equal to the span L of the beam. In contrast, in the case of a continuous beam, L_0 must be taken differently in the zones of positive bending moments (b_{eff}^{+}) and negative bending moments (b_{eff}^{-}) (where only the tensioned reinforcement is concerned), according to the following diagram (Fig 1.8):

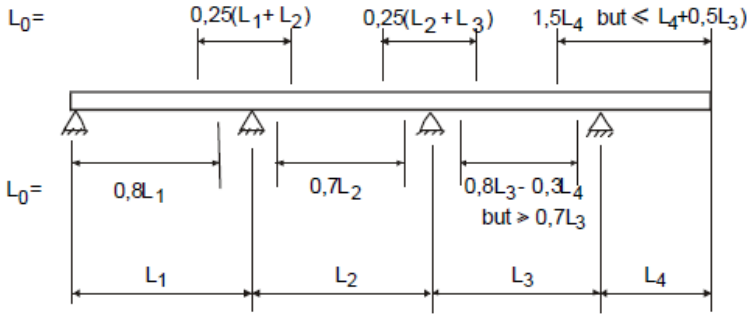

Figure 1.8: Lengths L_0 for the determination of effective width.

1.7.2- The second moment of area of composite beam cross-section

To calculate the second moment of area of the composite beam cross-section, the theory of homogenized sections is used, which allows replacing the concrete section with an equivalent steel section using an equivalent coefficient (n) defined by:

$$n = {E_a}/{E_c} \qquad (1.10)$$

Where: E_a:is the longitudinal elasticity modulus of the steel;

E_c: is the longitudinal elasticity modulus of the concrete;

Eurocode 4 [27], (section 3.1.4.2) proposes to adopt the following values for the elasticity modulus of concrete:

$E_c = E_{cm}$: for short-term actions.

$E_c = E_{cm}/3$: for long-term actions.

$E_c = E_{cm}/2$: in the other cases.

With E_{cm} is the average value of the secant elasticity modulus [KN/m2]

According to Eurocode 2 [33] (section 3.1.2.5) E_{cm} can be calculated by the following expression:

$$E_{cm} = 9{,}5(f_{ck} + 8)1/3 \qquad (1.11)$$

With: f_{ck} compressive strength of concrete cylinder [KN/mm2].

The second moment of area of the composite cross-section depends on the compressive concrete (uncracked section) in case of sagging bending moment or the tensile concrete (cracked section) in case of the hogging moment.

a) Second moment of area of uncracked section (sagging bending moment)

The second moment of area I_m^+ of the composite section is calculated assuming that the concrete is uncracked in case of a sagging bending moment. Moreover, the calculation of the distance between the neutral axis and the lower face of the steel beam Z_m allows to calculate the second moment of area I_m^+ of the composite section:

-Neutral axis in the slab:

$$Z_m = h - \frac{nA_a}{b_{eff}^+}\left[-1 + \sqrt{1 - + \frac{2b_{eff}^+}{n\,A_a}\,(h - Z_a)}\right] \qquad (1.12)$$

$$\Rightarrow I_m^+ = I_a + A_a\,(Z_m - Z_a)^2 + (h - Z_m)^3\,{b_{eff}^+}/{3n} \qquad (1.13)$$

-Neutral axis in the steel beam:

$$Z_m = \frac{1}{A_a + \frac{A_c}{n}}\left[A_a \times Z_a + \frac{A_c}{n}\left(h - \frac{h_c}{2}\right)\right] \qquad (1.14)$$

$$\Rightarrow I_m^+ = I_a + A_a(h - Z_a)^2 + \frac{A_c}{3n}\,h_c^2 - A_m(h - Z_m)^2 \qquad (1.15)$$

a) Second moment of area of cracked section (hogging bending moment at supports)

The second moment of area I_m^- is calculated by including the reinforcing bars located in the effective width of concrete slab b_{eff}^- with neglecting the cracked concrete section. In this case, the neutral axis is located in the steel beam:

$$Z_b = \frac{A_a \times Z_a + A_s \times Z_s}{A_a + A_s} \qquad (1.16)$$

$$\Rightarrow I_m^- = I_a + A_a\,(Z_a - Z_m)^2 + A_s\,(Z_s - Z_m)^2 \qquad (1.17)$$

With:

A_a : is the cross-section area of the steel beam;

A_s : is the cross-section area of the reinforcing bars;

A_c : is the cross-section area of the concrete slab ($A_c = b_{eff}^+ \times h_c$);

A_m: is the composite cross-section area ($A_m = A_a + {A_c}/{n}$)

I_a : the second moment of area of steel beam.

The other notions are shown in Fig 1.9.

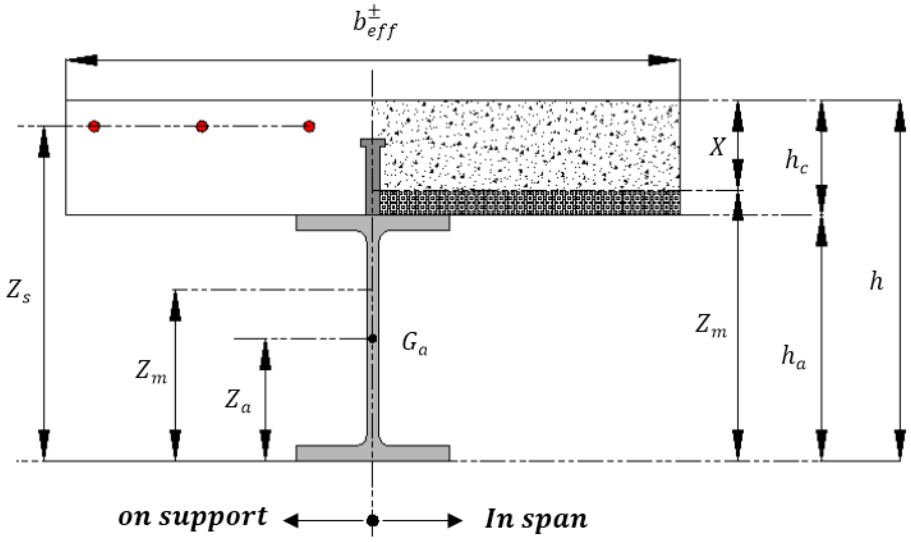

Figure 1.9: Notation for a composite cross-section in span and on support.

1.7.3- Classification of composite beams cross-section

In the analysis of composite beams, it is important to consider the possibility of local buckling. This is done by defining the class of section. Details description of the different classes and how they are determined for a particular composite section are given here for simply supported beams (in positive bending). The general description of the different classes according to Eurocode 4 [27], is as follows:

Class 1 and 2: the section is capable of developing the full plastic bending moment $M_{pl.Rd}^{+}$. In addition, class 1 sections can also rotate after the formation of a plastic hinge, but this is not important for simply supported beams.

Class 3: because of local buckling in the part of the steel section in compression, the full plastic moment resistance cannot be achieved, although the stresses in the extreme fibers of the steel section can reach yield.

Class 4: local buckling in the steel section occurs before yield is reached in the extreme fibers.

The curves of the moment-rotation behavior corresponding to each class of cross-section are presented in Fig1.10.

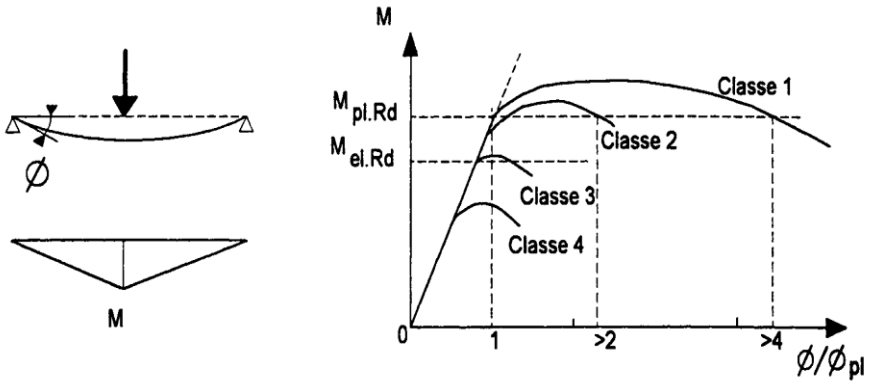

Figure 1.10 Classification of composite beams cross-section

1.8- Dimensioning of the shear connection

The connection at the interface of the steel-concrete composite beam (i.e., number and spacing of the connectors) can be determined by an elastic and plastic calculation method.

1.8.1- Elastic calculation of the shear connection

When the connected composite beam acts in an elastic way then the shear flow, V (shear force per unit length), between the concrete slab and the steel section may be calculated from:

$$V = \frac{T.S}{n.I_m} \qquad (1.18)$$

Where:

T: is the applied vertical shear force at the point considered;

I_m: is the second moment of area of the equivalent section;

S: is the first moment of area of concrete slab about the elastic neutral axis;

n: is the equivalent coefficient.

It can be seen, from the above equation, that the longitudinal shear forces that must be carried by the connection will vary depending upon the vertical shear present. However, the number of connectors (N) on the examined span (L) is given by the following formula:

$$N = \frac{V \times L}{P_{Rd}} \qquad (1.19)$$

V: is the shear force per unit length;

L: is the length span of the connectors distribution;

P_{Rd}: is the shear resistance of a connector.

1.8.2- Plastic design of the shear connection

a) Full connection

For a sagging bending moment in a composite beam simply-supported or in a continuous composite beam with ductile connectors, the total longitudinal shear force V_l exerted on each critical length (i.e. length between two successive critical cross-sections) should be calculated as follows:

$$V_l = F_{cf}$$

$$F_{cf} = min\left(\frac{A_a \times f_y}{\gamma_a} \ , \frac{0{,}85 \times b_{eff} \times h_c \times f_{ck}}{\gamma_c}\right) \qquad (1.20)$$

For a hogging bending moment in intermediate support of a composite beam with ductile connectors, the longitudinal shear force supported by the connectors is given by:

$$V_l = F_{cf} + \frac{A_s \times f_{sk}}{\gamma_s} \qquad (1.21)$$

The number of connectors assumed to be ductile, is calculated by

$$N_f = {V_l}/{P_{Rd}} \qquad (1.22)$$

b) Partial shear connection

The connection in the composite beam is called " partial connection ", when the number of connectors used N is less than the number of connectors needed for a complete connection N_f along a critical length. The degree of connection is defined by the ratio N/N_f . Partial connection can only be valid if the cross-sections are of class 1 or 2. As a result, the total longitudinal shear force transferred by the connectors along the critical length is reduced.

$$V_l^{red} = N.P_{Rd} < V_{lf}$$

In the same way, the moment resistance of the critical section is reduced:

$$M_{pl.Rd}^{+(red)} < M_{pl,Rd}^{+}$$

An analytical relationship can be established between the reduced moment resistance $M_{pl.Rd}^{+(red)}$ and the number of connectors N on the critical length. This relation is represented in Fig 1.11 by the curve ABC.

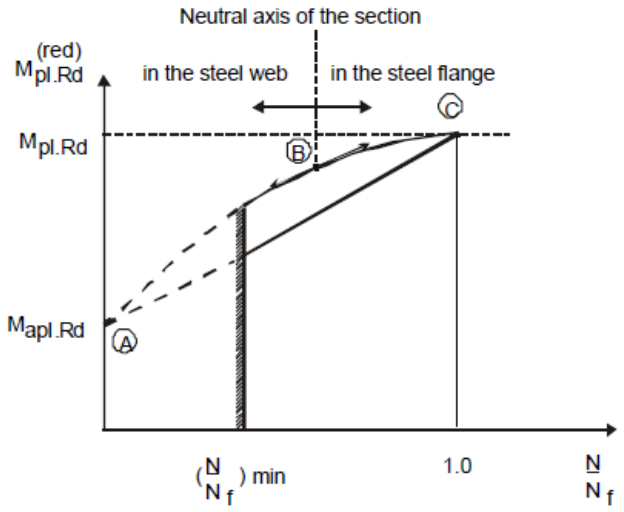

Figure 1.11 Resistant moment in terms of the degree of connection

According to Eurocode 4 [27], the reduced moment resistance $M_{pl.Rd}^{+(red)}$ can be calculated by a simplified method. This method consists of replacing the curve ABC with the line AC and calculate analytically the resisting moment using the following expression:

$$M_{pl,Rd}^{+(red)} = M_{apl,Rd} + \frac{N}{N_f}(M_{pl,Rd}^{+} - M_{apl,Rd})$$

- For $N/N_f = 1$ (complete connection) the resistant moment is not reduced and is equal to $M_{pl,Rd}^{+}$
- For $N/N_f = 0$ (no connectors), the reduced resistant moment is the moment of plastic resistance of the steel beam alone, $M_{apl,Rd}$.

According to Eurocode 4 [27], if the degree of connection is very low, the ABC curve or its AC simplification becomes invalid because the failure occurs by the shearing of connectors before reaching the reduced resisting moment. However, the following indications can be used to

evaluate the degree of connection according to the span of the composite beam and the geometry of the composite cross-section:

- For a solid slab and a steel profile with equal flanges

$$N/N_f \geq 0.4 \quad \text{if} \quad L \leq 5m$$

$$N/N_f \geq 0.25 + 0.03L \quad \text{if} \quad 5m \leq L \leq 25m$$

- For a solid slab and a steel profile in which the area of the lower flange does not exceed three times the area of the upper flange:

$$N/N_f \geq 0.4 + 0.03L \quad \text{if} \quad L \leq 20m$$

1.9-Conclusion

Shear connections in composite beam applications have a long history of both practical use and extensive research. However, the security of composite beams is essentially based on the efficiency of the connection system because most of the observed failures occur in the connection at the steel-concrete interface. The numerous studies conducted on shear connectors over the past 70 years have shown that there is no ideal connector available. The choice of a particular connector depends as much on its cost and ease of installation as on its mechanical performance.

Experimental part

Chapter 2:

Materials and Push-Out Specimens Fabrication

2.1- Introduction

This chapter presents the materials properties that have been used in the experimental tests such as concrete, connectors steel (headed studs, channel shear connectors), and the steel of the reinforcement bars. A detailed explanation of the construction of the hydraulic test machine that has been used to achieve the experimental tests was also presented. In addition, the measuring instruments such as electronic acquisition system, displacement measurement, load measurement, and their calibration were also presented. However, a new push-out test setup was developed and used to achieve the experimental program. This new test setup is different than the standard push-out test setup, and its detailed description is given in this chapter.

2.2- Material properties

2.2.1- Concrete

The concrete was ordered from a local ready-mix concrete supplier and was identical for all specimens. The casting of concrete is done in a horizontal position as it does in the construction process. After casting of concrete for the specimens, the concrete has been properly vibrated using a vibrator to eliminate air voids adjacent to the connectors. As an example, Fig. 2.1 shows the configuration of the specimens before and during casting. After that Eight concrete cylinders (160 mm in diameter x 320 mm in length) were prepared. The compressive strength was determined using a hydraulic press with a maximum capacity of 3000 kN, and the average compressive strength on the 62nd day, which was the start day for the push-out and pull-out tests are listed in Table 2. 1. The tensile strength and the elastic modulus of the concrete were calculated according to the procedure proposed by [33] are also listed in Table 2. 1.

Figure 2.1: Casting in a horizontal position (before and during casting).

Formwork plays a key role in concrete slabs of the push-out specimen. Therefore, steel molds were made by using sheet steel with 2 mm of thickness. The demolding was done about 48 hours after concreting and the specimens were hardened in the open air.

Table 2.1: Mechanical properties of concrete.

Compressive strength of concrete f_c (MPa)	Tensile strength f_{ctm}(MPa)	Young's modulus E_c (MPa)
31.9	3.01	32462

2.2.2- Steel

The other materials properties used in the experimental tests such as steel of shear connectors and reinforcing bars were determined based on the tensile tests performed on normalized specimens. Two identical tensile coupon specimens for each type of shear connectors and reinforcing bars were prepared (Fig 2.2) and (Fig 2.3). The tensile coupon specimens of channel shear connector steel were cut out from UPN 100 metal profile using Wire Cut Machine. While mechanical turning was used to make those of headed studs steel.

The dimensions of the plate and circular tensile coupon specimens are prepared according to the European standard EN ISO 6892-1 [34]. The loading was applied slowly by increments of the load until the specimen was broken. On the other hand, the load-displacement results obtained have been converted to stress-strain curves, as illustrated in Figure 2.4. Yielding behavior was observed for the tensile tests. The results of the tensile tests are shown in table 2.2. This table contains the average yield strength, the ultimate strength, and the elongation. However, the grade of the beam sections is ST275.

Figure 2.2: Tensile strength testing of channel shear connectors.

Figure 2.3: Tensile strength testing of headed studs.

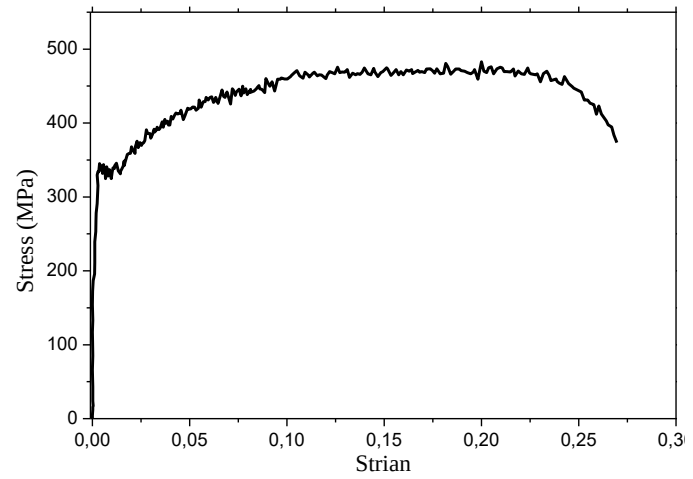

(a)

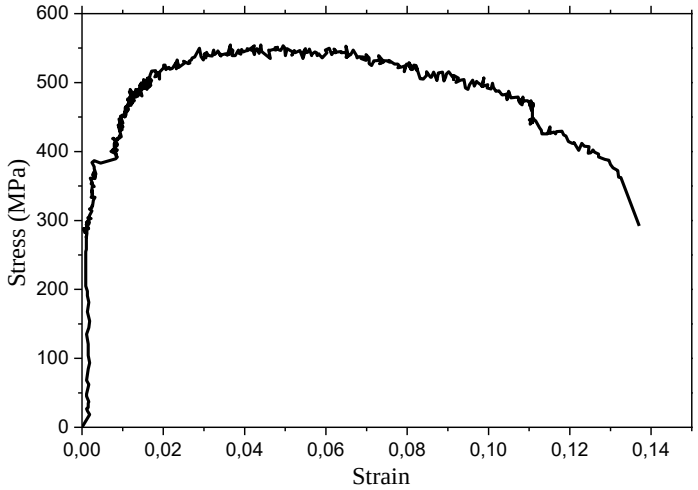

(b)

Figure 2.4: Tensile behavior: a) Steel of channel connectors, b) Steel of headed stud connectors.

Table 2.2: Geometric and mechanical properties of steel materials.

Specimens	Flange width, t_f (mm)	Web thickness , t_w (mm)	Steel grade	Av. Yield strength, f_y (MPa)	Av. Ultimate strength, f_u (MPa)	Av. Elongation (%)
Steel of channel shear connectors	8.5	6.2	S275	327	481	27
Steel of stud shear connectors	-		S235 J2+C450	389	554	13.8
Steel of reinforcing bars	Ø 10		S400	392	656	13
HEB 240 Steel	17	10	S275	-	-	-

2.2.3- Welding procedure

As shown in Fig. 2.5, channel and headed stud shear connectors were welded to the flange of the steel sections through a standard Arc welding (Stick welding),. Electrodes used are ESAB (E6013) type of 3.2 mm diameter × 350 mm long, with mechanical properties of 400 MPa yield strength and 510 MPa ultimate strength. Figure 2.6 shows the headed studs used in the specimens. The studs are of Nelson type with 19 mm diameter at the shank, 32mm diameter at the head, and 100 mm of height.

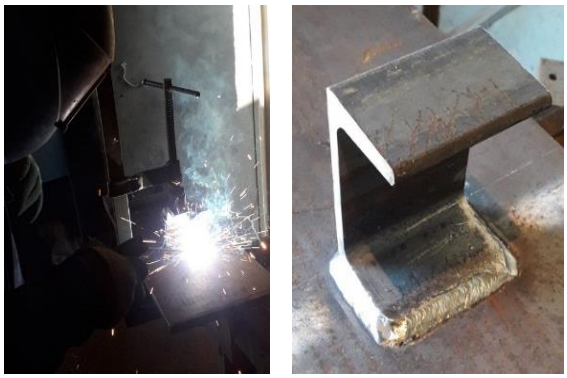

Figure 2.5: The welding process of the channel shear connector (during and after welding).

Figure 2.6: The headed stud shear connectors used in the specimens.

2.3- Hydraulic machine

The unavailability of a test machine led us to manufacture a new one to carry out our experimental research. This hydraulic machine was made in a workshop by the author using steel profiles, jack loading, electric engine, hydraulic pump, and some electric and electronic parts.

The structure of this hydraulic machine is designed to support a load capacity higher than 1000 kN. Thus, the structure of this test machine was built by using two types of steel profiles HEA200 for the columns and UPN240 for the beams (Fig 2.7). However, to increase the stiffness of the four beams, longitudinally half of UPN 240 welded on each beam, as shown in fig 2.7. On the other hand, to verify the stability of the machine's structure we performed the following calculations:

a) Beam section

- The inertia moment of the cross-section (a-a)(Fig 2.7) is : $I = 9.262 \times 10^7\ mm^4$.
- The length of the beam is: $L = 1220\ mm$.
- The steel beam grad is ST275, hence, the yield strength f_y is $275\ MPa$.
- The gravity center of the cross-section (a-a)(Fig 2.7) is: $y = 187.8\ mm$

The beams of this machine are stressed in simple bending, hence:

$$f_y > M \times y/I \quad \text{with} \quad M = p \times \frac{L}{4} \quad \Rightarrow \quad P < f_y \times I \times 4/(L \times y)$$

$$\text{So } P < 275 \times 9.262 \times 10^7 \times 4/(1220 \times 187.8) \Rightarrow P < 444674.31\ N$$

With two pairs of beams we conclude that the load resisted is 1778.69 kN.

b) Column section

- The area of the cross-section HEA 200 is: $A = 5383\ mm$
- The steel columns grad is ST275, hence, the yield strength f_y is $275\ MPa$.

The columns of this machine are loaded in simply tensile, hence:

$P \leq 0.9 \times f_y \times A/\gamma_M \quad \Rightarrow\ P \leq 0.9 \times 5383 \times 275/1.25$

So $P \leq 1065834\ N$

With two columns we conclude that the load resisted is 2131.66 kN.

c) Bolts

- The number of bolts that joint the columns with the beams is 16.
- The diameter of each bolt is $d = 18mm$.
- The cross-section area of each bolt is $A = 192\ mm^2$
- The steel bolts grad is 8.8 with an ultimate strength $f_u = 800$ MPa

We assume that the bolts are stressed only in shear force. Hence, according to [35]:

$$N = 0.6 \times f_u \times A/\gamma_M \Rightarrow N = 0.6 \times 800 \times 192/1.25 \ = 92160\ N$$

So $F = N \times 16 = 1474.56\ kN$.

Note: The diametrical pressure resistance at the bolt holes in the column flanges and beam webs was neglected because they are reinforced with steel plates by welding (Fig. 2.7).

On the other side, the diameter of the jack loading axis is 115 mm with a displacement of 350 mm, and the inside diameter of its cylinder is 140 mm. Furthermore, the pressure capacity of the hydraulic pump is 515 Par, which produced a maximum load of around 792 kN. As a result, the load applied by the jack loading is less than that resisted by the element of the structure machine (i.e., beams, columns, bolts), and this later is secured.

On the other hand, the displacement speed of the jack loading axis varies from 0 to 0.1 mm/s. As a note, the displacement speed chosen in our experimental tests is 0.008 mm/s. The electric engine used has a capacity of three horses and 700 rpm.

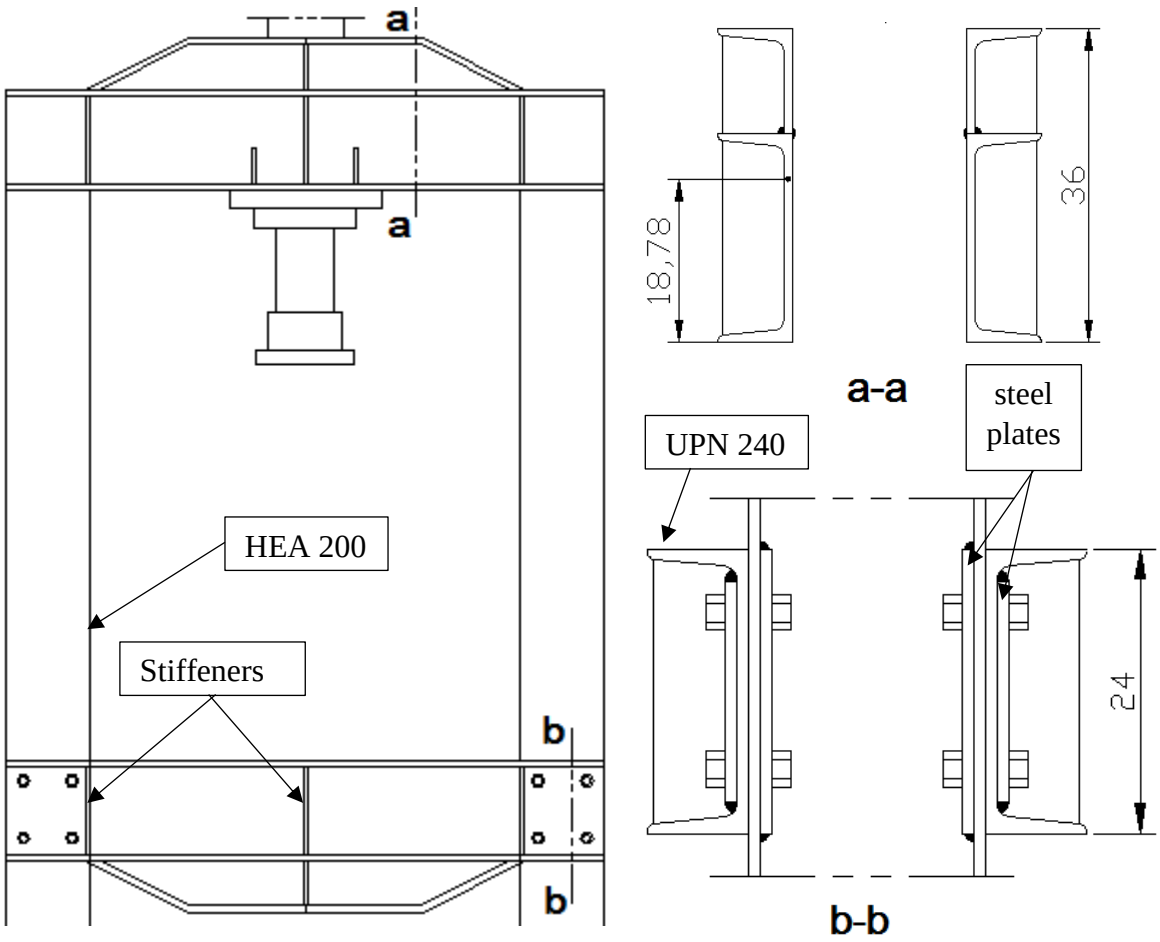

Figure 2.7: Descriptive design of the hydraulic machine structure.

2.4- Measuring instruments

2.4.1- Load measurement

The hydraulic machine is equipped with a load sensor to measure the loads applied to the specimen. Its maximum capacity is 300 Par. This sensor has electrical wires to join the electronic acquisition system, as shown in Fig 2.8.

Figure 2.8: Load sensor.

2.4.2- Displacement measurement

A linear potentiometer (LVDT) was used to measure the displacement. Its effective travel is 100 mm, and it has three electrical wires to join the electronic acquisition system, as shown in Fig 2.9.

Figure 2.9: linear potentiometer (LVDT).

2.4.3- Electronic acquisition system

This system is composed of an electric transformer, an electronic card called Arduino, and a LabVIEW program [36]. The purpose of each party is as follows:

- The electric transformer is used for a lower voltage power input.
- Arduino is an open-source platform used for building electronics projects. Arduino consists of both a physical programmable circuit board (often referred to as a microcontroller) and a piece of software, or IDE (Integrated Development Environment) that runs on the computer, used to write and upload computer code to the physical board. In addition, Arduino does not need a separate piece of hardware (called a programmer) in order to load new code onto the board it can simply use a USB cable.
- The LabVIEW program [36] is composed of two parts. The first is called " Front Panel " which is the interface that the user will interact with to control the Arduino. Then the second

is called "Block-Diagram" where the program will be written. This program was elaborated by two professors from the electrical engineering departement of Setif University.

2.4.4- Calibration of sensors

The use of a sensor always involves a calibration law that will allow passing from the electrical measurement to the estimation of the corresponding physical quantity. In addition, the calibration of a sensor is translated generally by a calibration curve that expresses the relationship between the physical quantity, and the measurement that is given by the sensor. This curve does not express a functional relationship but a correlation between two quantities. Most often it uses a regression technique to establish the calibration law.

The calibration of the linear potentiometer was done with the assistance of a measurement comparator, as shown in Fig 2.10. However, the calibration of the load sensor was realized by an institution specialized in the field. The load cell used has a capacity of 3000 kN, as shown in Fig 2.11.

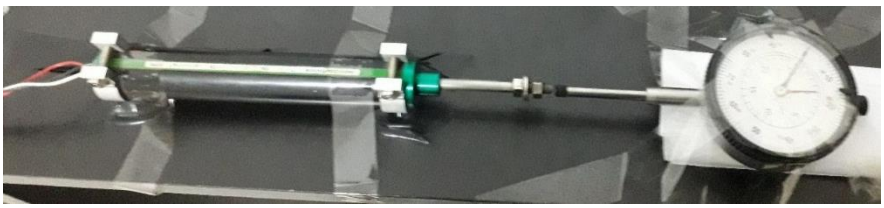

Figure 2.10: Calibration of the linear potentiometer.

Figure 2.11: Calibration of the load sensor.

2.5- New push-out test setup [37]

The study of shear connectors by the ancient regulations such as Eurocod4 [27] involves using a steel beam piece and two concrete slabs. Those latter connected to the two flanges of a steel beam by connectors. However, the push-out test failure in this case sometimes happens on one side only, and the other side remains connected due to the eccentricity between the jack loading axis and the two shear planes [38-40] (Fig 2.12). This phenomenon created a divergence between the results of the two sides due to the unequal loading between the two shear planes [41]. To overcome this issue, some researchers used the clamping mechanism procedure for the concrete slabs [41, 42]. As a note, the effect of this procedure (clamping mechanisms) was investigated in chapter 4 of this thesis. However, many researchers have been used a single concrete slab through various setups [32, 43-45].

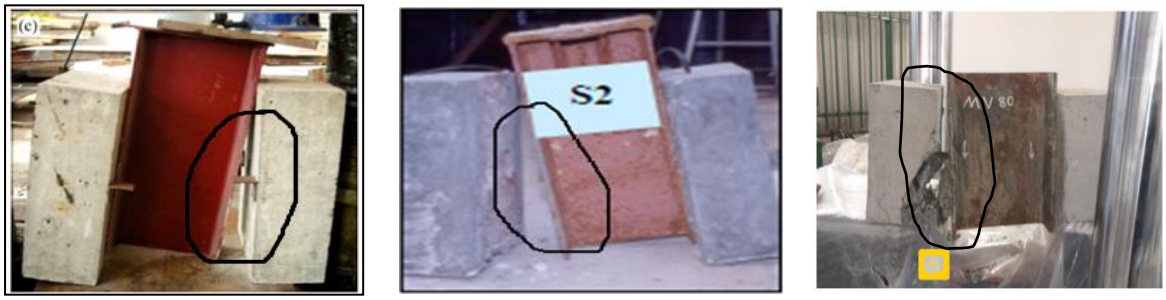

(a). [38] (b). [39] (c). [40]

Figure 2.12: Undesirable failure (One-sided failure).

In this study, a new push-out test setup was developed. The latter consists of concentrating the load on the flange where the shear plane is located and replacing the other side of the specimen (half steel section with concrete slab) with a moving system that ensures the specimen movement in one direction only.

2.5.1- The moving system components

Figure 2.13 shows an overview of the new push-out test setup with the moving system. The two main parts that make up this moving system are the guiding part and the moving part as follows:

The guiding part contains two pairs of HEM 120 (12.5× 21×126×140 mm^4) steel beams (A) connected perpendicularly by welding. The first pair is fixed to the machine pillar by four threaded rods grade 8.8 (M20) (B), using four UPN 80 steel beams. Also, the bottom HEM 120 of this pair is connected by welding with two UPN 140 steel beams for placing and fixing to

the machine base by two bolts (M18). The second pair carry the roller bearings. For ensuring and guiding the displacement, eight roller bearings KR52 type were placed vertically (C). Each one resists a static load of 27 kN. And four roller bearings of type NUTR20 were placed horizontally (D). Each one resists a static load of 39 kN.

The moving part consisted of three elements (E), (G), and (H). The element (E) slides on the roller bearings. Since the roller bearings are manufactured from hard metals, it has used a steel plate (25×140×600 mm^3) of XC48 metal type for the element (E). The latter has been heat-treated (hardened) to a hardness of 40 Rockwell to resist the contact pressure. Then, to be very straight, a rectification of its surfaces was made by a machine called the surface grinder. After that, this element (E) was fixed by seven bolts (M18) (F) with a steel plate I (25×40×600mm^3) (G). This element (G) was connected by welding with another steel plate I (10×70×600mm^3) (H), which contains four holes (d=18mm) to connect with the T sections web by using a couple of steel plates I (12×150×600mm^3) (I) and eight bolts (M18) (J).

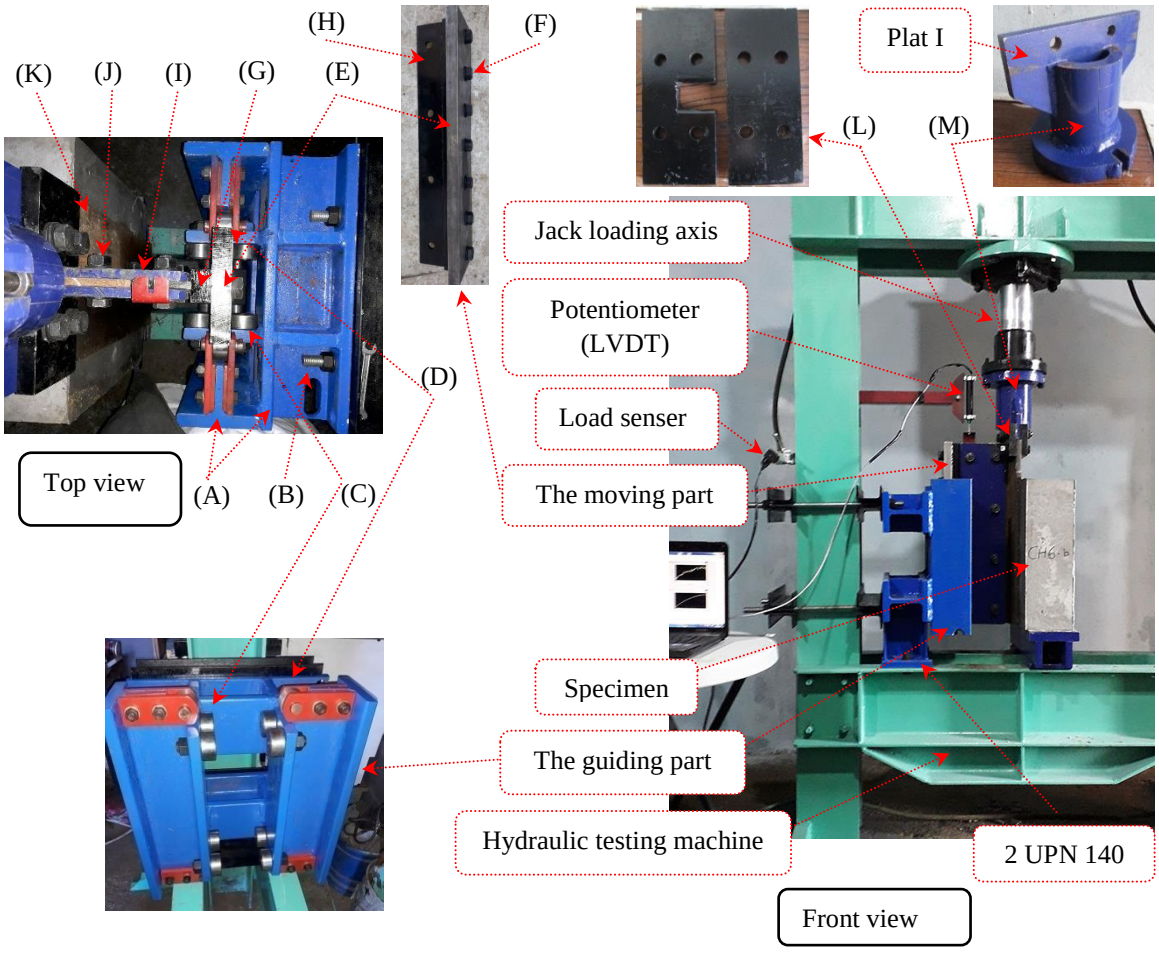

Figure 2.13: Push-out test setup.

2.6- Concision

In this chapter we have presented the experimental procedure adopted in the realization of the push-out tests. In addition, we have also presented in detail the new push out test setup. As it is known, the experiment tests are expensive and take a lot of time. Besides, it need a lot of arrangements such as:

1) Provide the necessary materials that are used in the experimental tests (i.e., connectors, steel profiles, reinforcing bars, and concrete).
2) Availability of a hydraulic machine test with a capacity of load higher than that applied on the specimen.
3) Effective and accurate measuring tools. (i.e., displacement sensor, load sensor, and electronic acquisition system).
4) The yield strength, the tensile strength, and the maximum elongation of the shear connector material, as well as the concrete compressive strength, should be determined.

Chapter 3: Push-out tests on developed channel shear connectors

3.1-Introduction

Five new shapes of channel shear connectors are offered and studied in this chapter. Using a new test setup, twelve push-out tests and three pull-out tests were carried out under monotonic loading to evaluate the effect of the following parameters on the ultimate load capacity, ductility, and also on the concrete: (i) reduction of channel shear connector length at the two plastic hinges indicated by Baran and Tobkaya [32], as illustrated in Fig.3.1. (ii) reducing the top flange to 70% and 50%. In addition, the effect of the reduction of the channel shear connector head in the new shapes on the work of the connector to prevent separation of the concrete slab was also investigated.

Firstly, the description of the push and pull-out specimens is presented. Then, the results of push-out tests such as; the failure modes, the load-slip behavior, the concrete slabs, the bending deformation capacity, the height between the two plastic hinges that appeared near the base of the channel connectors, and the ductility factor were revealed and discussed. As for the pull-out test, the effect of the new channel shapes on the concrete slab uplift was also revealed and discussed. In addition, an overall discussion was performed, including a comparison between the new and the standard push-out test setup.

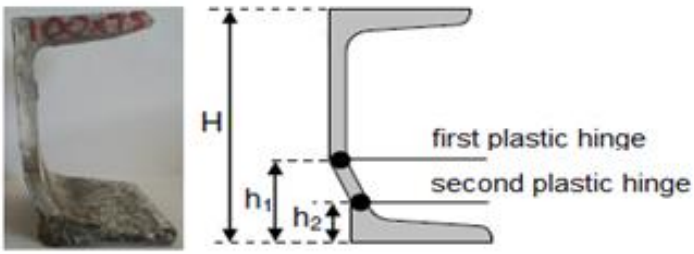

Figure 3.1: Idealized failure mechanism of channel shear connectors [32].

3.2- Description of specimens

3.2.1- Push-out specimens

Twelve push-out specimens were divided into six groups. Each group includes two identical specimens. Group CH1 (a, b) includes the specimens of the ordinary channel shear connector shape that have been used as a reference (a benchmark), while the other groups include five new channel shear connector shapes presented in Fig.3.2. All channel shear connector shapes are embedded in normal concrete strength. The manufacturing of the new shapes was very easy by piercing and cutting the UPN100 steel section. Given that recently, the

availability of advanced equipment on construction sites, these two procedures (piercing - cutting) are becoming very easy. Therefore, the manufacture of these shapes is affordable.

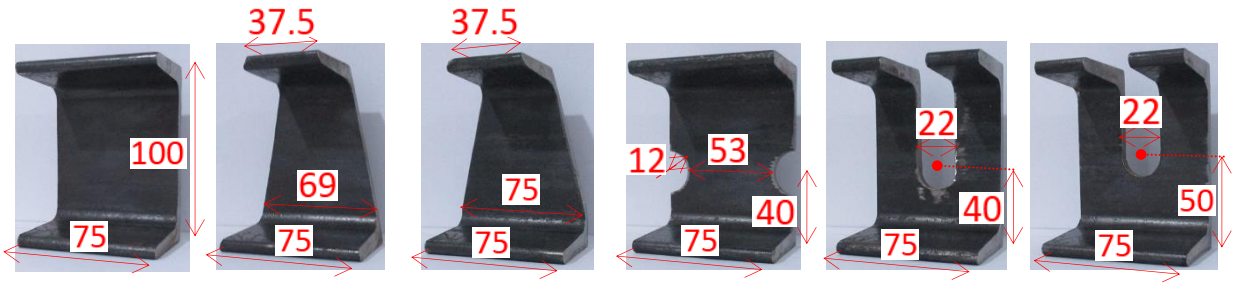

a- CH1 (a, b, c) b- CH2 (a , b, c) c- CH3 (a, b) d- CH4 (a, b) e- CH5 (a, b, c) f- CH6 (a, b)

Figure 3.2: Geometric details of the proposed channel shear connector shapes for each group (All dimensions in mm).

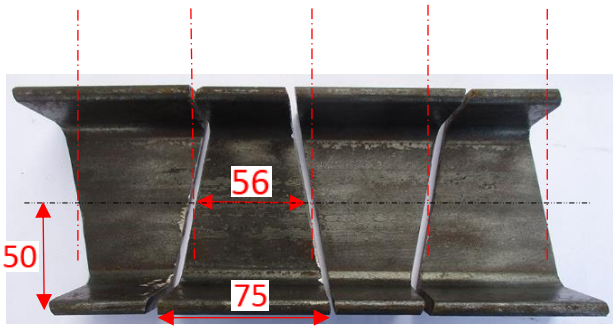

Figure 3.3: Transversal cutting of CH2 shape (uni; mm).

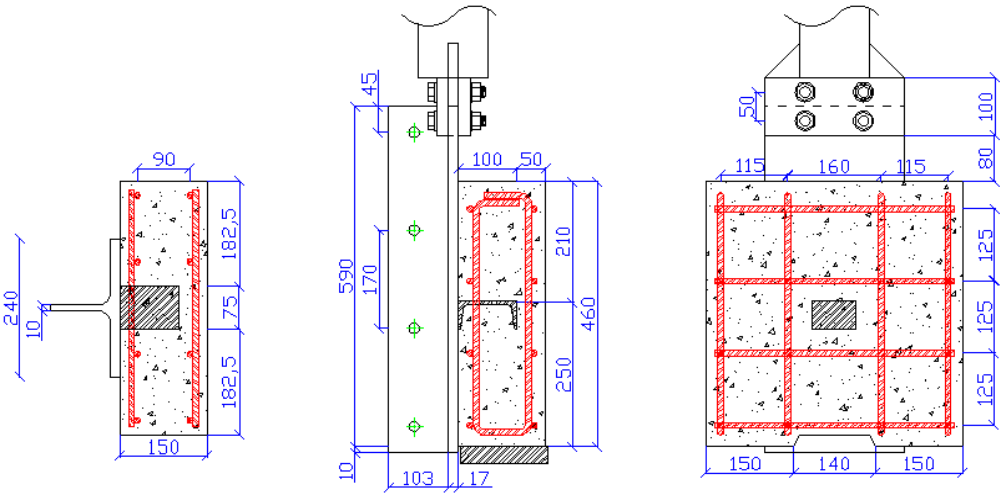

Top view Front view Side view

Figure 3.4: Details of push-out test specimen (uni: mm).

3.2.2- Pull-out specimens

Arıkoğlu et al. 2020 [46] were investigated the performance of channel shear connectors in steel-concrete composite beams with precast slabs. In conclusion, they advised that future research should focus on revealing the uplift resistance of these shear connectors. Therefore, to explore the effect of the reduction of the channel shear connector head in this study on the work of the shear connectors to prevent the concrete slab uplift, three specimens of pull-out test were prepared including CH1-c, CH2-c, and CH5-c shear connector shapes (Fig.3.2). The details of these specimens are given in Fig.3.6. However, figure 3.7 shows an overview of the pull-out test setup.

Figure 3.5: Applying load on the push-out specimen.

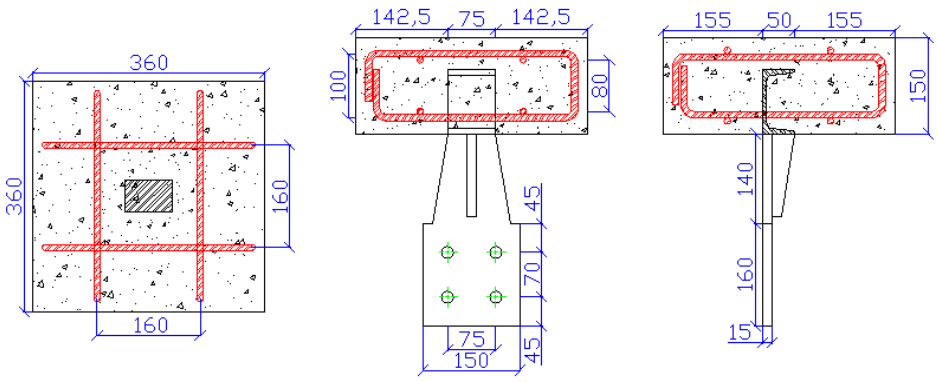

Figure 3.6: Details of pull-out test specimen (All dimensions in mm).

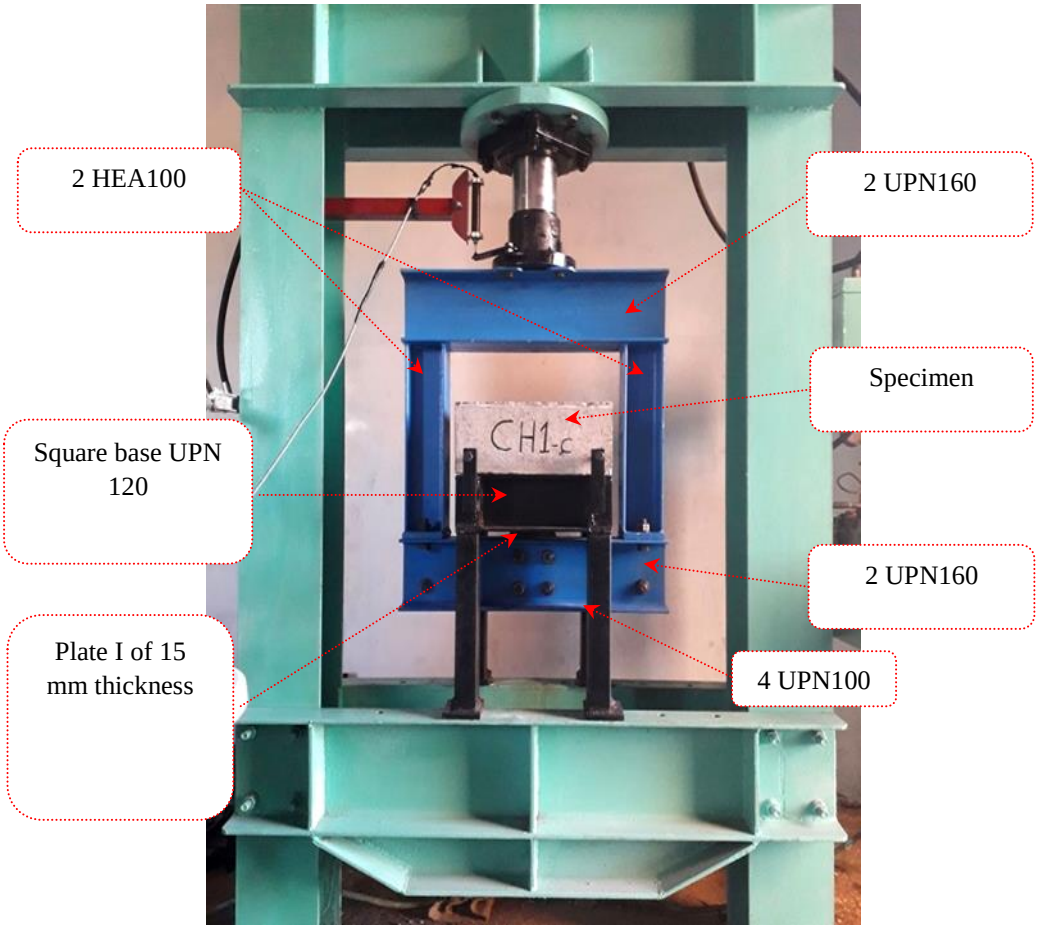

Figure 3.7: Pull-out test setup.

3.3- Test results

3.3.1- Push-out test

3.3.1.1- Failure modes

During the execution of tests, the cracking appeared from the bottom of the concrete slab and started to propagate with the increase of applied loading until it reached the middle of the concrete slab. After the tests, the cracks were a little thick at the bottom and thin at the middle of the concrete slab.

Figure 3.8 shows the failures of the specimens that yielded high ductility for each group. The failure modes observed from the push-out tests were concrete cracking-splitting in CH1 specimens (Fig. 3.8 (a)) while the concrete cracking was the failure mode observed in all other specimens, as illustrated in Fig. 3.8 (b, c, d, e, and f). In addition, the third failure mode was the deformation of connectors. No fracture of the channel shear connector occurred in all specimens, and the concrete slab remained connected to the steel section.

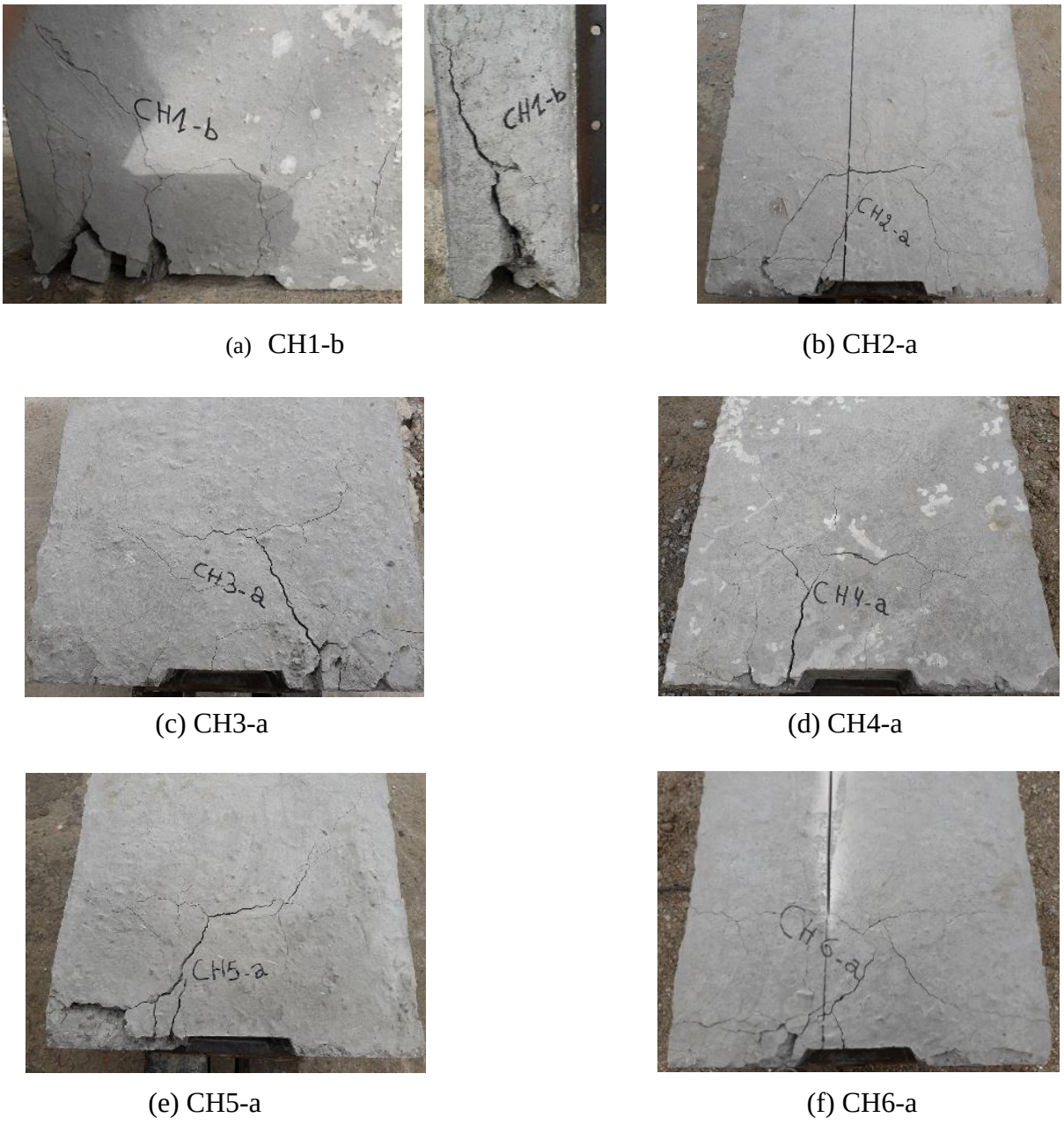

(a) CH1-b (b) CH2-a

(c) CH3-a (d) CH4-a

(e) CH5-a (f) CH6-a

Figure 3.8: Typical failure modes: (a) concrete cracking-splitting; (b, c, d, e, and f) concrete cracking.

3.3.1.2- Load-slip behavior

A comparison between the load-slip curves of the two reference specimens CH1 (a, b) against those of the new shear connector shapes is presented in Fig 3.9 . It can division the load-slip curves into three stages. The first stage is the elastic stage which the load-slip curves were very steep when the load was below 0.65-0.75 P_u, P_u is the ultimate load.

The second stage is the plastic stage which the slope of the load-slip curves decreases when the load is between 0.65-0.7 P_u and P_u. The third stage was the unloading stage. However, it should be noted that in the elastic stage, the load-slip curves of all specimens were almost identical and the difference was in the plastic stage.

Table 3.1 summarizes the ultimate strength, the ultimate slip which is equivalent to the 10% drop in ultimate strength for each specimen, and the average between specimens of the same gender. It also summarizes a comparison of the average of the CH1 group specimen with the averages of the specimens in the other groups.

From this comparison, it is concluded that: (i) the ultimate strength of CH2 and CH5 groups were almost similar, while the ultimate strength of CH3, CH4, and CH5 groups increased slightly to 2.3%, 3.9%, and 5.1%, respectively. (ii) the ultimate slip of the CH2, CH3, and CH5 groups increased by about 19% to 1.99 mm,1.98 mm, and 1.93 mm, respectively, while the ultimate slip of the CH4 group was 1.57 mm (about 15%). As for the CH6 group, its ultimate slip was considerable, with an increase of about 31% to 3.16 mm.

The decrease in channel shear connector length at the second plastic hinge for the CH2 group compared to the CH3 group caused a slight decrease in ultimate strength (about 1.7%), while the ultimate slip was identical.

3.3.1.3- Concrete slabs

From Fig. 3.8, it can be seen that the CH1 specimen was more affected by concrete cracking. Moreover, to inspect cracks inside the concrete slabs and the deformation patterns of channel connectors, the concrete slabs of the specimens that yielded high ductility for each group were sawed longitudinally, as shown in Fig.3.10.

The position of the longitudinal sawing axis is plotted on specimens CH2-a and CH6-a, as indicated in Fig.3.10 (b) and Fig.3.10 (f). It can be classified specimens in terms of the concrete cracks into three classes as follows: the specimen CH1-b is in the first class since it was most affected by the concrete cracking as shown in Fig.3.10 (a). CH3-a and CH4-a specimens are in the second class, as shown in Fig.3.10 (c and d). Finally, CH2-a, CH5-a, and CH6-a specimens are the least affected by concrete cracking, as shown in Fig.3.10 (b, e, and f). It can be seen that the concrete cracks in front of the connector were higher than the other side. It can also see that the specimens that were less affected by concrete cracking achieved higher ultimate slip (i.e. higher ductility).

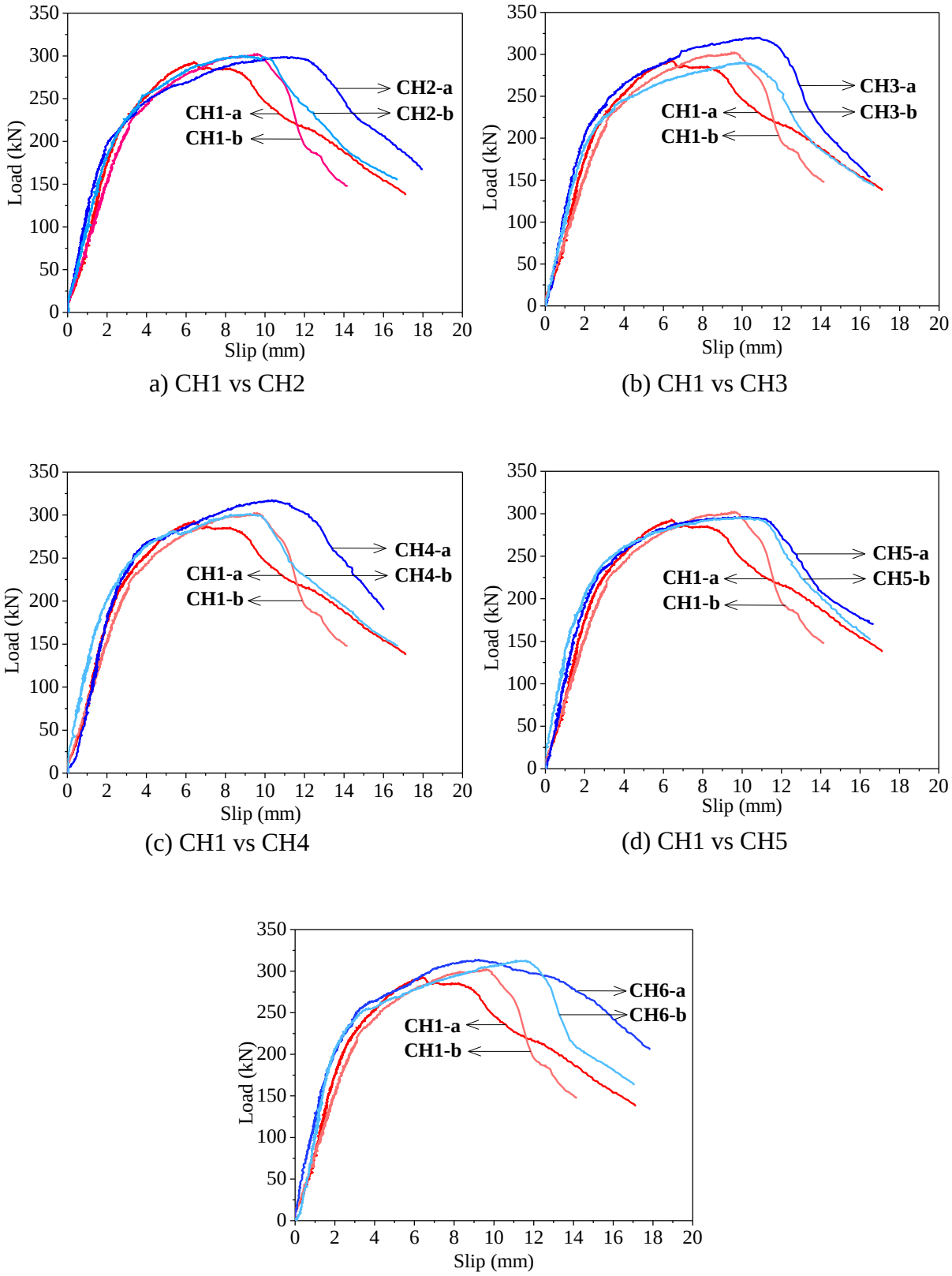

a) CH1 vs CH2

(b) CH1 vs CH3

(c) CH1 vs CH4

(d) CH1 vs CH5

(e) CH1 vs CH6

Figure 3.9: Load-slip curves of push-out tests.

Table 3.1: Push-out tests results of channel shear connectors.

Specimens		Ultimate load (kN)	Average ultimate load (kN)	Ultimate slip (mm)	Average ultimate slip (mm)	Average each specimen / Average CH1	
						Load	Slip
CH 1	-a	293.23	297.9	9.42	10.12	1	1
	-b	302.58		10.82			
CH 2	-a	298.79	299.61	13.32	12.11	1.005	1.196
	-b	300.44		10.91			
CH 3	-a	319.88	304.99	12.42	12.10	1.023	1.195
	-b	290.10		11.78			
CH 4	-a	317.48	309.67	12.79	11.69	1.039	1.155
	-b	301.51		10.60			
CH 5	-a	296.17	295.82	12.20	12.05	0.993	1.190
	-b	295.47		11.90			
CH 6	-a	313.69	313.18	13.77	13.28	1.051	1.312
	-b	312.67		12.80			

3.3.1.4- Ductility factor

For a better understanding of ductility performance, the ductility factor is a good choice [47]. Figure 3.10 gives an overall elastoplastic load-slip curve reproducing those observed in the measurement, from which the shear connector ductility factor, μ, is defined.

Two straight lines were designated as preliminary stiffness and ultimate strength in the load-deflection curve. The intersection of those two lines was taken as an equivalent yield displacement Δ_y. The maximum deflection, Δ_{max}, was defined as the deflection at which the 10% drop in ultimate loading occurs. The expression, Δ_{max}/Δ_y, gives the value of the required ductility factor. In general, the greater the ductility factor, the greater the amount of inelastic redistribution of applied loads [48]. Among all six groups, the better ductility was on the part of the CH6 group.

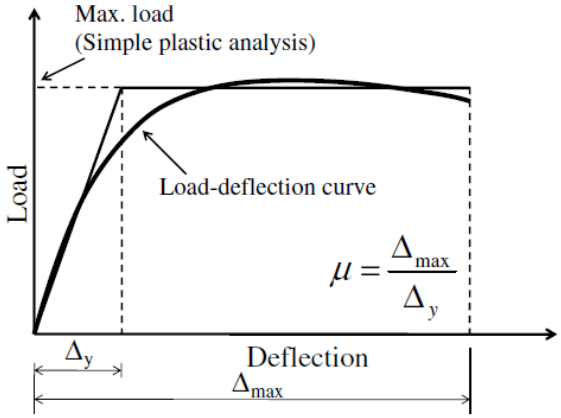

Figure 3.10: Definition of ductility factor [48].

3.3.2- pull-out test

3.3.2.1- Failure mode

The failure of all three specimens was due to a concrete breakout. Pyramid failure surfaces are developed, as shown in Fig. 3.11, with slight bending deformation of the connector head, the latter is produced after the creation of a plastic hinge on the web.

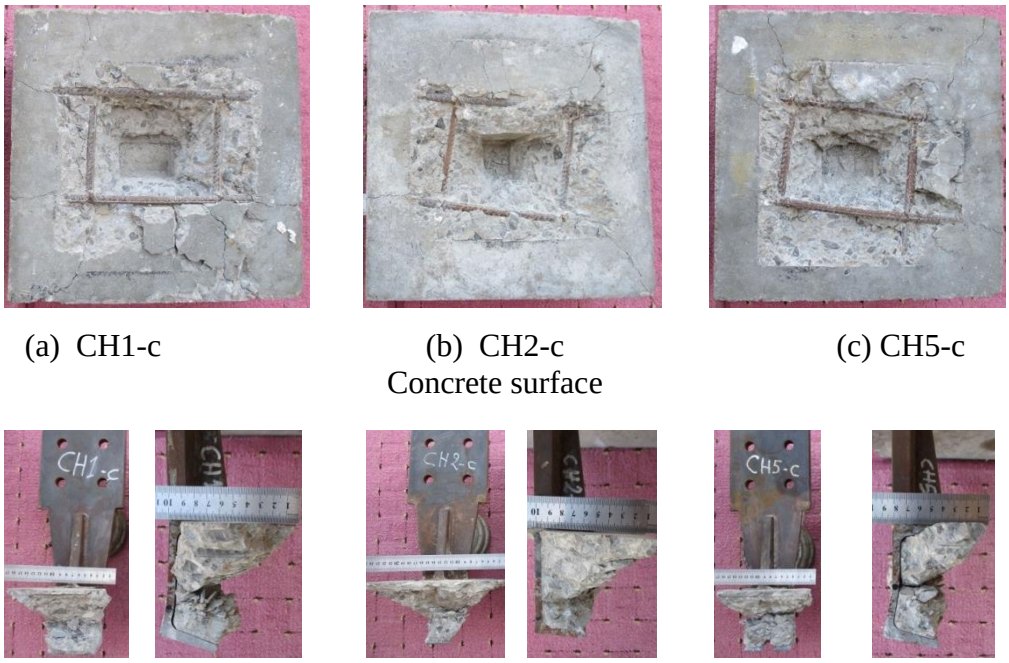

(a) CH1-c (b) CH2-c (c) CH5-c

Concrete surface

Front view Side view Front view Side view Front view Side view

(a) CH1-c (b) CH2-c (c) CH5-c

Channel shear connectors surface

Figure 3.11: Typical failure of pull-out tests.

3.3.2.2- Load-slip behavior

The load-slip curves of the three specimens CH1-c, CH2-c, CH5-c, are shown in Fig. 3.16, while the ultimate load and ultimate slip results are summarized in Table 3.2. It is noticed that the specimen CH2-c yielded a decrease in the ultimate tensile strength of about 21% and a slight increase in the ultimate tensile slip of about 3% compared to CH1-c. However, the CH5-c specimen yielded an increase in the ultimate tensile strength of about 4.9% and a decrease in the ultimate tensile slip of about 15% compared to CH1-c.

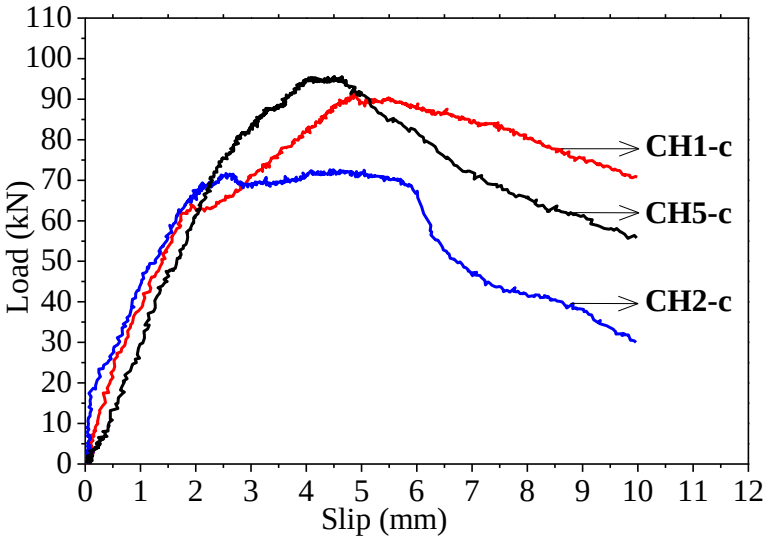

Figure 3.12: Load-slip curves of pull-out tests.

Table 3.2: Pull-out tests results.

Specimens	Ultimate load (kN)	Ultimate slip (mm)	Each specimen / CH1-c	
			Load	Slip
CH1-c	91.40	5.49	1	1
CH2-c	72.49	5.70	0.79	1.03
CH5-c	95.91	4.71	1.04	0.85

3.4- Discussion

Previous studies mentioned above concluded that increasing the length of the channel shear connector negatively affects the concrete slab. Moreover, the crack initiation load rises with increasing channel size, number, and length of channels [49].

On the other hand, the specimen with 100 mm high channels is more flexible than that with 75 mm high shear channels. Wherein, the amount of slip at the ultimate load was 6.5-9 mm compared to 4-8 mm for the 75 mm high shear channels [50]. But, the requirement Eurocode-4 for an ideal plastic behavior of the shear connection is 6 mm slip. In addition, a parametric study including 1680 simply supported beams with solid slabs planned according to Eurocode 4 was conducted by Zona and Ranzi 2014 [51] to evaluate the influence of various parameters on the predicted slip demand in the shear connection at the ultimate limit state. The results show that, in the cases of a partial shear connection (η= 0.4), propped construction, and sections with equal flanges or bottom flange twice or three times the top flange, the slip demand was between 6-23 mm when the span length was 20-40 m.

Therefore, the two new shapes CH6 and CH2 of shear channels can be useful to avoid the negative effect of longer channel connectors and shorter channel connectors on the concrete slab and ductility consecutively.

3.5- Design codes

Table 3.5 illustrations a comparison between the ultimate load values of the experimental tests and those predicted by some design codes and the previous research (see chapter 1). The results of the comparison demonstrated that Eq. (1.6) agrees well with the test results, whereas Eq. (1.4) and Eq. (1.5) are very conservative. As for Eq (1.7), the results were greater than the test results in this study, and it should be mentioned that using of concrete slab clamping mechanism by Baran and Topkaya 2012 [32] in their experimental tests perhaps led to an increase in the ultimate strength with which they established their equation.

Table 3.5: Experimental ultimate load capacity against those of predicted design codes.

Specimens	Ultimate load capacity (kN)					Eq. (1.4) /Test	Eq. (1.5) /Test	Eq. (1.6) /Test	Eq. (1.7) /Test
	Test	Eq. (1.4)	Eq. (1.5)	Eq. (1.6)	Eq. (1.7)				
CH1	296.76	265.6	179.3	294.9	355.2	0.90	0.60	**0.99**	1.19
CH2	299.61					0.89	0.59	**0.98**	1.18
CH3	304.99					0.87	0.58	**0.96**	1.16
CH4	309.67					0.86	0.58	**0.95**	1.14
CH5	295.82					0.90	0.60	**1.00**	1.20
CH6	313.18					0.85	0.57	**0.94**	1.13

3.6- Conclusion

The results of twelve push-out and three pull-out specimens were presented. Investigations were realized using a new push-out test setup to study the behavior of the channel shear connector shapes proposed. Upon analysis of the study results, the following conclusions were drawn:

1) The new push-out test setup used in this study guaranteed the movement between the two elements (steel section-concrete slab) in one direction only.
2) The new channel shear connector shapes provided great results in ductility, whereas the results of ultimate strength were slightly tangible for the CH3, CH4, and CH6 groups.
3) The performance improvement of these new channel shear connector was at the plastic stage, while in the elastic stage it was almost identical to the ordinary shear channel.
4) The failure modes observed were cracking-splitting of concrete in CH1 specimens and concrete cracking in all other specimens. The concrete slab of the CH1 group were more affected by concrete cracking.
5) According to the pull-out tests, and the steel-concrete transverse separation produced in the push-out tests, the reduction of the channel shear connector head in the new shapes does not affect the work of the connector to prevent concrete slab uplift.
6) The best performance was achieved by the CH6 and CH2 groups. In addition, specimens from these groups are the least affected by concrete cracking.
7) The empirical equation developed by (Pashan 2006) agrees well with the push-out test results.

Note: this chapter was published by the author in the article [37].

Chapter 4:

Push-out tests on the developed headed stud shear connectors

4.1- Introduction

In this chapter, a modified shape of headed stud sized 19 mm in diameter and 100 mm in length is proposed and studied. The performance of this new shape was compared with that of two other ordinary-headed studs. The first has the same diameter and length, and the second has 16 mm of diameter and 100 mm of length. Eight experimental push-out tests using the new test setup shown in the previeuse chapter were achieved under monotonic loading. The purpose is to evaluate the influence of the following parameters: (i) the clamping mechanism of concrete slabs; (ii) the diameter of headed studs; (iii) reduction of stud diameter to 16mm from 20 mm of the bottom shank of stud until the head, as shown in Fig. 1 (c).

4.2- Description of specimens

The experimental program consists of eight push-out specimens divided into three groups. Group N°1 contains three specimens included ordinary headed studs with a diameter of 19 mm and a height of 100 mm shown in Fig. 4.1 (a). The first specimen on the group N°1 ST1-a is subjected to a different procedure than the other seven specimens. This procedure was the clamping mechanism of the concrete slab, as illustrated in Fig. 4.2. The other two specimens ST1-b and ST1-c are used as a reference. Group N°1 contains three identical specimens included ordinary headed studs of diameter 16 mm and a height of 100 mm (Fig. 4.1 (b)). The last group includes a new geometric parameter shown in Fig. 4.1 (c), and the details of the specimens are shown in Fig. 4.3. The connector shapes used in the specimens of the ST3 group were manufactured by mechanical turning.

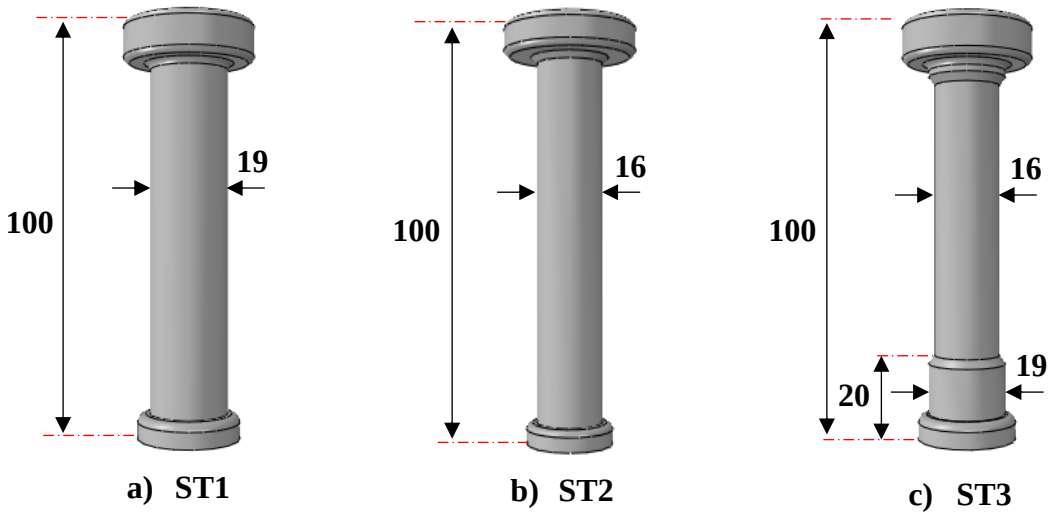

Figure 4.1: The geometric details of headed stud for each group (All dimensions in mm).

On the other hand, the slip between the steel beam and the concrete slab would occur when the studs deform [52]. The deformation occurs due to the effects of bending moment and starts from the bottom of the connector until a given height value. The height value influenced by many parameters such as the type of concrete, the diameter, and the height of the shear connector. Table 1 summarizes the height of the bending arm given by some researchers [16, 17, 53, 54] used ordinary concrete and headed studs of 19 mm diameter and 100 mm length. It noted that the height of the bending arm in the bottom shank of headed studs is varied between 18mm and 25mm. Therefore, the reduction of stud shank in the ST3 specimens is started from 20 mm.

Table 4.1: The height of the bending arm that given by some researchers.

Researchers	d (mm)	L (mm)	f_{ck} (MPa)	Tests types	length of bending arm (mm)
Xiaoqing Xu and al [16]	19	100	34.1	Experimental	25
Weichen Xue and al [53]	19	100	30,5	Experimental	18
Chen Xu and Sugiura [17]	19	100	30	FEA	18
Xiaoqing Xu and Liu [54]	19	100	34.1	FEA	22

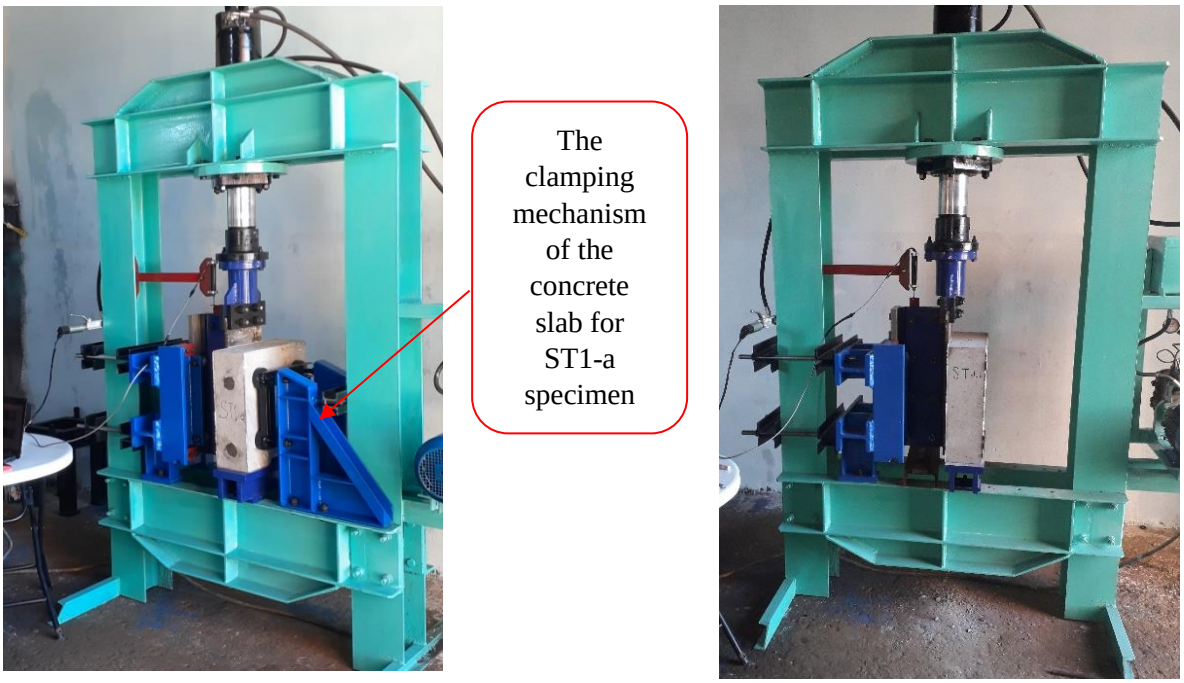

(a) (b)

Figure 4.2: push-out setup; (a) ST1-a specimen; (b) the other specimens.

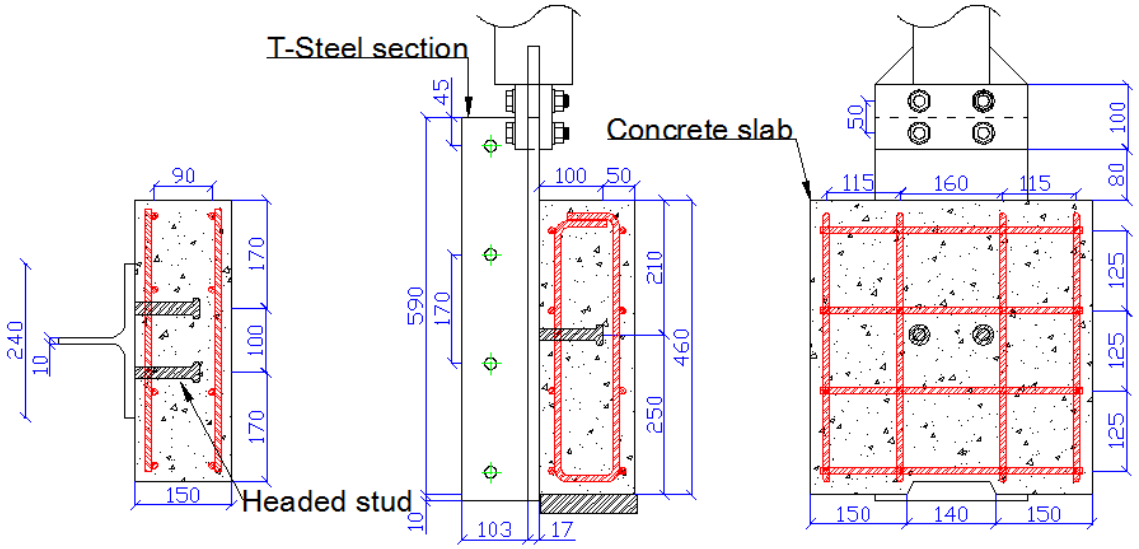

Figure 4.3: Details of push-out test specimen (All dimensions in mm).

4.3- Test results

4.3.1- Load-slip behavior

Figure 4.4 demonstrates a comparison of the load-slip curves of the reference specimens ST1 against those of the other specimens. As the curves obtained by the channel connectors in the previous chapter, it can divide the curves into three stages. In the first stage, the load increases linearly with slip due to the small deformation of the connectors, and the slipping-load curves are steep when the load was less than 0.68-0.78 P_u. P_u is the ultimate load capacity per stud. It can consider this stage is the elastic stage. Then, in the next stage, the rise of the load slip curves declines when the load is between 0.68-0.78 P_u and P_u. It can consider this stage the plastic stage. Afterward, in the last stage, the load systematically decreases, and then a shearing of the connectors occurs immediately.

Table 4.2 summarizes the results of push-out tests. Column (2) in this table shows the ultimate load capacity per stud P_u of each specimen and its average values shown in column (4). Column (3) shows the ultimate slip δ_u of each specimen when the load has reduced by 10% (0,9Pu) from its peak, and its average values are shown in column (5). Column (6) shows the average slip value δ_m, which corresponds to the ultimate strength P_u. Columns (7) and (8) show the ratio of averages load P_u and slip δ_u of ST1-a specimens and the other groups compared to the reference specimens ST1 (b, c).

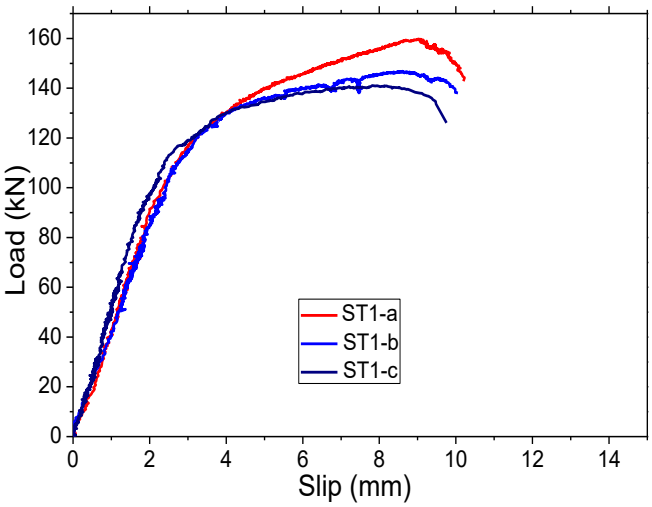

a) (ST1-a) vs (ST1-b and ST1-c)

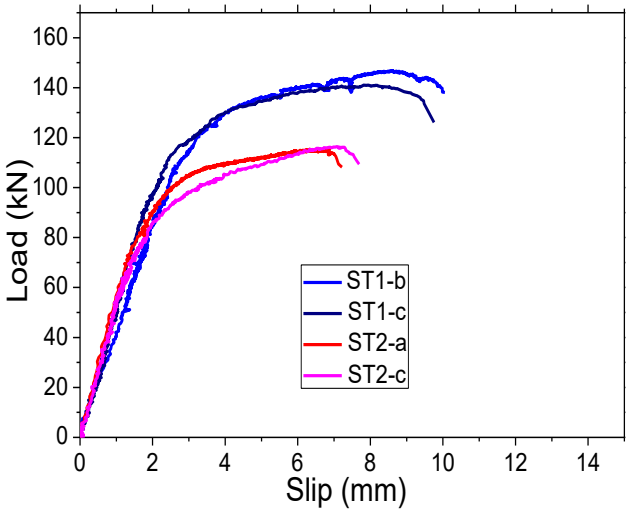

b) (ST1-b and ST1-c) vs (ST2-a and ST2-c)

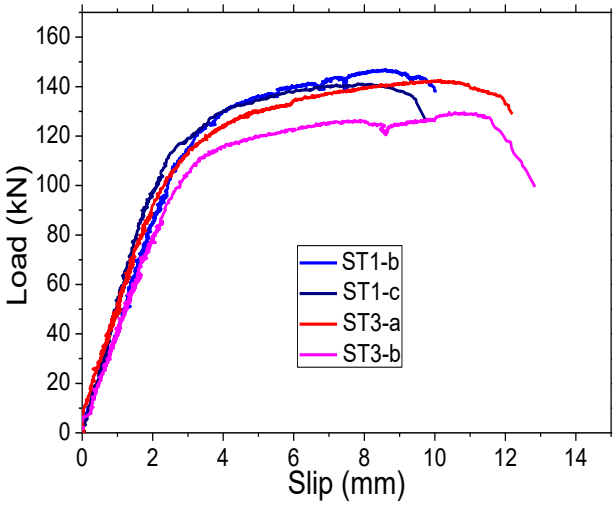

c) (ST1-b and ST1-c) vs (ST3-a and ST3-b)

Figure 4.4: Load-slip curves of headed studs push tests.

Table 4.2: Push-out tests results of headed stud connectors.

Specimens		P_u (kN)	δ_u (mm)	Avr $P_u(kN)$	Avr δ_u (mm)	Avr $\delta_m(mm)$	Avr. each. sp / Avr. ST1 (b, c)	
							P_u	δ_u
(1)		(2)	(3)	(4)	(5)	(6)	(7)	(8)
ST 1	-a	159,73	10,20	159,73	10,20	9,00	1,11	1,03
	-b	146,80	10,05	143,91	9,90	8,21	1	1
	-c	141,03	9,75					
ST 2	-a	115,4	7,21	115,89	7,45	6,88	0,80	0,75
	-b	-	-					
	-c	116,38	7,69					
ST 3	-a	142,53	12,19	136,02	12,17	10,46	0,94	1,22
	-b	129,52	12,15					

4.3.2- Failure modes

The failure in all specimens was a complete separation between the concrete slab and the T-steel section due to fracture of headed studs just above the weld collar, as shown in Fig 4.5. Meanwhile, no concrete cracks occurred on the surfaces of the specimens. Except that, in front of the weld and the lower part of studs, as shown in Fig 4.6. It can note that the crushing length of concrete in the specimens containing the head studs of 19 mm diameter was between 70 and 95 mm. But it was between 60 and 70mm in the specimens containing the head studs of 16 mm diameter. However, in all specimens, the headed studs were subjected to bending deformation at the bottom shank.

Figure 4.5: Failure pattern of specimens.

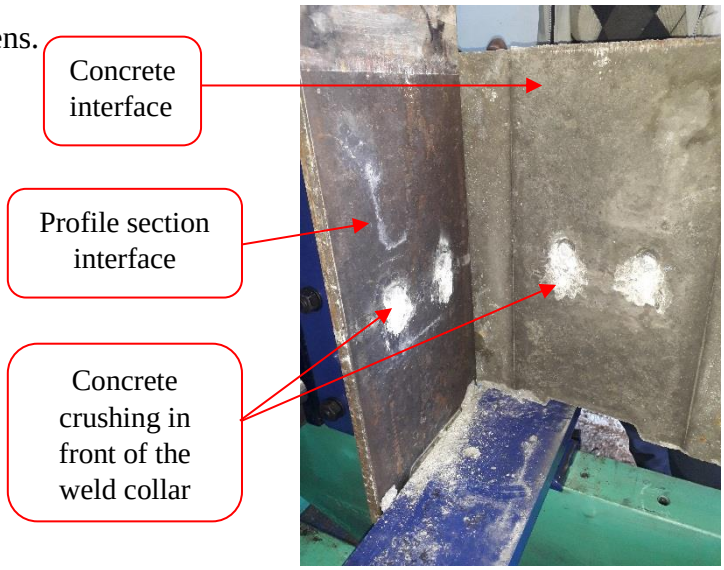

(a) Specimens of the first group (ST1)

(a) Specimens of the second group (ST2)

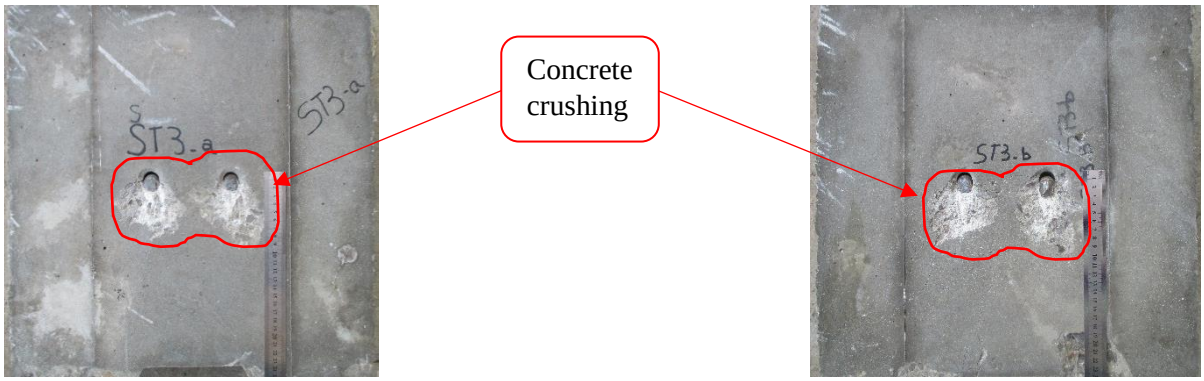

(a) Specimens of the third group (ST3)

Figure 4.6: Concrete interface crushing.

4.3.3- Bending deformation of studs

To inspect the deformation of headed studs, the concrete slabs of the specimens that realized high ductility for each group were demolished after the tests and the headed studs were taken out, as shown in photographs given in Fig. 4.7. It can be seen that a plastic hinge is created on the bottom shank of each stud. Moreover, it can be seen that the ST3 shape gives better deformation. Figure 4.8 shows the representative deformed shape of the headed stud after failure.

The behavior of headed studs during the tests can be divided into three stages, as shown in Fig 4.8. In the first stage (elastic stage), the reaction force comes from the stud shank and the weld collar. This stage corresponds to when the slip between the concrete slab and the profile section is less than 2 mm. Stage II will be when the slip value is higher than 2 mm and lower than the ultimate slip. The reaction force in this stage comes only from the shank of the headed stud because the hardness of the weld caller caused the crushing of the concrete (Fig. 4.5) (Fig. 4.6). In stage II, the shank of the stud started to deform, and the reaction force was combined by axial and shear forces, as shown in Fig. 4.8 (stage II). Finally, at the last stage the deformation of the shear studs becomes higher, and the shearing of headed studs occurs immediately.

a) ST1-a b) ST1-b c) ST3-c d) ST3-a

Figure 4.7: Headed studs' deformation.

Table 4.3 summarizes the geometric results of the bending deformation of the studs in each group. Where h: is the height of bending part (mm), e: is the height between the edge of the weld and the point where the plastic hinge is located (mm), Δ: is lateral deformation of headed stud shank (mm). t: is lateral deformation above the area where the plastic hinge is located (mm). However, the tangents of the bending deformation angles are getting by the following equitation: $tg\ \theta = \Delta - t / e$.

On the other hand, the relationship between the lateral deformation of the headed stud shank and slip at the interface steel-concrete is shown graphically in Fig. 4.9 (a). And the relationship between the tangential deflection and the slip is shown in Fig. 4.9 (b). It can be

detected that the slip value in the steel-concrete interface increased linearly with increasing the lateral deformation and the bending deformation of headed studs. In addition, the lateral deformation did not represent the value of an ultimate slip and was smaller for all specimens.

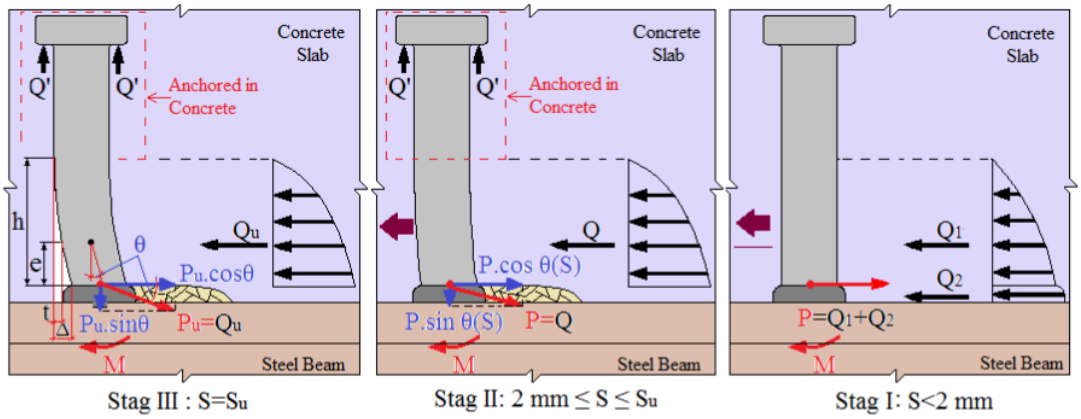

Figure 4.8: Representative deformed shape of headed stud.

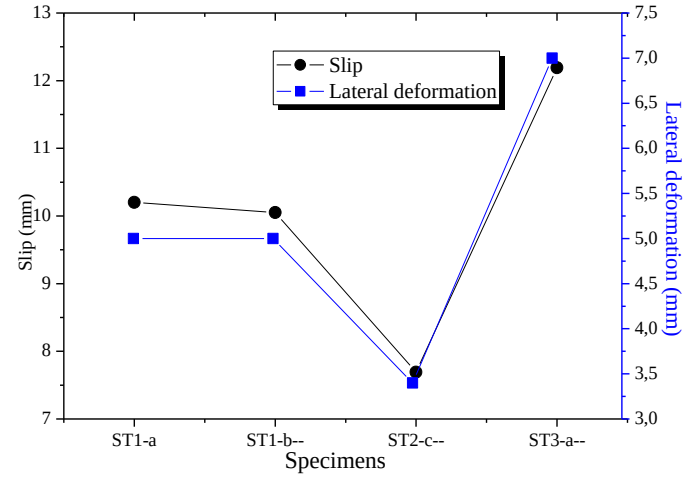

(a)

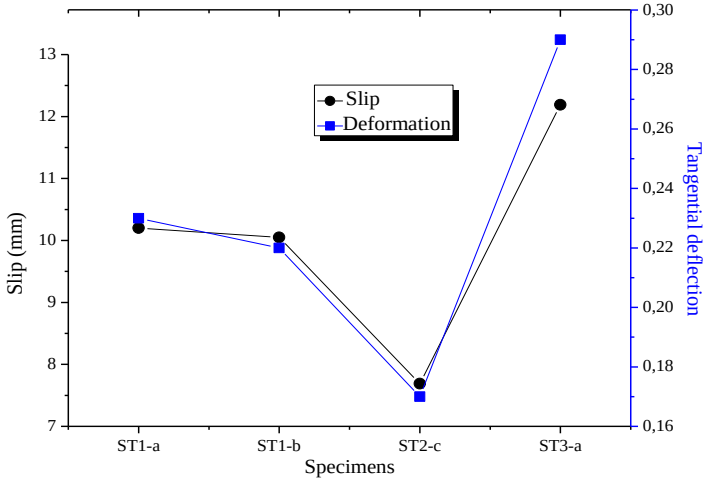

(b)

Figure 4.9: Graphic relationship: (a) slip-lateral deformation; (b) slip-deflection.

Table 4.3: Locations of plastic hinge.

Specimens	Δ (mm)	h (mm)	e (mm)	t (mm)	θ (°)	tg (θ)	δ_u (mm)	H-d (mm)
ST1-a	5	46	17,2	1,0	13,0	0,23	10,20	100-19
ST1-b	5	45	16,8	1,2	12,7	0,22	10,05	
ST2-c	3,4	36	13,5	1,0	10,0	0,17	7,69	100-16
ST3-a	7	50	18,7	1,5	16.3	0,29	12,19	100-19

4.4- Parametric study

4.4.1- Effect of concrete slab clamping mechanism

In the push test, the concrete slab clamping mechanism has been used in many studies [10, 20-23]. Due to this, we chose to study the effect of this procedure in this chapter. The results of load-slip curves shown in Fig. 4.4 (a) indicate that using the concrete slab clamping mechanism in the ST1-a specimen increased the ultimate strength by about 11% and slightly increased the ultimate slip by about 3% compared to the reference specimens ST1(b, c). Hence, it can give recommendations for future research. The use of a concrete slab clamping mechanism in the push-out test increased the ultimate load and ultimate slip of the connectors. Therefore, it cannot obtain the correct load-slip performance. As mentioned earlier (chapter 3), using the concrete slab clamping mechanism perhaps led to an increase in the ultimate strength. Thus, this is confirmed by the results of this chapter.

4.4.2- Effect of headed stud diameters

As the load-slip curves indicate in Fig. 4.4 (b), the ultimate load capacity is influenced significantly by the decrease in stud diameters. Therefore, the specimens of group ST2 (a, c) containing 16 mm diameter headed studs gave an ultimate strength and ultimate slip less than 20% and 25% consecutively compared to the reference specimens ST1(b, c). However, the headed studs of 19mm diameter have better bending deformation than the headed studs of 16 mm diameter.

4.4.3- Effect of headed studs shape in group ST3

The comparison between the load-slip curves of the specimens ST3 (a, b) and the reference specimens ST1 (b, c) is shown in Fig. 4.4 (c). The results showed that this new shape of the headed stud did not affect the performance of these specimens in the elastic part and was almost

similar to reference specimens ST1 (b, c). In contrast, when the load exceeds 0.68 to 0.75 times the ultimate load value, the performance is different between the two groups. Whereas,, the ST3 specimens (a, b) gave an increase of about 22% in ultimate slip and a slight decrease in the ultimate strength of about 6%. However, the comparison between the stud deformation of this group (ST3) against that of ordinary stud ST1 given in Fig 4.7 shows that the new shape of the stud (ST3) had better deformation capacity and better ductility than the ordinary headed stud.

4.5- Provisions of design codes

Table 4.4 demonstrates the ultimate load values obtained from the push-out tests against those predicted by some design codes (see chapter 1). The comparison shows that Eq. (1.3) is in accord with the test results, whereas Eq. (1.1) and Eq. (1.2) are very conservative.

Table 4.4: Comparison of experimental and predicted values for ultimate load capacity.

Specimens	Ultimate load (kN)				Eq. (1.1) /Test	Eq. (1.2) /Test	Eq. (1.3) /Test
	Test	Eq. (1.1)	Eq. (1.2)	Eq. (1.3)			
ST1	143,91	111.64	109.89	156.99	0.77	0.76	**1.09**
ST2	115,89	79.16	77.93	111.33	0.68	0.67	**0.96**
ST3	135,98	111.64	109.89	156.99	0.82	0.80	**1.15**

4.6- Conclusion

In this chapter, eight push-out tests were conducted to study the behavior of headed studs with a deferent parameter such as; (i) the clamping mechanism of concrete slab (ii) diameter of headed stud connector; (iii) new shape of headed stud connector. Upon analysis of the results the following conclusions were drawn:

1. The failure in all specimens was a complete separation between the concrete slab and the T-steel section due to fracture of headed studs just above the weld collar.
2. Using the procedure of concrete slab clamping mechanism in the ST1-a specimen increased the ultimate strength by about 11%, and slightly increased the ultimate slip by about 3% compared to the reference specimens ST1(b, c). Therefore, as a recommendation for future research, using a concrete slab clamping mechanism in the push-out test does not provide the correct results.
3. The slip in the steel-concrete interface increased linearly with increasing the lateral deformation and the bending deformation of headed studs. However, the lateral

deformation does not represent the value of an ultimate slip and is lower than it on all specimens

4. The 16 mm diameter head studs gave an ultimate strength and ultimate slip less than 20% and 25% consecutively compared to 19 mm diameter headed studs.
5. The new shape of the headed stud (ST3) has better deformation and better ductility than the ordinary stud shape.
6. In terms of the bearing capacity of headed stud connectors, the results of the empirical equation given by American National Standard ANSI/AISC 360-05 [29] are in accord with the test results.

Numerical part

Chapter 5:

Finite element analysis of push-out tests.

5.1- Introduction

Numerical analysis has proved to be an alternative to experimental push-out tests with lower costs and less time. Moreover, more parameters can be evaluated in the numerical analysis with reasonably accurate results, especially, when the numerical methods are supported by experimental results. Furthermore, three-dimensional (3D) finite element models can simulate more complex structures and can provide full behavioral details, such as the distribution of stresses and strains at all points in the structure. Therefore, recently this method has presented significant value.

The purpose of this chapter is to develop a three-dimensional (3D), finite element model, using the finite element software ABAQUS [18] to simulate the non-linear push-out test on some type of shear connectors. The proposed model was validated by comparing the numerical results against those of some experimental push-out tests from previous chapters. These specimens are the channel shear connector CH1 specimen and the specimens of new channel shapes CH2 and CH6, which had a better performance from chapter three, as well as the headed stud specimens ST1, ST2, and ST3 from chapter four. The results compared are load–slip curves, deformation patterns of shear connectors, and the failure modes. In addition, the I-shape shear connector was studied in this chapter and its results were compared with those of channel shear connector CH1. Afterward, a parametric study is carried out to discover the effect of concrete compressive strength and the connector's steel grade on the performance of shear connectors.

5.2- Finite element model

5.2.1- General

Numerical analysis was carried out based on our previous experimental work on push-out specimens presented in chapters three and four. Therefore, the geometry of the specimens is shown in Fig. 3.4 and Fig. 4.2 for channel and stud shear connectors in chapters three and four, respectively. Both material and geometric nonlinearities were taken into account in this study. However, to obtain accurate results from the numerical analysis, all components of the push-out test must be properly modeled. The main components are the steel profile, concrete slab, shear connectors, and reinforcing bars. Only half of the specimen was modeled just like the experimental specimens in previous chapters, as shown in Fig 5.1. Concrete damage plasticity models and nonlinear material constitutions were established in the analytical investigation. The following subsections presented the details of the FE analysis.

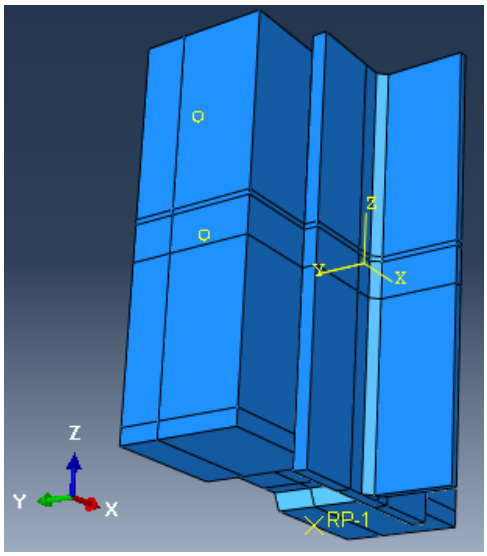

Figure 5.1: FE Model of push-out specimen.

5.2.2- Interactions and constraint conditions

In the push-out simulation, the interactions of the steel beam - concrete and the connectors - concrete are the most important part. Thus, the surface to surface contact between the different components is employed. Normal contact and tangential behavior contact available in the contact property option of ABAQUS were used. The normal hard contact is used to transfer pressure between the contacting surfaces, with possible separation in case of negative pressure in the normal direction. Tangential friction was adopted using the penalty contact method of ABAQUS for the interaction of connectors surfaces and the surrounding concrete, as shown in Fig 5.2. Where Fig 5.2 (a), Fig 5.2 (b), and Fig 5.2 (c) illustrate the interaction contact of channel shear connector, headed stud connectors, and I-shape connector, respectively, with the surrounding concrete. In this interaction, the friction coefficient was taken as 0.2, which was referenced from the study of Qinghua H et all [55]. In the push-out experiments, the steel beam flange surface in contact with the concrete slab is usually greased to reduce friction [38, 56]. Therefore, a frictionless contact interaction was applied to the steel beam flange and the concrete slab interface, as illustrated in Fig 5.2 (d). The flange surface of the steel beam and the surfaces of the connector are assumed to be the master surfaces. Concrete surfaces are assumed to be slave surfaces.

The base of the concrete slab is constrained to a reference point using a function of rigid body and tie nodes, as shown in Fig 5.2 (e). Whereas, embedded regions were used for simulation of the reinforcing bars inside the whole concrete slab, as shown in Fig 5.2 (f). The connector and the steel beam flange were merged using retain function.

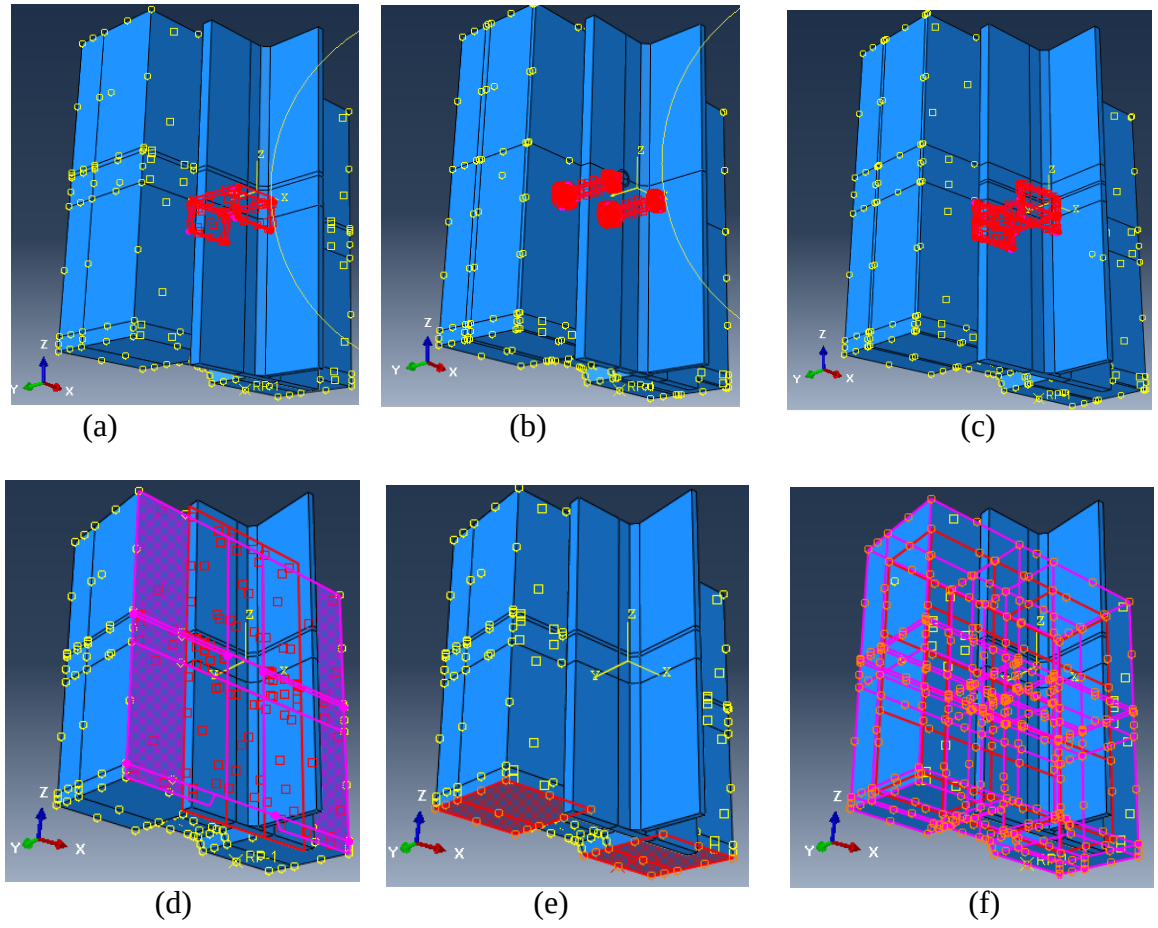

Figure 5.2: Interaction and constrain conditions of the specimens: (a, b, c, d) Interaction contact; (e) rigid constraint; (f) Embedded constraint of reinforcing bar.

5.2.3- Boundary and loading conditions

In this analysis, static general used in the ABAQUS standard was applied. In addition, linearly increased displacement controlled by amplitude and smooth step-functions was applied in the reference point located in the bottom surface of the concrete slab, as illustrated in Fig 5.3 (a). The load was measured automatically as the total reaction forces were determined at the top cross-section of the steel beam. The reaction forces represent the action forces at the connector. The slip was measured as the relative displacement between the nodes on the steel flange and the concrete slab.

There are two boundary conditions of this FE model as follows. The symmetric boundary condition was applied to the surface at the symmetric planes of the specimen, as shown in Fig. 5.3 (b). The displacement of the X direction was zero. The nodes at the top flange of the steel beam cross-section were constrained for all translational degrees of freedom, as shown in Figure 5.3 (c).

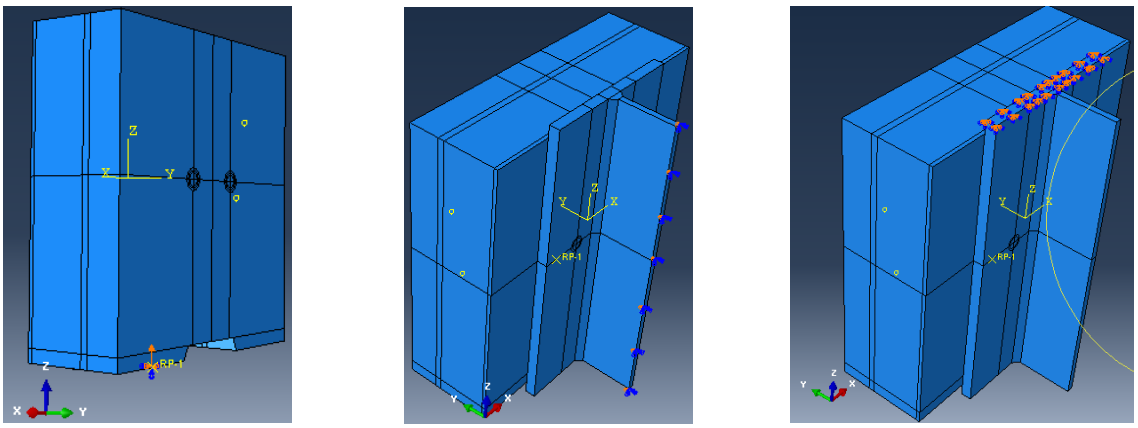

a) linearly increased displacement

b) symmetric boundary condition X=0, U2=0, U3=0

c) boundary condition X=0,Y=0,Z=0

Figure 5.3: Boundary condition in the specimen.

5.2.4- Material properties of concrete

The notion of concrete constitutes a wide range of materials. Whose properties are quantitatively and qualitatively different for typical tests (compression and tension) [57]. To model the non-elastic behavior of reinforced concrete the concrete damage plasticity model available in the ABAQUS material library was used. This model can be used for both static and dynamic analyses. And primarily based on two main failure mechanisms namely tensile cracking and compressive crushing of concrete [58]. The stress-strain relationship for the concrete damage plasticity model is shown in Fig 5.4. As shown in this figure, when the concrete specimen is unloaded from any point on the strain softening branch of the uniaxial nonlinear stress-strain curve, the unloading response weakened, due to which the elastic stiffness of the material appears to be damaged (or degraded) [59].

The simplified concrete damage plasticity (SCDP) model that was developed by Milad H et all [60] is adopted for this FE analysis. This simplified CDP model of the concrete, including a damage parameter, strain hardening/softening rules, and certain other elements, were presented for concrete grades C20, C30, C40, and C50. Figure 5.5 demonstrates the stress-strain curves of compressive and tensile behavior for the C30 concrete grade used in our analysis. The SCDP model of concrete grade C20 and C40 were also used in the section of the parametric study below. In addition, the other material properties for concrete with the simplified concrete damage plasticity (SCDP) model are as follows: the density (γ) was taken 2450 Kg/m2, the material dilation angle (Ψ) was taken at 31, the eccentricity (ε) was taken to be 0.1. The ratio of biaxial compressive strength to uniaxial compressive strength (fb0/fc0) was taken as 1.16, and the tensile-to-compressive meridian ratio (K) is 0.67.

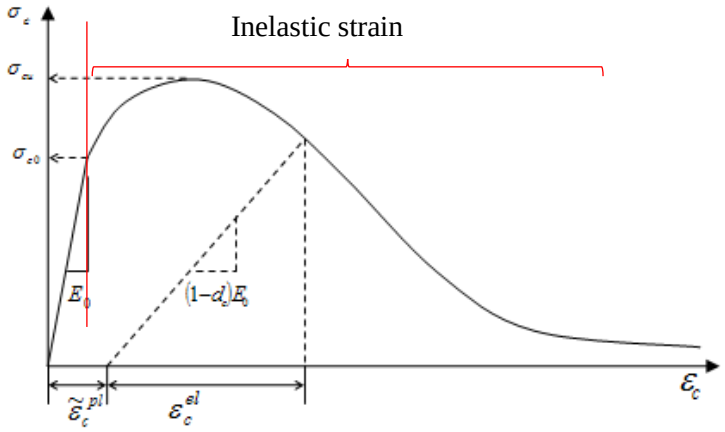

(a)

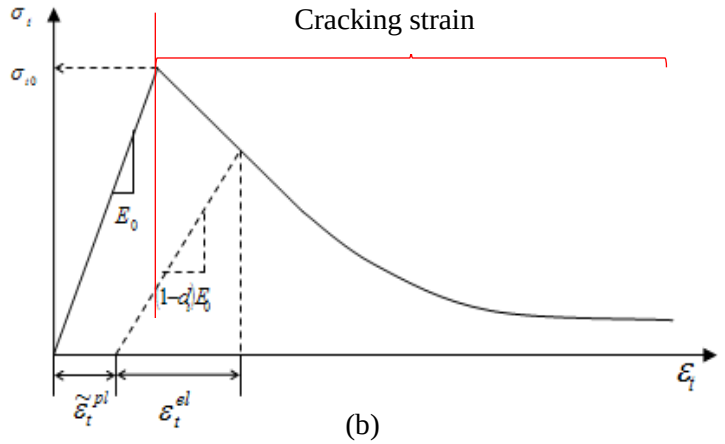

(b)

Figure 5.4: Graphical representation of the damage parameters in relation with uniaxial nonlinear stress-strain behavior. [59]; (a) Compression, (b) tension.

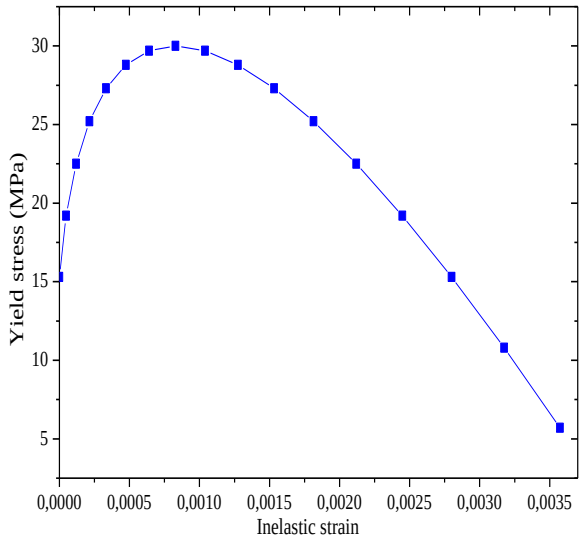

(a)

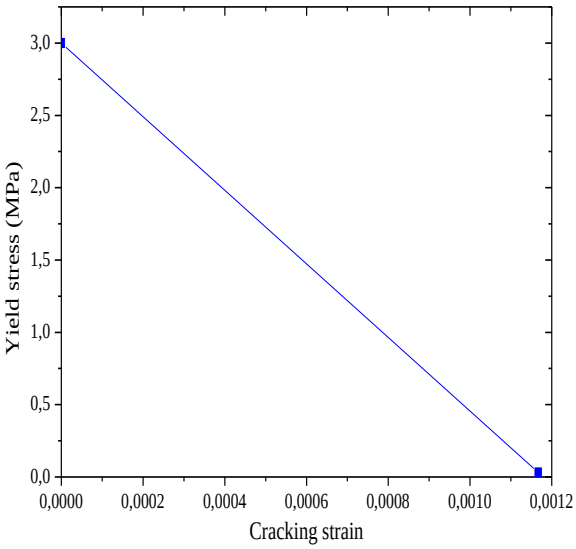

(b)

Figure 5.5: Stress-strain curve for 30 MPa concrete [60]; a) Compressive behavior; b) tensile behavior.

5.2.5- Material properties of steel

The material properties of the shear connector are of great importance in the push-out test simulation. Thus, the elastic-plastic material model is employed in this study based on the nominal behavior of the stress-strain curve shown in Fig 5.6. The steel of connectors and reinforcing bars were modeled using an isotropic hardening material. The ultimate strength and yield of the steel from the chapter 2 are used in this FE analysis. The elasticity module (Es) is taken as 205 GPa, 202GPa, 200GPa for channel shear connectors, headed stud connector, and reinforcing bar, respectively. Poisson ratio (υ) and the density (γ) are taken as 0.3, and 7850 Kg/m2 respectively.

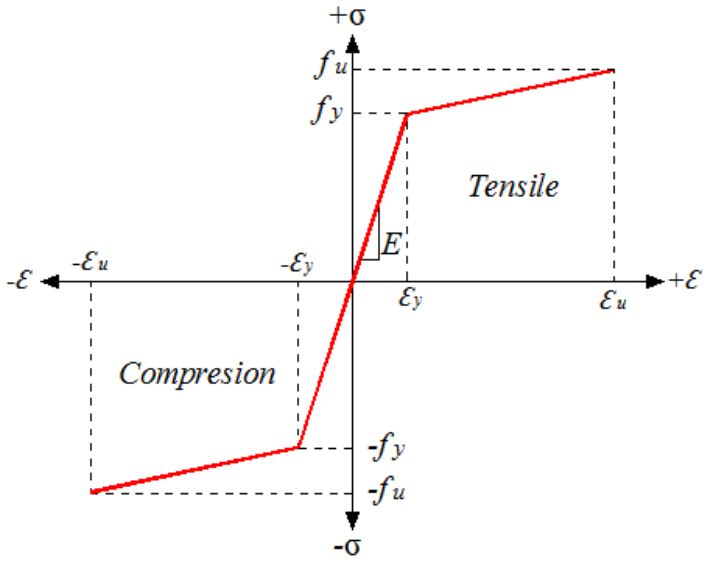

Figure 5.6: Stress-strain curve of steel.

5.2.6- Finite element type and mesh

The common element mesh type available in the ABAQUS library used for solid structures is C3D8R. This element is a brick element with eight nodes, and each node has three translational degrees of freedom. It can be efficiently used in nonlinear analysis of properties including plasticity, contact, failure, large displacements, and damage. Hence, the steel beam, concrete slab, and shear connectors in this FE analysis were all meshed through the C3D8R element. While the reinforcing bars are meshed by using the T3D2 element available in the ABAQUS library as well. This element (T3D2) is a truss element with two nodes, and each node has three translational degrees of freedom.

Figure 5.7, Figure 5.8, and Figure 5.9 show the finite element type and mesh of the channel shear connector specimens, I-shape shear connector specimens, and headed stud specimens, respectively. Each part of the specimen was partitioned and meshed independently. In order to decrease the analysis time, a smaller mesh size (8 mm) was applied at the connectors and the surrounding concrete region, while an appropriate mesh size (16 mm) was applied to

the rest of the model. As result, the mesh number of channel shear connector specimens is more than 17000 elements. However, the mesh number of headed stud elements is more than 20000 elements. As for the I connector specimen, its mesh number is about 17775 elements.

The weld collar of headed stud connectors contributes to a significant portion of the shear strength and should be taken into account in the analysis [61] and [62]. Due to that, the modeling of the weld collar is taken into consideration in this simulation, as shown in Fig. 5.9.

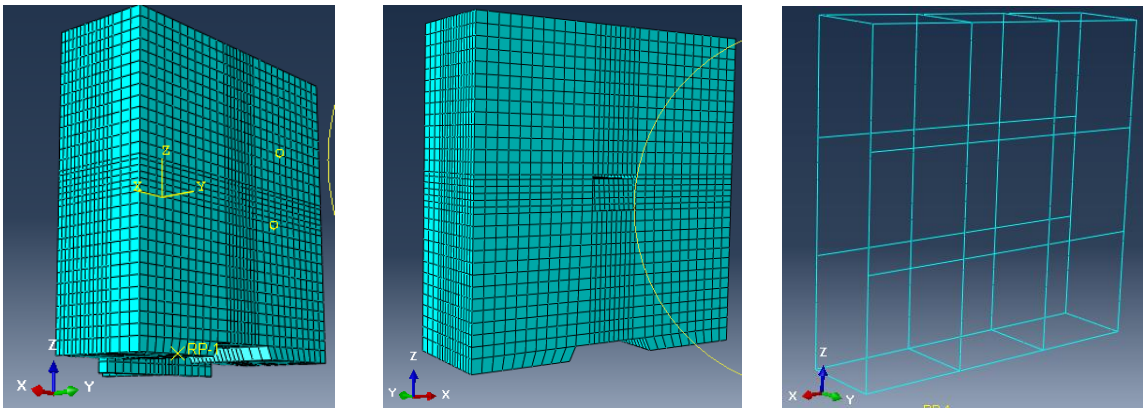

(a) (b) (c)

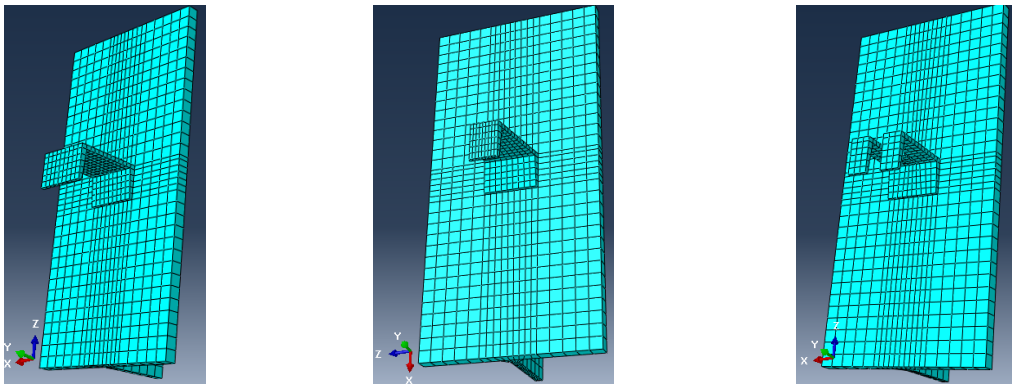

(d) (e) (f)

Figure 5.7: Mesh of channel connector specimen; a) whole specimen; b) concrete slab; c) reinforcing bars; d) CH1 shape; e) CH2 shape; f) CH5 shape.

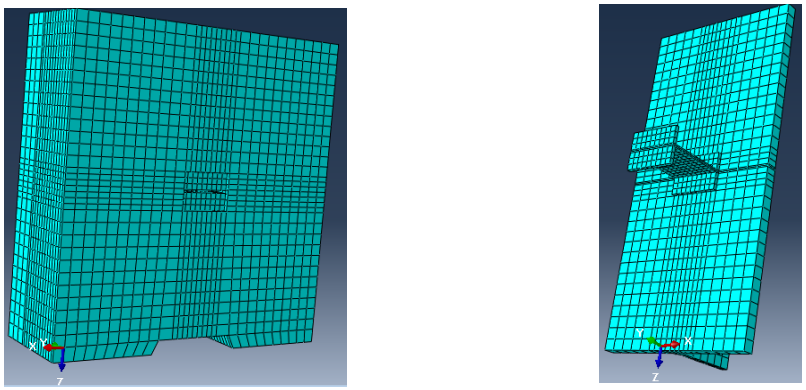

(a) (b)

Figure 5.8: Mesh of I shape connector specimen; a) concrete slab; b) I shape connector.

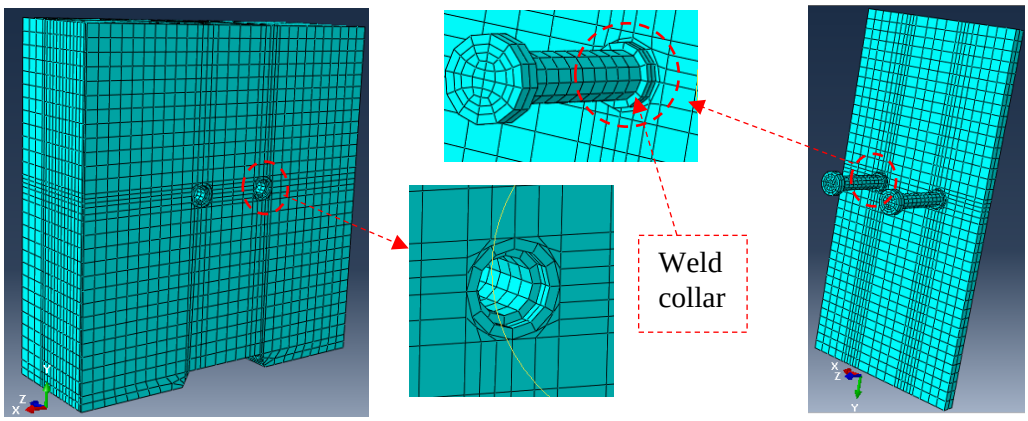

(a) (b)

Figure 5.9: Mesh of headed stud specimen; a) concrete slab; b) stud connectors.

5.3- Analysis results and comparison

This section presents the comparison between the FE simulation against the experimental tests concerning push-out results, load–slip curves, bending deformation patterns of shear connectors, and the failure modes. Moreover, the comparison of the FE analysis results between the CH1 channel connector specimen and the I connector specimen was presented in this section as well.

5.3.1- FE simulation vs experimental results.

Numerical results of channel shear connector specimens and headed stud specimens with a concrete strength C30 are presented in this section. These numerical results were compared against the experimental test results from chapters three and four, as indicated in Table 5.1. Besides, this table presented the comparison of the slip value δ_m, which corresponds to the numerical ultimate strength P_u (i.e., the peak load) against the average of those obtained in experimental tests for each group. Good agreement of ultimate load results between experimental and FEA is found in channel shear connector specimens CH1, CH2, and CH6. It can also observe that the ultimate load results between experimental and FEA of headed stud connector specimens ST1 and ST3 are almost in agreement. Whereas the ultimate load obtained by finite element analyses of the ST2 specimen, which contains 16 mm diameter headed studs, is approximately 15% lower than that obtained from the experimental test. As a note, for specimens ST1, ST2, and ST3 the ultimate load capacity presented is per stud. However, the comparison of the slip value δ_m of each FEA specimen versus those of experimental tests shown that: (i) for specimens CH1, CH2, and CH3 that contain channel shear connectors, the ultimate loads in the FEA correspond to 4.55, 5.79, and 7.65 mm of slip δ_m, respectively. While they correspond to 6.64, 9.87, 10.33 mm, respectively, in the experimental tests. (ii) As for ST1, ST2, ST3 specimens which contain headed stud connectors the ultimate loads in the FEA

correspond to 7.42, 6.17, 8.92 mm of slip δ_m, respectively. While they correspond to 8.21, 6.88, 10.46 mm in the experimental tests.

Table 5.1: Experimental results and numerical results comparison.

Specimens	Experimental results		FE results		U. load(Exp)/ U. load(FEA)	δ_m(Exp)/ δ_m(FEA)
	Ultimate load (kN)	$\delta_m(mm)$	Ultimate load (kN)	$\delta_m(mm)$		
CH1	297.9	6.64	295.24	4.55	1	1.45
CH2	299.61	9.87	299.45	5.79	1	1.7
CH6	313.18	10.33	319.74	7.63	0.98	1.35
ST1	143,91	8,21	136.29	7.42	1.05	1.1
ST2	115,89	6,88	100.53	6.17	1.15	1.11
ST3	136,02	10,46	141.01	8.92	0.96	1.17

5.3.2- Comparison of (load – slip) curves of experimental and FE simulation

The load-slip curve is an important basis for analyzing the mechanical behavior of shear connectors. The comparisons of experimental and numerical load-slip curves of all the push-out specimens are illustrated in Fig.5. 10, and Fig.5. 11. It can observe that three stages were identified in the typical load–slip curves of all shear connectors as follows:

- At the first stage, these curves were steep with small slips, indicating elastic behavior and large stiffness. The comparison at this stage showed that the curves obtained from FEA were steeper than those from the experimental push tests for specimens CH1, ST1, ST2, and ST3. In which the slips in the FEA are smaller than those of experimental tests. This difference is due to the fact that in the experimental tests, specimens may suffer from uncertain initial defect which is difficult to simulate in material model. Whereas slightly diverge in steep curves between the FEA and experimental tests for the CH2, CH3 specimens.
- The next stage was a nonlinear curve where both load and slip increased. In this stage also the stiffness reduced slowly with the slip for all specimens. It can see that FEA predicts the peak strength of all specimens with good accuracy, except for the ST2 specimen. But, there is an obvious difference in the curves of FEA against those of experimental tests for CH1, CH2, and CH3 specimens. This is due to the difference between the slip value δm, which corresponds to the peak load (ultimate strength Pu).

As for the load-slip curves of specimens ST1 and ST3, they are in perfect agreement in this stage.

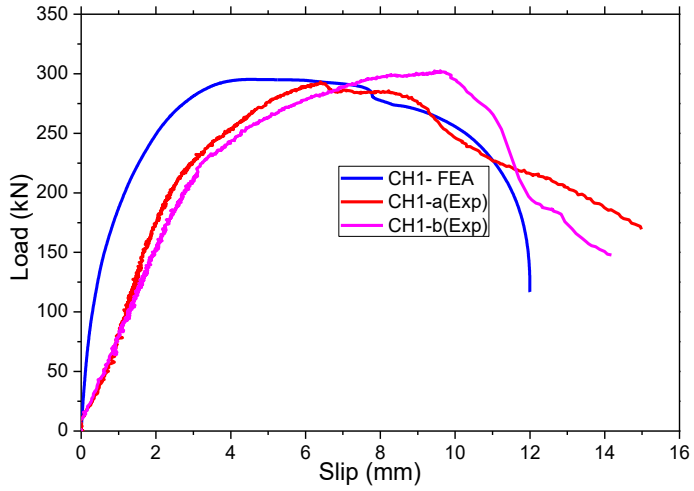

(a)

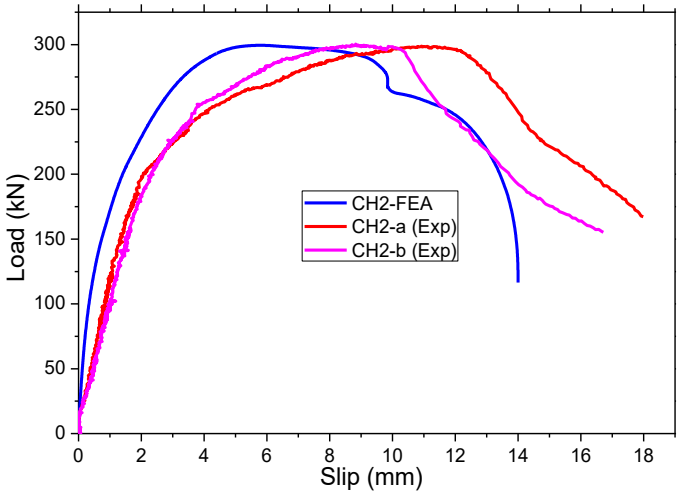

(b)

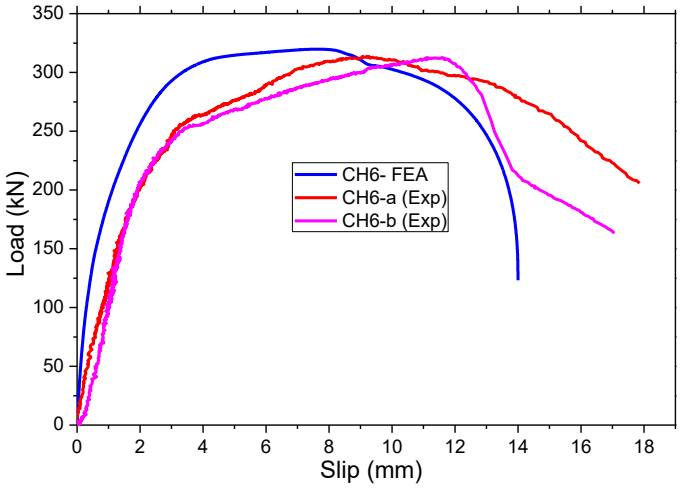

(c)

Figure 5.10: Finite element curve vs experimental curves of shear channels groups: a) CH1 group; b) CH2 group; c) CH6 group.

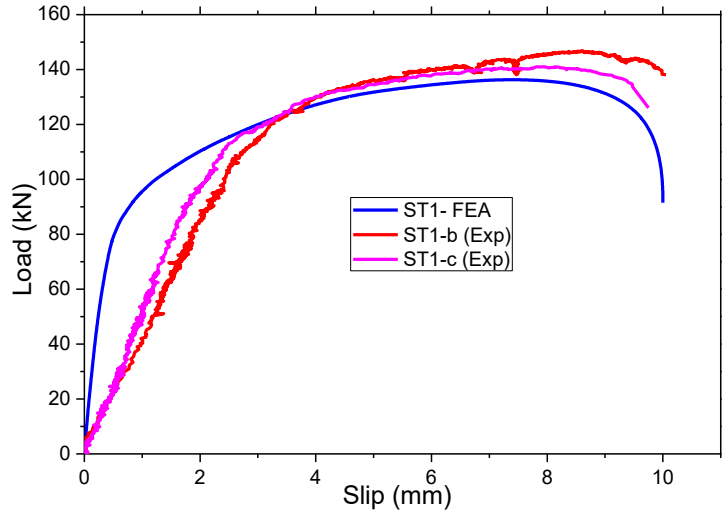

(a)

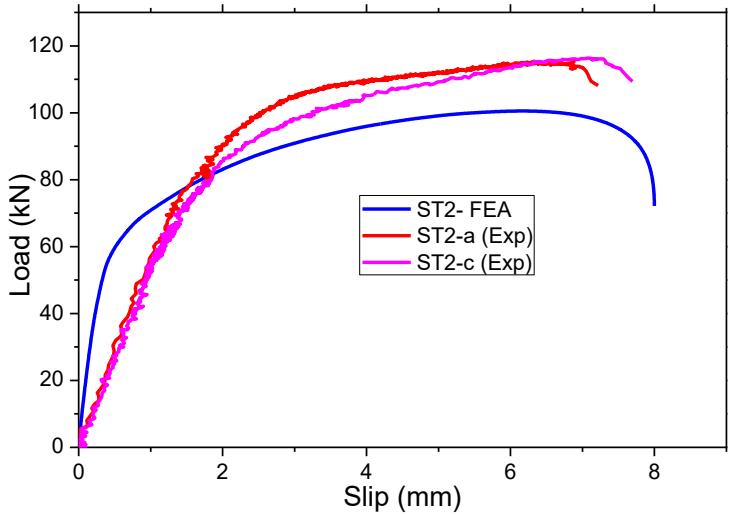

(b)

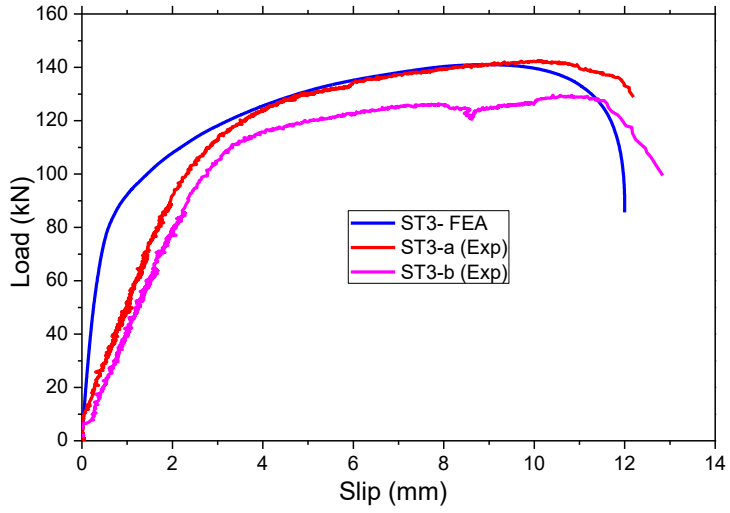

(c)

Figure 5.11: Finite element curves vs experimental curves of headed stud connectors groups: a) ST1 group; b) ST2 group; c) ST3 group.

- The last stage is located beyond the peak load, the slip continued to increase as the load decreased for all specimens.

5.3.3- deformation patterns of shear connectors

Deformation and stress distributions in FE simulation have been recorded. Therefore, the finite element deformation patterns of the shear connectors on the whole specimens (except the I connector specimen) are compared against those in the experimental push-out tests, as shown in Fig 5. 12 to Fig 5. 17. From this comparison, it should be noted that the deformation pattern of all connectors in both finite element and experimental tests was at the bottom. It should be also noted that in the FE analyses the deformation behavior of three-channel connector shapes CH1, CH2, and CH3 are agree well with those in experimental tests. Moreover, good agreement as well between the FE analyses and the experimental tests concerning the void formed behind and above the channel connectors, as illustrated in Fig 5.12 (c), Fig 5.13 (c), and Fig 5.14 (c). As for the deformation behavior of headed studs in the specimens, ST1 and ST2 are slightly similar between FE analyses and experimental tests, as presented in Fig 5.15 (b), Fig 5.16 (b). While the new headed stud shape deformation (ST3) looks similar in both FEA and experimental tests, as shown in Fig 5.17 (b).

5.3.4- Stress - strain distribution and failure modes

As in the experimental tests, the failure mode of the push test was also investigated in the FE simulation. The failure mode in the FE simulation was obtained depending on the stress-strain distribution as well as tensile and compressive damage of the concrete slab.

a) Shear connectors: it can depend on Mises stress distribution to identify the failure mode of each specimen. Fig.12 (a), Fig.13 (a), and Fig.14 (a) show the Mises stress distribution of channel shear connector specimens CH1, CH2, and CH3, respectively. It can be observed that the stress regions in the channel shear connectors were greatest at the web bottom in the three specimens CH1, CH2, and CH3. Knowing that the ultimate and yield strength of channel connectors adopted in the FEA are the same as those of experimental tests, which are 481MPa and 327MPa, respectively. Hence, the highest Mises stress contours of CH1, CH2, and CH3 specimens are 333MPa, 339MPa, and 334MPa, respectively, as presented in Fig.12 (a), Fig.13 (a), and Fig.14 (a). This means that channel connectors CH1, CH2, and CH3 are yielded due to being subjected to stresses slightly higher than the yield strength and considerably lower than the ultimate strength of the channel connector webs (481MPa). In other words, those channel shear connectors are yielded without any shearing failure in the FE analyses. Thus, a good

correlation of failure mode between the FE analyses and experimental push-out tests for the channel connectors CH1, CH2, and CH3.

As for the headed stud connectors, the Mises stress distribution is presented in Fig.15, Fig.16, and Fig. 17. It can be observed that the stress regions in the headed stud connectors were greatest at the bottom, exactly just above the weld collar. However, the highest Mises stress contours of ST1, ST2, and ST3 are 551 MPa, 550 MPa, and 536 MPa, respectively. The ultimate strength of studs' steel is 554 MPa, and it is near to the highest Mises stress contours.

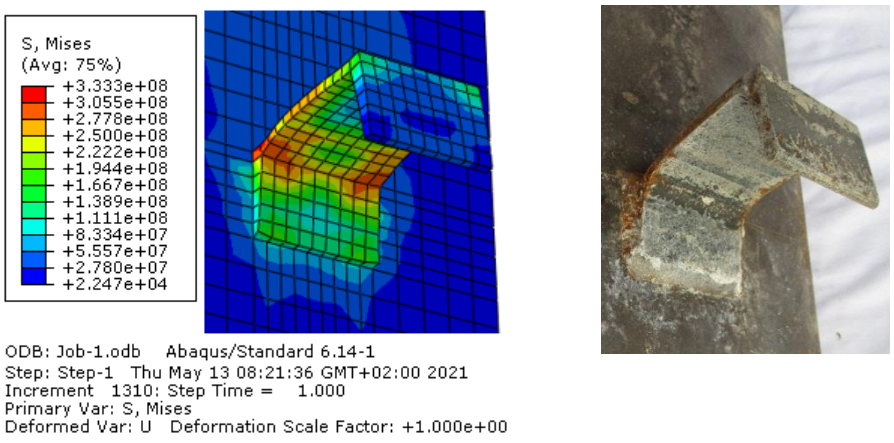

a) 3D view of stress Mises distribution

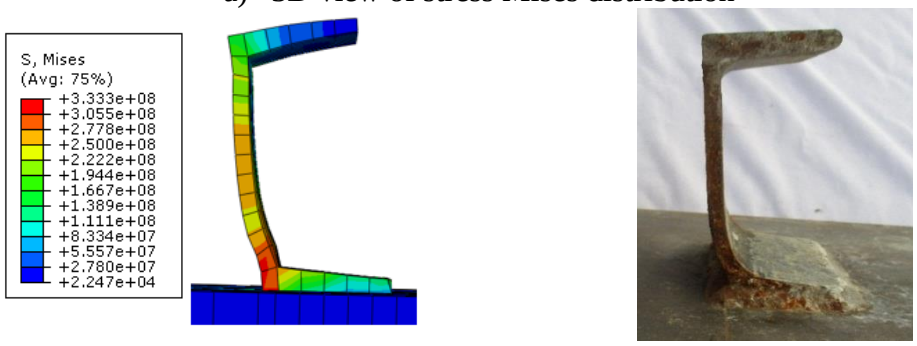

b) Side view of stress Mises distribution and channel deformation

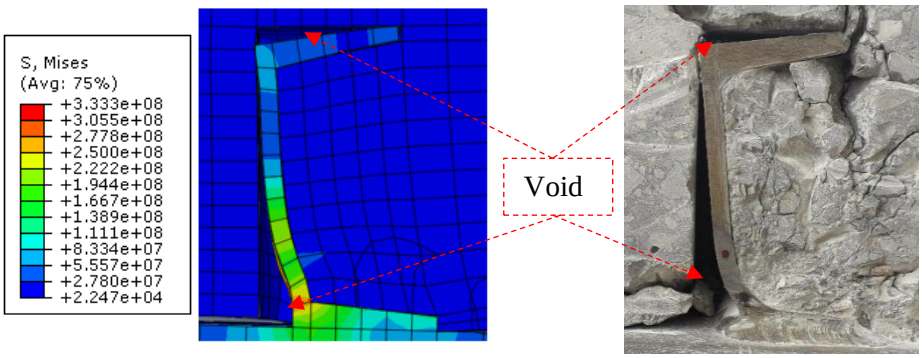

c) Side view with surrounding concrete

Figure 5.12: Shear channel deformation of FE analysis versus experimental tests for CH1 specimen.

Hence, these results supported the conclusion that the failure mode of shear connection observed from FE analyses is the shearing of headed stud shanks just above the weld collar. Consequently, it can say that a good agreement of failure mode between experimental and numerical results for all of the push-out tests.

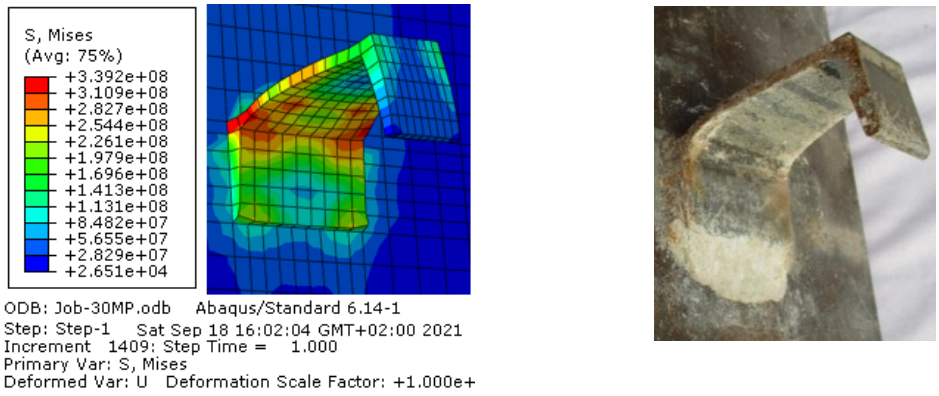

a) 3D view of stress Mises distribution

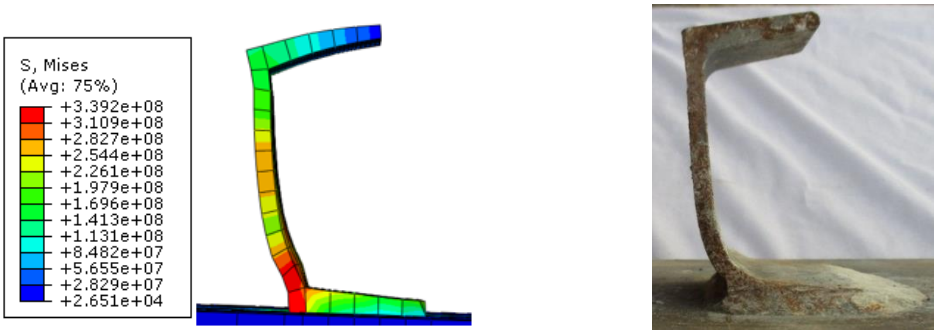

b) Side view of stress Mises distribution and channel deformation

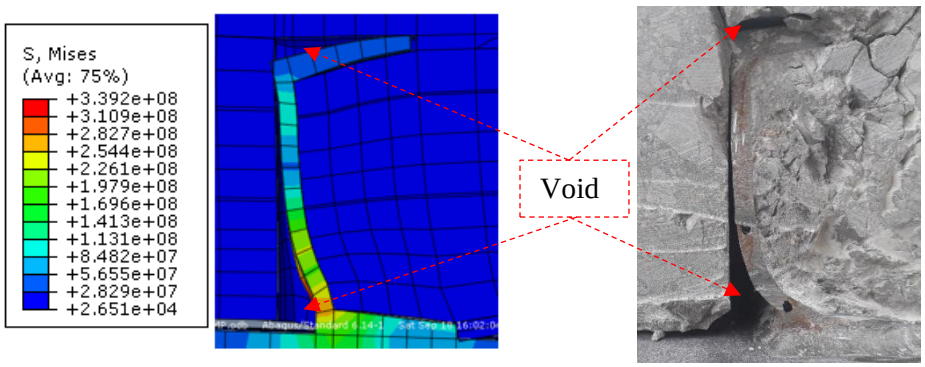

c) Side view with surrounding concrete

Figure 5.13: Shear channel deformation of FE analysis versus experimental tests for CH2 specimen.

b) Concrete slabs: the equivalent plastic deformation was inspected in the FE model to examine the damage process of concrete slabs. In ABAQUS, the equivalent plastic strain is denoted as PEEQ, which is an important parameter to reflect the plastic status of a structure.

When the value of PEEQ of an element is greater than zero, it is indicated that the element begins to yield [62]. Figure 5. 18 shows the equivalent plastic strain of concrete in FEA against the concrete slap failure of the experimental specimen (CH2). It can be seen that in the experimental specimen the concrete crushing was in front of the connector. This mode of failure is confirmed by the maximum plastic strain in the FEA which is in the same region.

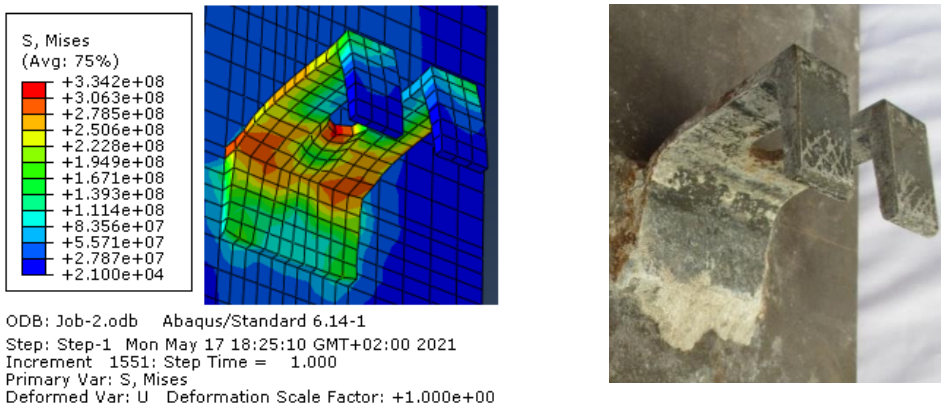

a) 3D view of stress Mises distribution

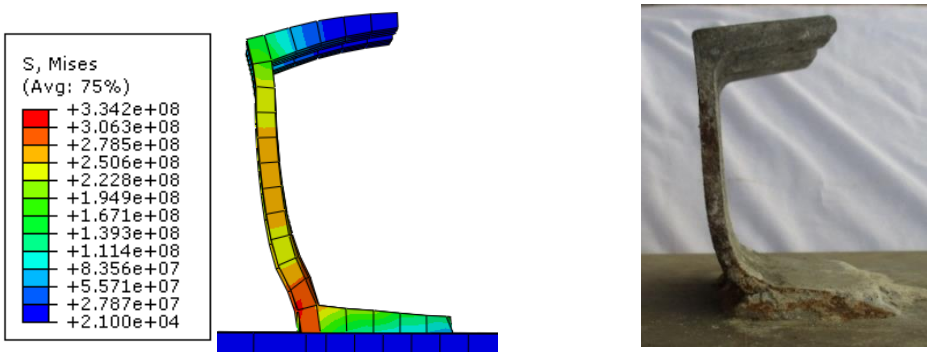

b) Side view of stress Mises distribution and channel deformation

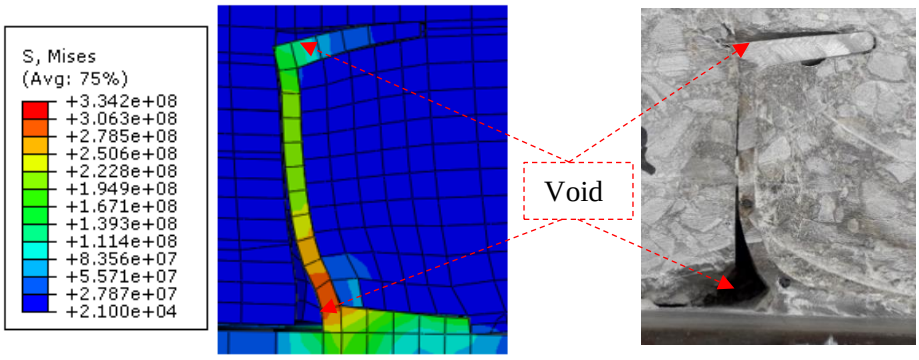

c) Side view with surrounding concrete

Figure 5.14: Shear channel deformation of FEA vs experimental tests for CH6 specimen.

As for the ST1 and ST2 specimens of headed stud connectors in the experimental test, the concrete is crushing in front of the weld, and the lower part of stud shanks. The maximum plastic strain in the FEA was also in the same region, as shown in Fig 5. 19 and Fig 5. 20. In

addition, it can be observed that the maximum plastic strain of the ST1 specimen is 0.299, while it was 0.277 for the ST2 specimen (Fig 5. 19 (a), and Fig 5. 20 (a)). Thus, the plastic strain of the concrete in front of the bottom of the 19 mm headed stud diameter is greater than that in front of the 16 mm headed stud diameter. However, the plastic strain of the concrete in the CH2 specimen (Fig 5. 18) is 0.349 and it is higher than those in the ST1, and ST2 specimens.

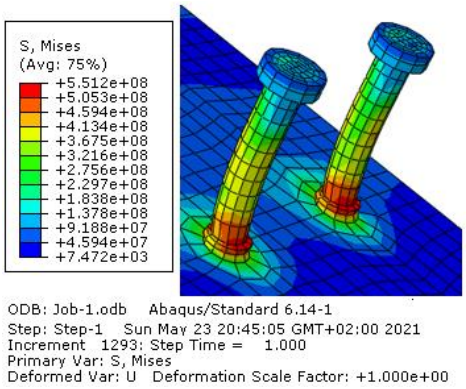

a) 3D view of stress Mises distribution and studs deformation

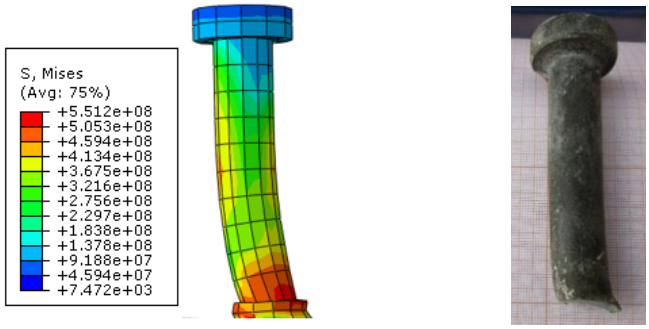

b) Side view of stress Mises distribution and stud connector deformation

Figure 5.15: Stud deformation of FEA Vs experimental tests for ST1 specimen.

On the other hand, it can also investigate the concrete damage process by using compressive and tensile damage parameters. Where any value greater than zero for compressive damage parameter at a given point represents a crashing of concrete. While any value greater than zero for the tensile damage parameter at a given point represents an open crack. Figure 5. 21 presents the tensile damage of FEA versus the concrete cracking in the experimental specimen CH2. There is a significant similarity between the FEA and the experimental specimen, where the cracks are in the bottom half of the concrete slab in both FEA and experimental test. However, the compressive damage in the FEA against concrete crushing in the experimental test for the ST1 specimen is shown in Figure 5. 22. According to this figure, the compressive damage in the FEA can represent the concrete compressive crushing of the experimental push test.

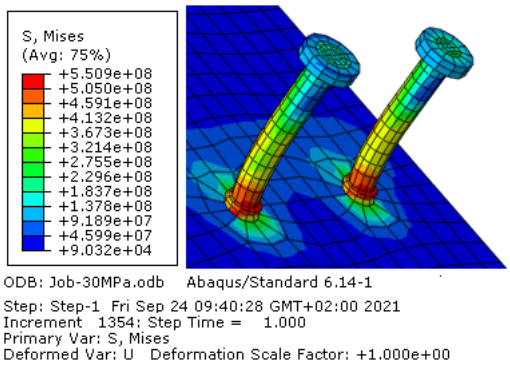

a) 3D view of stress Mises distribution and studs deformation

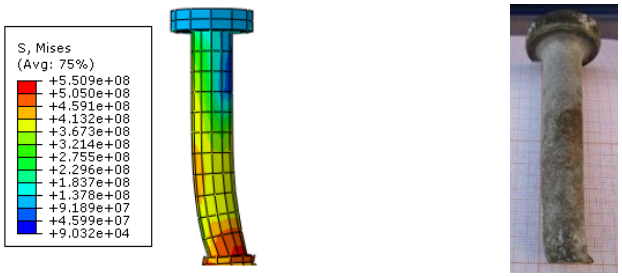

b) Side view of stress Mises distribution and stud connector deformation

Figure 5.16: Stud deformation of FEAVs experimental tests for ST2 specimen.

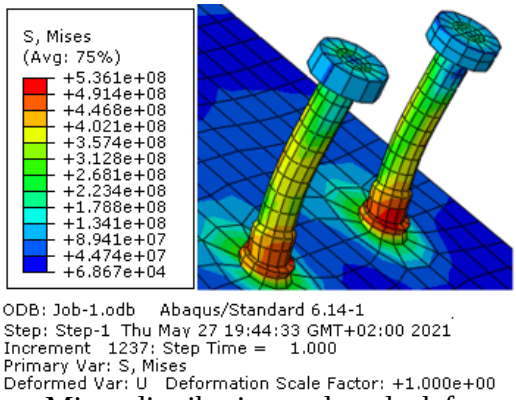

a) 3D view of stress Mises distribution and studs deformation

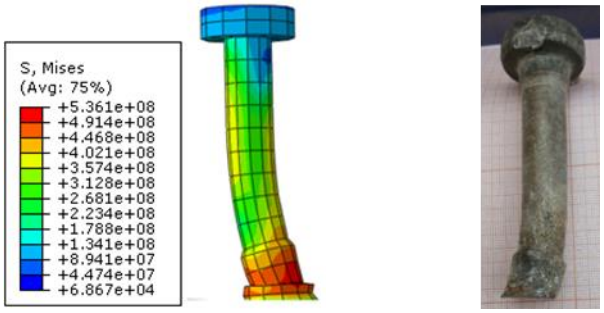

b) Side view of stress Mises distribution and stud connector deformation

Figure 5.17: Stud deformation of FEA vs experimental tests for ST2 specimen.

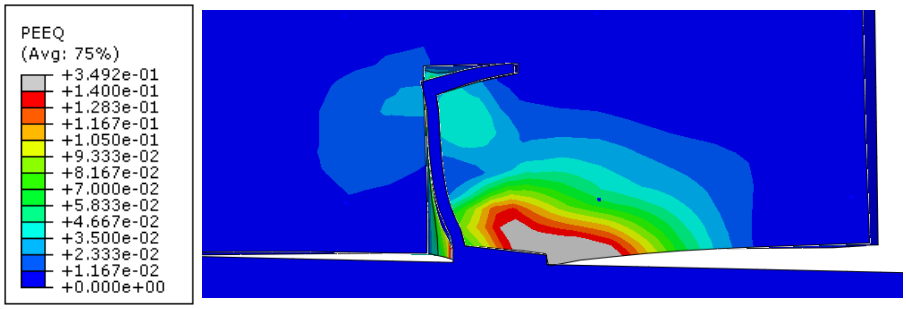

a) FE analyses

b) Experimental push test

Figure 5.18: Equivalent plastic strain of FEA Vs experimental tests for CH2 specimen.

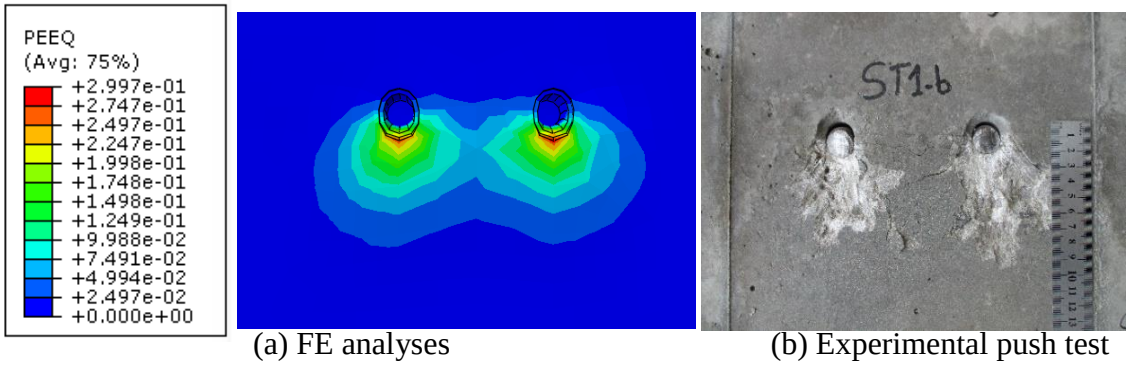

(a) FE analyses (b) Experimental push test

Figure 5.19: Equivalent plastic strain of FEA Vs experimental tests for ST1 specimen.

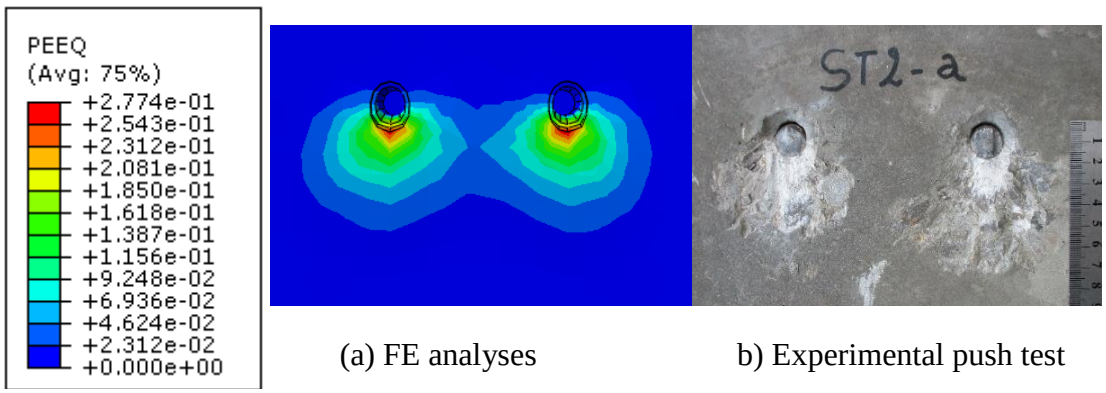

(a) FE analyses b) Experimental push test

Figure 5.20: Equivalent plastic strain of FEA vs experimental tests for ST2 specimen.

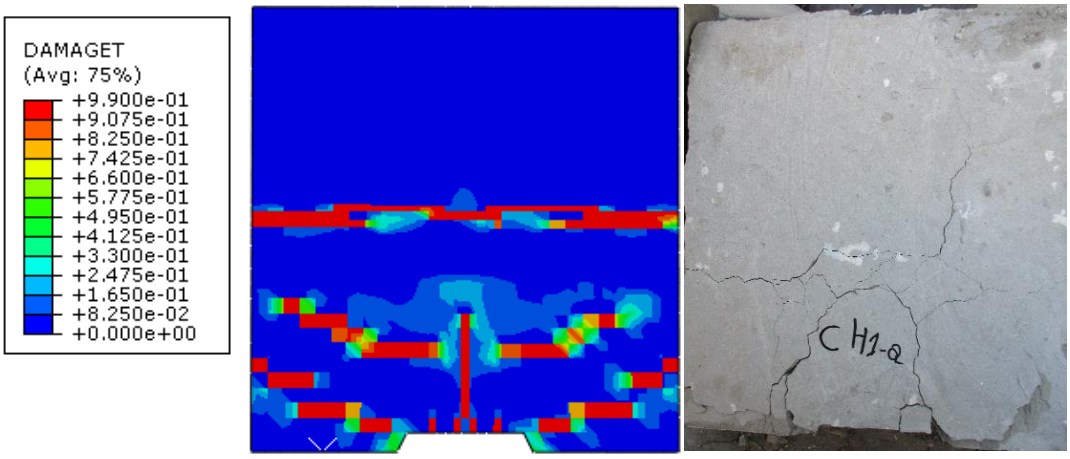

Figure 5.21: Tensile damage of FEA vs concrete cracking in the experimental test for CH1-a specimen.

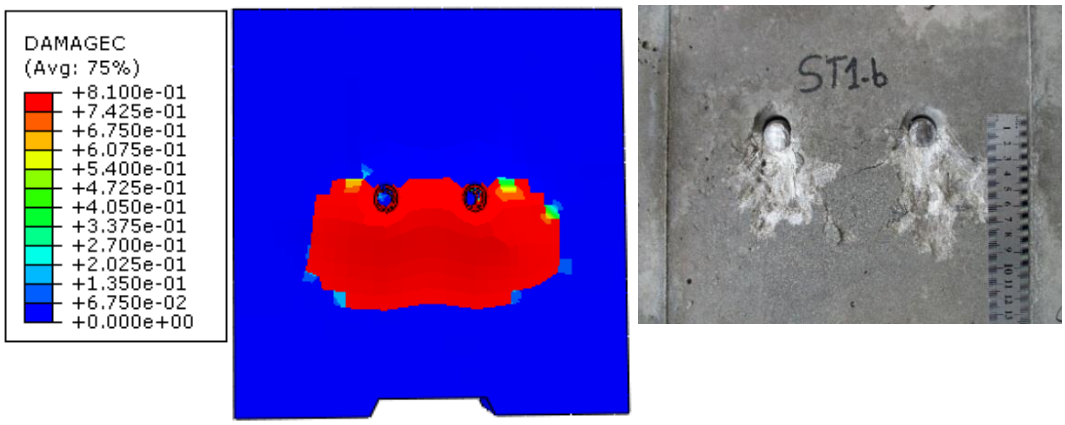

(a) FE analyses b) Experimental push test

Figure 5.22: Compressive damage in FEA vs concrete crushing in experimental test for ST1-b specimen.

c) reinforcing bars: Figure 5.23 shows the Mises stress distribution of specimens CH1 and ST1. The highest stress is found in the reinforcing bar located in front of the bottom of the shear connectors. According to the Mises stress contours, the highest stress is 185 MPa for the CH1 reinforcing bar and 322 MPa for the ST1 reinforcing bar. Although the concrete slab of specimen CH1 was more damaged than that of specimen ST1, the highest stress in the ST1 reinforcing bars was greater than that of CH1. However, in both specimens, CH1, and ST1, the values 185 MPa and 322 MPa of Mises stress are less than the yield strength of the reinforcing bar, which is 392 MPa. Hence, the reinforcing bars did not yield in both specimens.

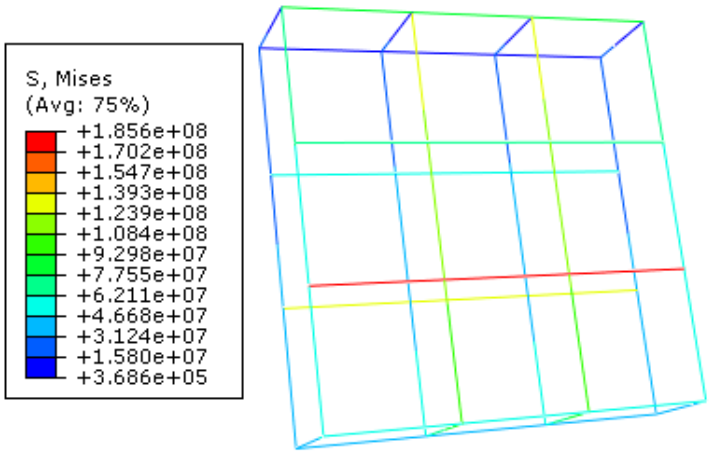

(a) CH1 specimen

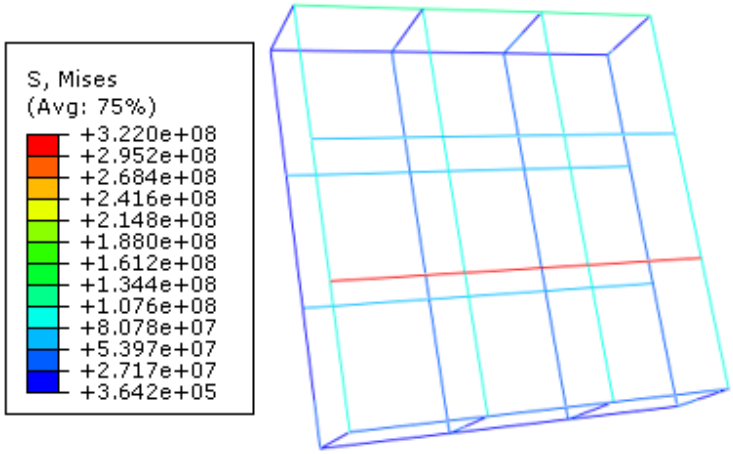

(b) ST1 specimen

Figure 5.23: Mises stress distribution in the reinforcing bars.

5.3.5- Channel shear connector vs I- shape shear connector

In the FE analyses specimens of channel connector CH1 and I- shape connector, the size was the same for both connectors, where the length was 75 mm, and the height was 100 mm for each connector. In addition, the steel property and the concrete strength were the same as well, with 327 MPa, 481 MPa of yield, and ultimate strength, respectively, for steel and 30 MPa of concrete strength. However, table 5.2 presents the comparison of the results of both connectors. Whereas, Fig 5.24 shows the comparison of the load-slip curves between the channel connector specimen and the I connector specimen. Good agreement between channel connector and I connector specimens are found in the elastic stage, while in the plastic stage, the ultimate shear capacity of the channel connector is greater than that of the I connector by about 19 %. As for the slip at the peak load (i.e. ultimate load capacity), it was 6.64 mm for the channel connector specimen and 3.75 mm for the I connector specimen. It can say that the higher ultimate shear capacity and ductility of the channel shear connector against the I-shape

connector are due to the difference in the web width for each connector. The web width of the channel connector is 6.2 mm, while that of the I-shape connector is 4.1 mm.

Table 5.2: I-shape shear connector vs channel shear connector results.

I-Shape shear connector specimen		Channel shear connector specimen		U. load (I connector)/ U. load (channel)	δ_m(I connector)/ δ_m(channel)
Ultimate load (kN)	$\delta_m(mm)$	Ultimate load (kN)	$\delta_m(mm)$		
239,33	3.75	295.24	6.64	0.81	0.56

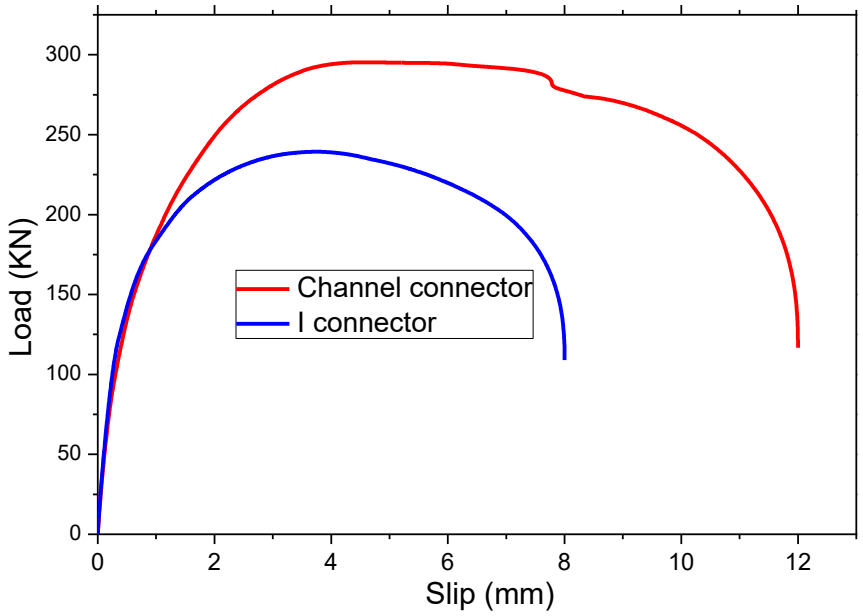

Figure 5.24: Channel shear connector curve vs I shape connector curve.

5.4- Parametric study

5.4.1- Effect of concrete grade

In this section, CH2, ST1, and I connector specimens were investigated with three different strengths of concrete 20MPa, 30 MPa, and 40 MPa. The results of ultimate load capacity and the slip value δ_m, obtained by the FE analyses are illustrated in Table 5.3. Whereas, the load-slip curves are demonstrated in Fig.5. 25.

As indicated in Table 5.3, it appears that the concrete strength significantly governed the ultimate load capacity of each specimen. As can be seen from the table, in the CH2 specimen, the increase in the compressive strength of concrete from 20 MPa to 30 MPa, provides an increase in the ultimate load capacity from 230.32 kN to 299.45 kN, which is more than a 30

% improvement in the load capacity. Then, when the concrete strength increased from 30 MPa to 40 MPa, the ultimate load capacity increased by about 19 % to reach 357.48 kN. However, For the ST1 specimen, when the compressive concrete strength increases from 20 MPa to 30 MPa, the ultimate load capacity increased from 110.27 kN to 136.29 kN which is approximately 23%. While when the compressive strength of concrete increased from 30 MPa to 40 MPa, the ultimate load capacity is raised by about 16% to attain 159.14 kN. As for the I-shape connector specimen, the ultimate load capacity increased from 179.18 kN to 239.33 kN, which is 33 % when the compressive strength of concrete increases from 30 MPa to 40 MPa. Furthermore, when the concrete strength is rises from 30 MPa to 40 MPa, the ultimate load capacity is improved by about 18 % to attain 282.53 kN.

On the other hand, the slip value δ_m of the CH2 specimen was higher when the concrete strength was 20 MPa. Whereas the slip values δ_m were almost similar in both concrete compressive strength 30 and 40 MPa. However, in the ST1 and I-shape connector specimens, the slip values increase with increasing the concrete compressive strength.

The comparison between the CH2 and ST1 specimens shows that they were approximately the same concerning the slip values δ_m. The slip values of the I-shaped connector specimen were about half of those of the CH2 and ST1 specimens.

Table 5.3: Effect of concrete compressive strength.

Specimens	Concrete strength (MPa)	FE results	
		Ultimate load (kN)	$\delta_m(mm)$
CH2	20	230.32	7.81
	30	299.45	5.78
	40	357.48	6.01
ST1	20	110.27	6.63
	30	136.29	7.41
	40	159.14	7.95
I-Shape connector	20	179.18	3.32
	30	239.33	3.75
	40	282.53	4.37

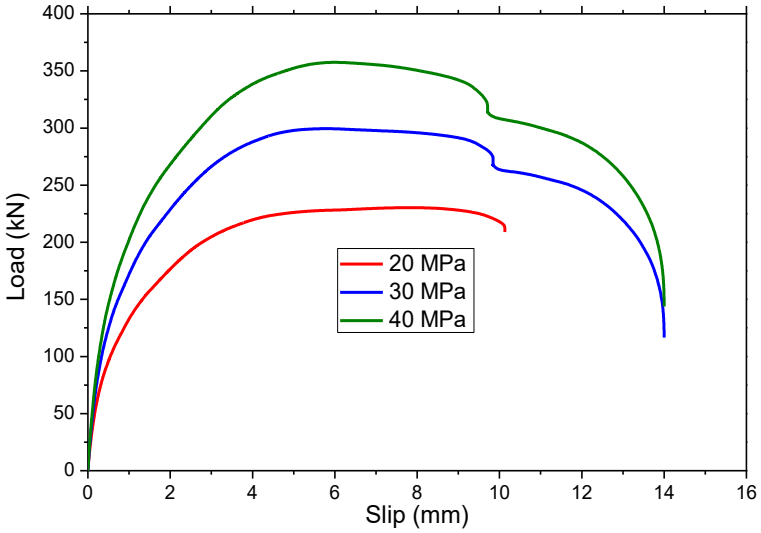

(a) Channel connector of CH2 specimen

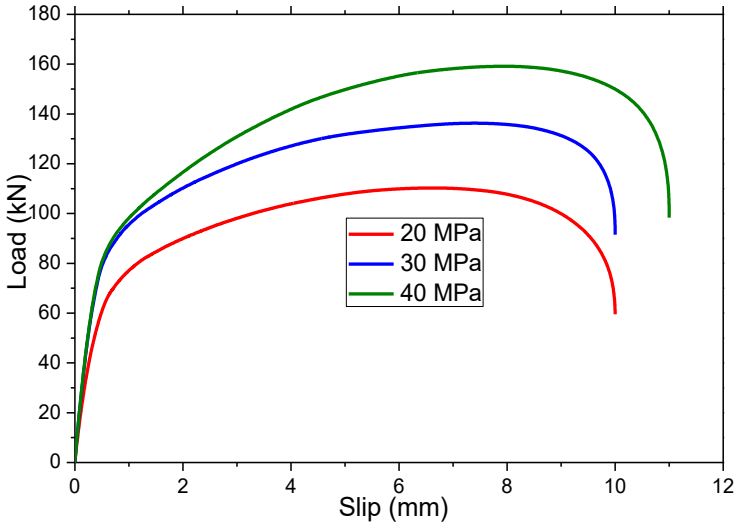

(b) Headed stud connector for ST1 specimen

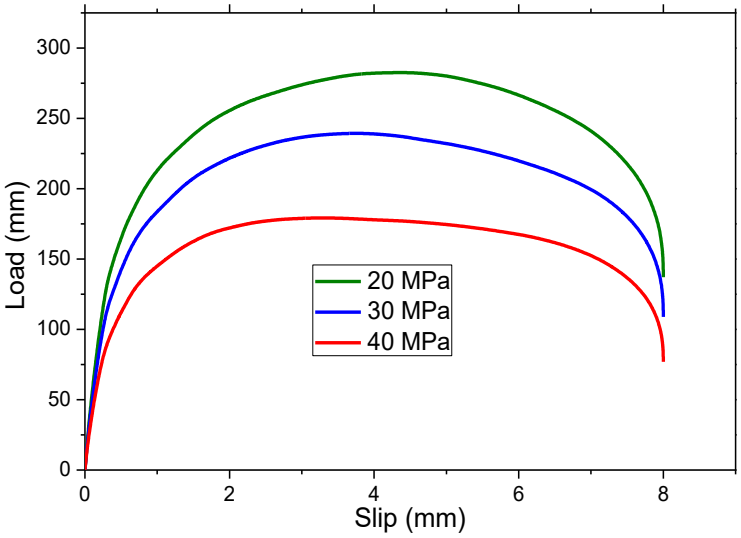

(c) I-shape connector

Figure 5.25: Load-slip curves of three different concrete strength.

5. 4.2- Effect of steel grade

To evaluate the influence of the connector's steel grade on the ultimate load capacity, two specimens CH2 and I-shape connector were investigated. The results of connector's steel with a yield strength of 327 MPa were compared against those of S235 steel grade. Table 5.4 illustrates the results of the ultimate load capacity of the channel shear connector CH2 and I-shape connector specimens. Figure 5.26 presents the load-slip curves of the two specimens with two different steel grades of each connector. It can be seen that decreasing the steel grade of the connectors provides a non-significant decrease in the ultimate load capacity. Where the decrease in the connector's steel grade by about 28% led to a decrease in ultimate load of around 3% for the CH2 specimen and 5% for the I-shape connector specimen.

Table 5.4: Effect of steel grade.

Specimens	Concrete strength (MPa)	steel grade		Ultimate load (kN)
		Yield strength f_y(MPa)	Ultimate strength f_u(MPa)	
CH2	30	235	360	289.69
	30	327	481	299.45
I-Shape shear connector	30	235	360	239.33
	30	327	481	225.58

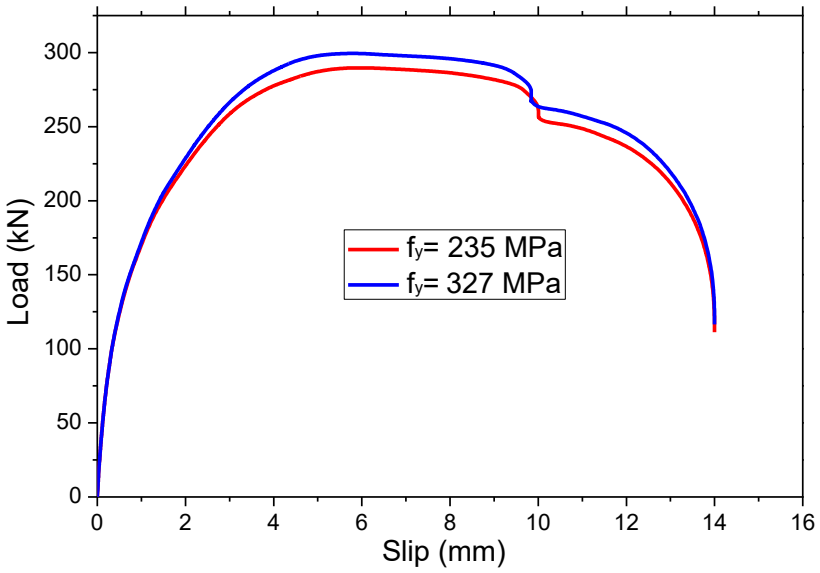

a) CH2 specimen

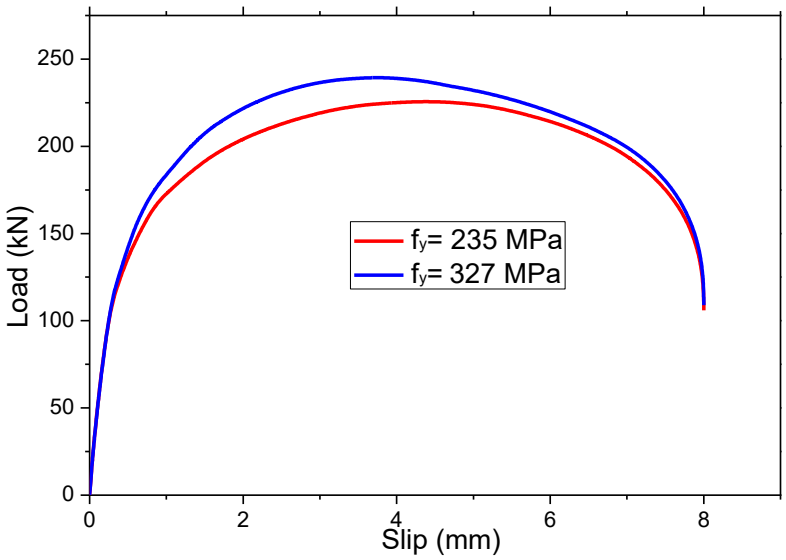

b) I-shape shear connector specimen

Figure 5.26: Effect of shear connector's steel grade.

5. 5- Conclusions

A three-dimensional finite element model has been proposed in this chapter to simulate the behavior of shear connectors in push-out specimens. The finite element software ABAQUS has been used. The validation of the proposed model was done by comparing the numerical results against some experimental push-out tests from the two previous chapters. Then, the validated model was used to simulate the I-shaped connector to compare its behavior with that of the channel shear connector. In addition, the effect of concrete compressive strength and connector steel grade was investigated. From the comparison of experimental and numerical results, we can draw the following conclusions:

1) In all specimens, good agreement was observed between the experimental and FE simulation in terms of ultimate load capacity. Except for the ST2 specimen, a 15% difference is seen for numerical and experimental results.
2) In both methods, finite element simulation and experimental teste, the observed failure mode was concrete cracking for channel connector specimens and connector shearing for headed stud specimens. As result, a significant similarity in failure mode was obtained for the experimental and numerical results for all push-out specimens.
3) Finite element analysis using the concrete damaged plasticity model is an efficient simulation method to predict the behavior of the shear connectors.
4) The ultimate shear capacity of the channel connector is greater than that of the I-shape connector by about 19 %. Furthermore, the channel shear connector has better ductility than the I-shape connector.

5) The concrete compressive strength significantly governed the ultimate load capacity of shear connectors. While the connector's steel grade does not have a significant effect on ultimate load capacity.

Chapter 6 :

Finite element analysis of steel-concrete composite beams.

6.1- Introduction

Steel-concrete composite beams have been widely used in different types of construction, where shear connectors are commonly welded through the top flange of steel beams to ensure full/partial composite action between the steel beam and the concrete slab. However, experimental tests on steel-concrete composite beams are very advanced, time-consuming, and require large test facilities [63-66].

In the previous chapters, the behavior of shear connectors was investigated using push-out specimens. However, in this chapter, the nonlinear behavior of some shear connectors is numerically studied using steel-concrete composite beam specimens. A 3D finite element model of a composite beam is developed using ABAQUS software version 6.14 [18]. This software can model the composite response without requiring information from push-out tests to define the behavior of shear connectors [67]. The accuracy of the suggested modeling approach was validated against experimental results available in the literature. The nonlinear material behavior of concrete is modeled using the concrete damage plasticity model, while the elastic-plastic bilinear model is used for steel.

The numerical results are presented and discussed, focusing on the load-deflection relationship of the composite beams, the slip at the steel-concrete interface, and the failure modes. Furthermore, a parametric study was carried out to evaluate the influence of various parameters, i.e., the degrees of connection, the concrete compressive strength, and the connector's steel grade.

6.2- Finite element analysis

6.2.1- Model geometry

Several specimens were prepared in this chapter using ABAQUS to study the connection behavior in steel-concrete composite beams. The specimens are simply-supported beams under a positive moment with double concentrated loads at the mid-span. The connectors investigated in these specimens are channel connectors CH1 and CH2 as well as headed stud connector ST1.

Each beam was 4.25 m long. The concrete slab was 14 cm thick and 65 cm wide, and the steel beam was IPE 300. Fig.6.1 shows the dimensions of the specimens, and Fig.6.2 shows a typical FE model consisting of five types of components, i.e., the concrete slab, shear

connectors, reinforcing bars, steel beam, and stiffeners. Stiffeners were welded to a steel beam to prevent local buckling of the web or flanges.

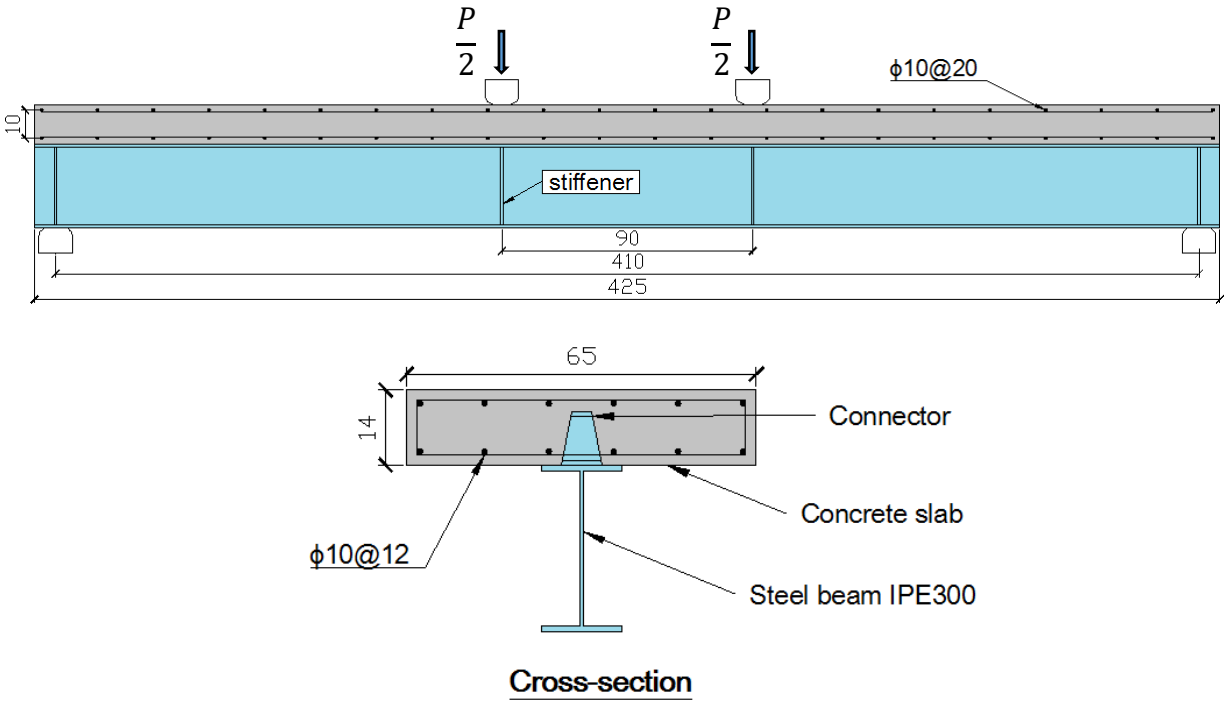

Figure 6.1: Composite beam dimensions (unit = cm).

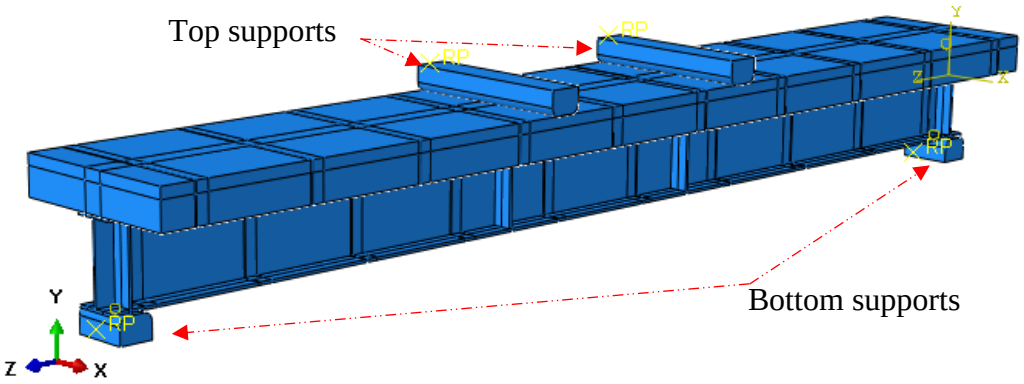

Figure 6.2: Finite element model.

6.2.2- Interactions and constraint conditions

Surface-to-surface interactions were considered for the contact surfaces between the shear connectors and the surrounding concrete, between the concrete slab and the top flange of the steel beam, between the concrete slab and the top supports, as well as between the steel beam and the bottom supports. In the normal direction, the hard contact function was used to prevent penetration between surfaces. Whereas, in a tangential direction, a penalty contact function was adopted using a friction coefficient of 0.2, as in the push-out tests (chapter five). Frictionless

contact interaction was applied between the bottom flange of the steel beam and the bottom supports. Figure 6.3 shows the different contact interactions between interfaces in the composite beams. Furthermore, in the surface-to-surface interaction, the master and slave surfaces should be defined. The surface with higher rigidity was defined as the master surface. Therefore, the surfaces of the steel beam and the shear connectors were defined as the master surfaces for their contact interactions with the concrete slab, while the concrete slap surfaces were defined as slave surfaces. For the interface between the top supports and the concrete slab, the bottom supports, and the steel beam, the top, and bottom supports interfaces were selected as the master surfaces. While the steel beam and the concrete slab interfaces were selected as slave surfaces. On the other side, all reinforcing bars were embedded in the concrete slab, as presented in Fig 6. 4.

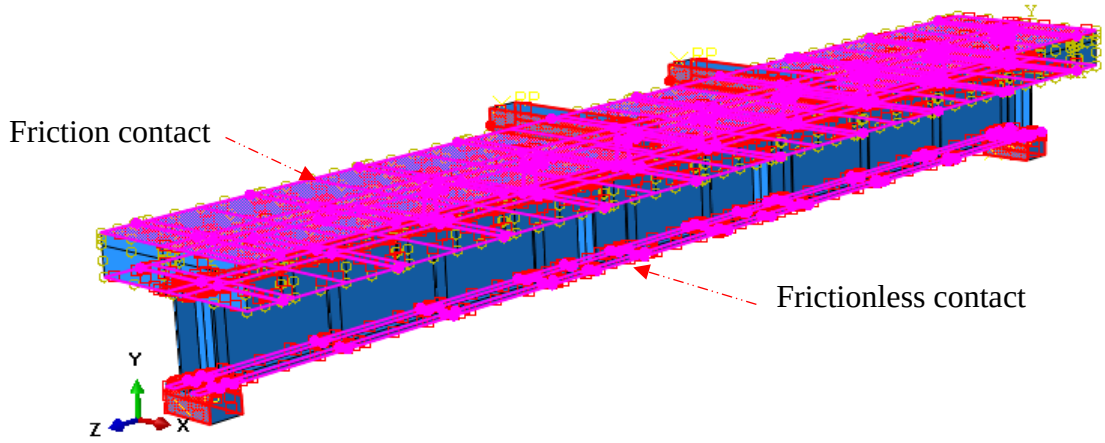

Figure 6.3: Contact interactions.

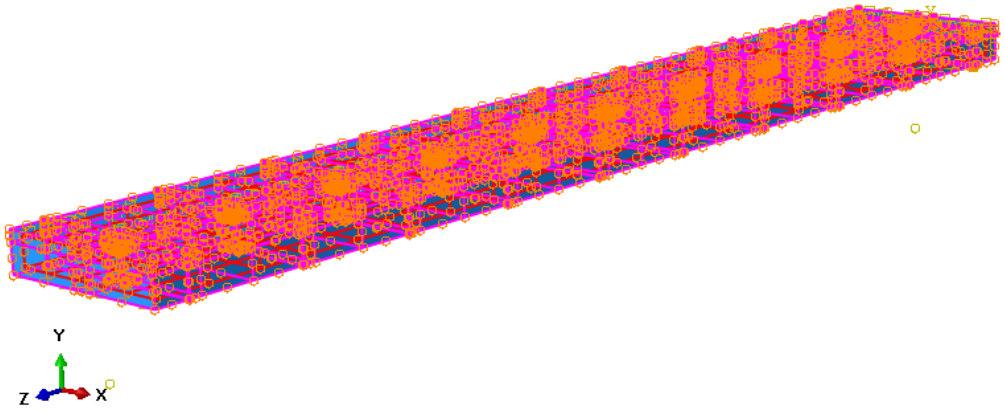

Figure 6.4: Reinforcing bars embedded in concrete slab.

6.2.3- Boundary and loading conditions

In general, the support conditions of simply-supported beams were either hinged or roller-supported. In contrast, the reference point is located in the bottom supports was restrained in all degrees of freedom, as illustrated in Fig 6. 5. Therefore, the use of frictionless contact between the steel beam and the lower supports was designed to ensure the correct simulation of the roller support.

As for the loading, a linearly increased displacement controlled by amplitude and smooth step functions was applied in the two reference points located in the top supports. The load was measured automatically as the sum of the reaction forces at the two reference points of the bottom supports. The deflection was measured as the average displacement between the two reference points of the top supports.

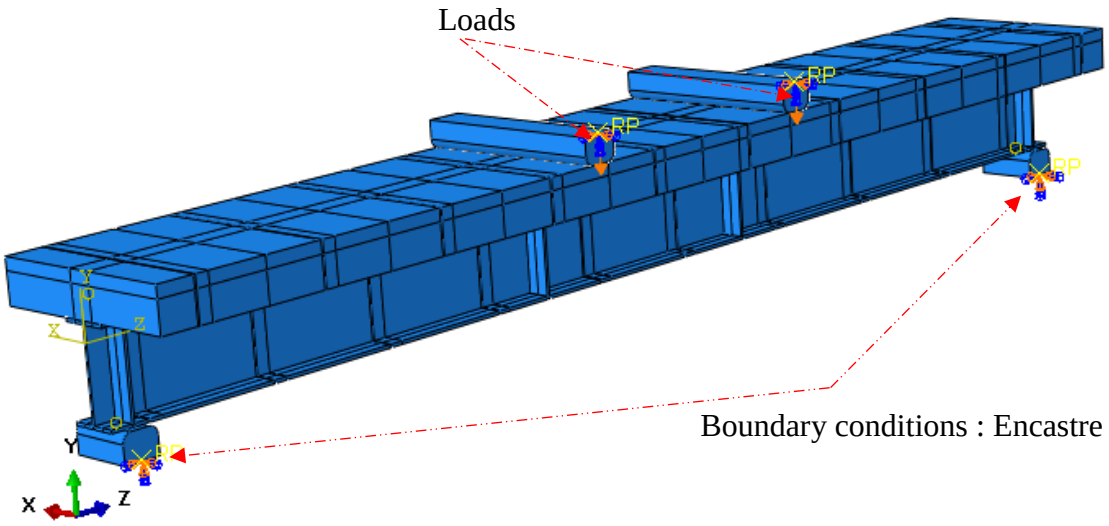

Figure 6.5: Boundary and loading conditions.

6.2.4- Material properties

a) concrete: as in the case of push-out specimens (section 5.2.4), the model used for concrete is multilinear in compression and bilinear in tension. The simplified concrete damage plasticity (SCDP) model developed by Milad H and all [60] is adopted, as well, for the finite element analysis of composite beam specimens. Furthermore, the CDP model includes four grades of concrete, namely C20, C30, C40, and C50.

b) steel: the material model used for the steel beam, the shear connectors steel, and the reinforcing bars steel is similar to that used in the push-out tests. This model is a bilinear elastic-plastic material model and is employed in this study based on the nominal behavior of the stress-strain curve shown in Fig. 5.6 of chapter five. The user must therefore introduce the following values:

- The elasticity modulus *E* and the Poisson's ratio ν.
- The yield strength f_y and ultimate strength f_u.
- The elastic strain ε_y and compressive strain ε_u.

6.2.5- Finite element type and mesh

The steel beam, concrete slab, shear connectors of the composite beams, and the four supports meshed through the C3D8R element. This element is a brick element with eight nodes, and each node has three translational degrees of freedom. Whereas, the reinforcing bars have meshed through the T3D2 element. This element is a truss element with two nodes, and each node has three translational degrees of freedom. Each part of the composite beams was partitioned and meshed independently. However, suitable element sizes for the different components were employed.

The mesh of the two composite beams of channel connector CH2 and headed stud connector ST1 is shown in Fig 6.6. In the longitudinal direction for the shear channels composite beams, the mesh size of the channel connectors, the steel beam elements under the channel connectors, and the surrounding concrete regions vary from 6 to 15 mm depending upon the geometric of the channel connectors.

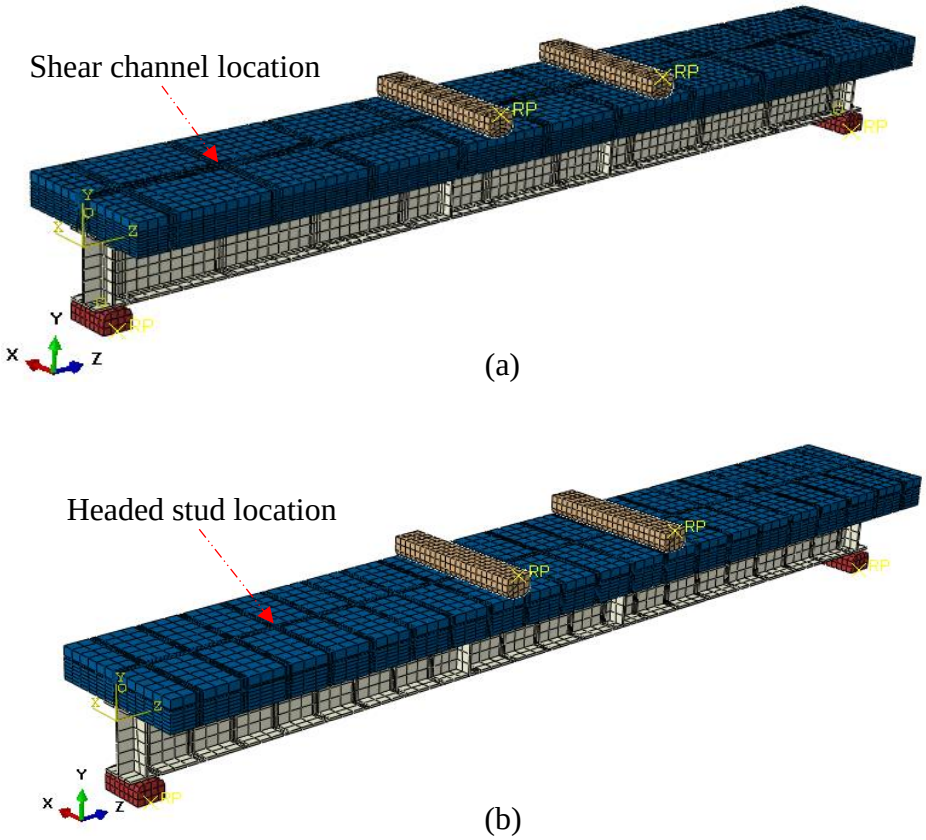

Figure 6.6: Finite element mesh: (a) Shear channel beam (b) headed stud beam.

In the transversal direction, the mesh size of the shear channels, the steel beam elements underneath, and the concrete in front and behind shear channels varies from 3 to 15 mm. However, the other regions have meshed with a maximum element size of 50 mm. As result, the mesh number of each shear channel composite beam is more than 20000 elements.

As for the headed stud composite beams, the mesh size ranged from 3 to 15 mm for headed studs, the steel beam elements underneath, and the surrounding concrete of studs. The other regions have also meshed with a maximum element size of 50 mm. The mesh number of each headed stud composite beam is more than 20000 elements.

Reinforcement bars were meshed using an element size of 100 mm, and a 30 mm mesh element size was used for the supports.

6.3- Validation of the developed model

To ensure the accuracy of the proposed model, the numerical results of two different examples are presented here and compared with those obtained experimentally. The first example is a simply-supported composite beam with a concentrated load at mid-span tested by (Wang 2017) [68]. The second example is a composite beam with double concentrated loads in the mid-span tested by (Xing 2016) [16]. The comparison focuses on the load-deflection relationship, interface slip of the composite beams, and the failure mode.

6.3.1- Composite beam tested by (Wang et al 2017) [68]

The first composite beam specimen SCB-1 tested by Wang 2017 [68] is selected as an example, which was simply supported and subjected to a monotonic concentrated load at the mid-span. The total length of the composite beam was 3200 mm, and the span was 3000 mm. A concrete slab that was 300-mm wide and 80-mm thick was used. The I-shaped steel beam was welded using a 10-mm-thick steel plate with a 120-mm-wide top flange, a 160-mm wide bottom flange, and a 150-mm web height. Two rows of stud connectors with a diameter of 13 mm were welded on the top flange of the steel beam with a transverse spacing of 60 mm, as shown in Fig. 6.7. The shear connection degree η in this composite beam (SCB-1) was 100%. However, the geometrical characteristics and the properties of the materials of this composite beam are collected in Table 6.1.

Figures 6.8 and 6.9 show a comparison between the numerical curves and those obtained experimentally. Figure 6.8 shows the evolution of the deflection in the function of the loading,

while Fig 6.9 concerns the slip distribution at the steel-concrete interface along the composite beam. This comparison shows that in the linear regime the finite element curve is in good agreement with the experimental curve and slightly diverges from the experimental curve in the nonlinear regime. In addition, the ultimate load capacity obtained numerically was 225.76 kN, and almost similar to that of the experimental test which was 228.41 kN, i. e., the divergence is negligible and about 1%. However, the slip distribution at the steel-concrete interface obtained in the finite element simulation is generally in conformity with that obtained in the experimental test.

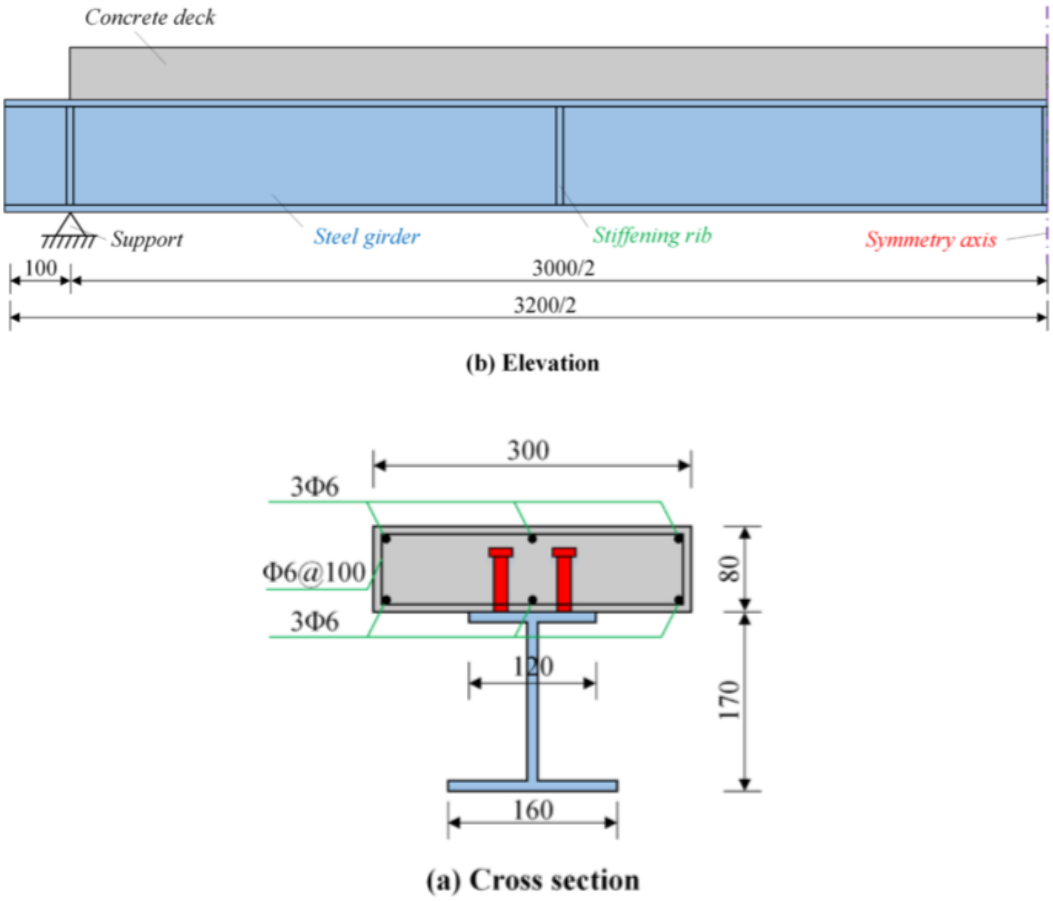

Figure 6.7: Dimension and reinforcement of specimen (unit = mm) [68].

On the other hand, in the experimental tests, the SCB-1 composite beam experienced flexural failure modes, where the steel beam yielded, and the concrete slab was crushed in the mid-span. Figure 6. 10 shows the failure modes in this FE simulation and those in the experimental tests of the SCB-1 specimen. It can be observed that the equivalent plastic strain (PEEQ) is located in the mid-span of both steel beam and concrete slab. In other words, the failure mode in this FE simulation is similar to that in experimental tests.

Table 6.1: Details of composite beam SCB-1.

Materials	geometrical characteristics	materials properties
Concrete Slab	$Width = 300\ mm$ $Thickness = 80\ mm$	$Density = 2500\ kg/m3$ $E_c = 2660\ MPa,\ \nu_c = 0.2$ $f_{ck} = 30\ MPa\ ,\ f_t = 3\ MPa$
Steel beam	$Cross\ section\ area = 4300\ mm^2$ $Total\ length = 3200\ mm$ $Span\ length = 3000\ mm$ $height = 170\ mm$ $Top\ flange = 10 \times 120\ mm$ $Bottom\ flange = 10 \times 160\ mm$ $Web = 10 \times 150\ mm$	$Density = 7850\ kg/m3$ $E_s = 200000\ MPa,\ \nu_s = 0.3$ $f_y = 352\ MPa,$ $f_u = 450\ MPa$ $\varepsilon_u = 0.15$
Steel of reinforcing Bars	$Transverse\ reinforcement$: 32Ø6 $Longitudinal\ reinforcement$: 6Ø6	$Density = 7850\ kg/m3$ $E_s = 200000\ MPa,\ \nu_s = 0.3$ $f_y = 300\ MPa, f_u = 400\ MPa$ $\varepsilon_u = 0.1$
Stud connectors	$Number\ of\ stud$: 28 $Stud\ spacing$: 215 mm $Height = 60\ mm$ $Diameter = 13\ mm$	$Density = 7850\ kg/m3$ $E_s = 200000\ MPa,\ \nu_s = 0.3$ $f_y = 400\ MPa, f_u = 529\ MPa$ $\varepsilon_u = 0.12$

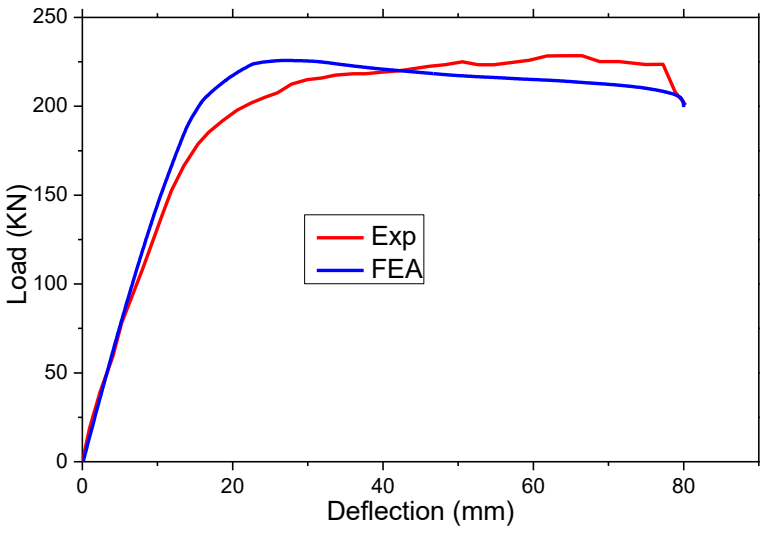

Figure 6.8: Load-deflection curves of SCB-1 specimen.

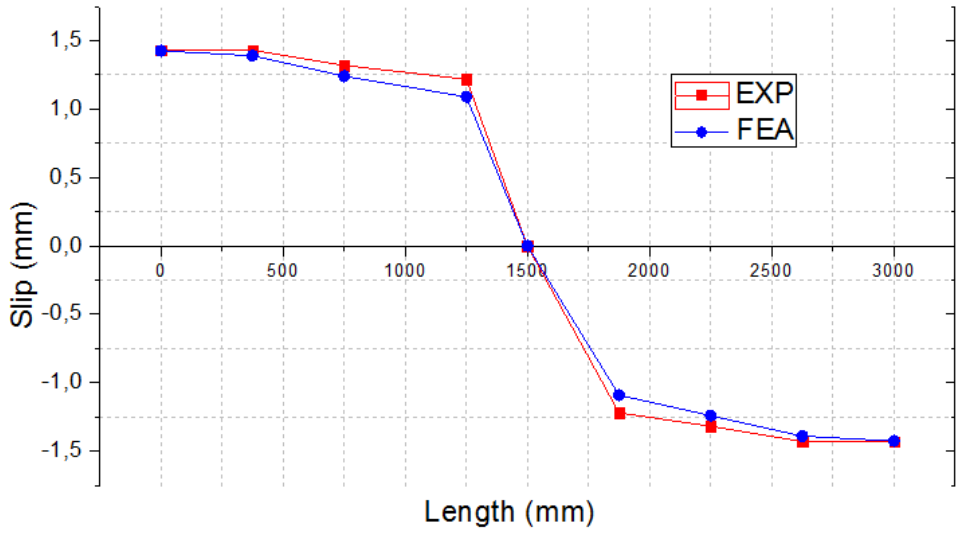

Figure 6.9: Slip distribution along the SCB-1 composite beam.

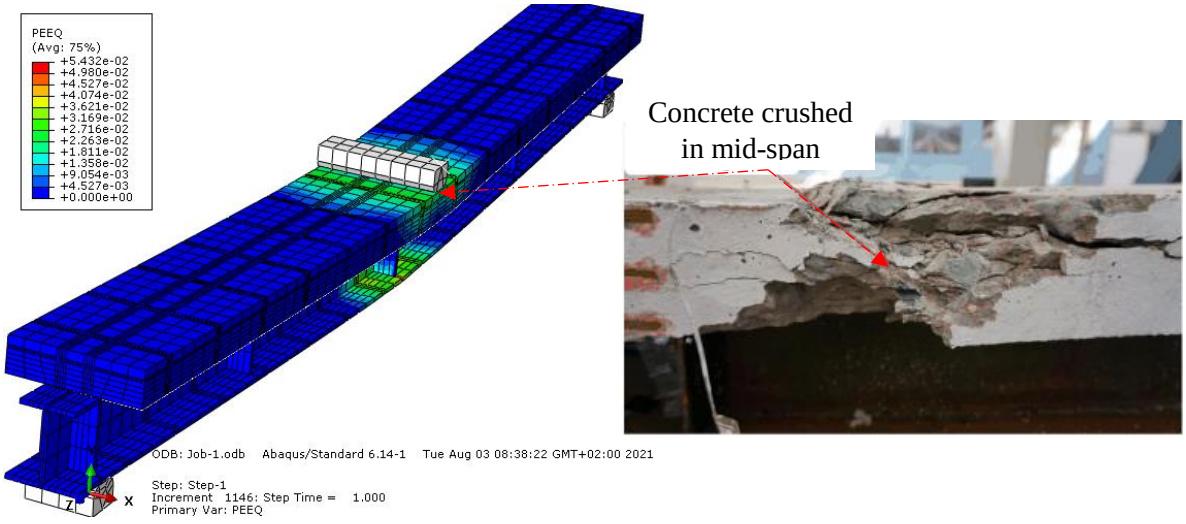

(a) (b)

Figure 6.10: Failure modes of SCB-1: (a) FE simulation; (b) experimental tests [68].

6.3.2- Composite beam tested by (Xing et al 2016) [16]

The second example selected is FBST-1 composite beam specimen that was investigated experimentally by (Xing et al 2016) [16]. This simply-supported composite beam was subjected to a monotonic load. The load at the mid-span was distributed to the two loading points, and the distance between them was 700 mm, as shown in Fig 6.11. The overall span of the composite beam is 3700 mm, where the shear span is 1500 mm. Stiffening ribs were established at the loading and support section. The section HW250 × 250 profile steel was selected as the steel beam. The length of this steel beam expands on both sides by 150 mm compared to the total

span. A concrete slab that was-600 mm wide and 130 mm thick was used and connected with a steel beam by a single row of headed studs.

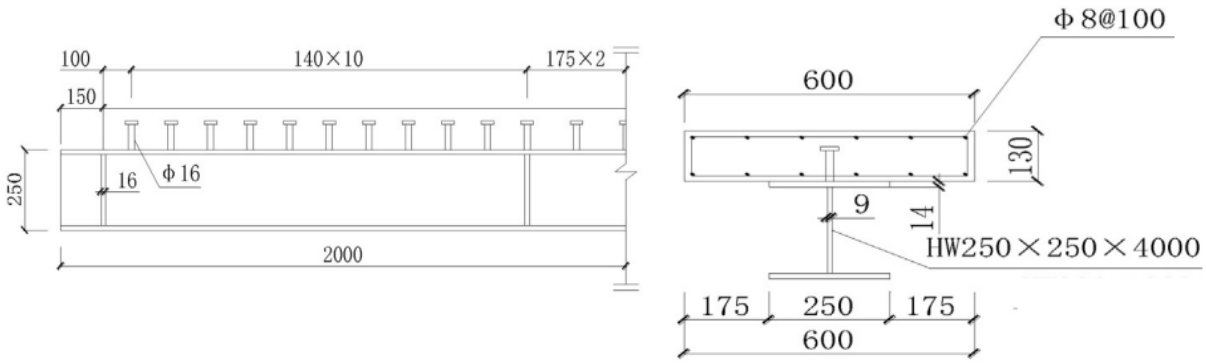

Figure 6.11: Layout of headed studs and cross section of FBST-1specimen (unit: mm) [16].

Table 6.2: Details of composite beam FBST-1.

Materials	geometrical characteristics	materials properties
Concrete slab	$Width = 600\ mm$ $Thickness = 130\ mm$	$Density = 2500\ kg/m3$ $E_c = 30000\ MPa,\ \nu_c = 0.2$ $f_{ck} = 40\ MPa, f_t = 4\ MPa$
Steel beam	$Cross\ section\ area = 8998\ mm^2$ $Total\ length = 4000\ mm$ $Span\ length = 3700\ mm$ $height = 250\ mm$	$Density = 7850\ kg/m3$ $E_s = 210000\ MPa$ $\nu_s = 0.3$ $f_y = 267\ MPa, f_u = 402\ MPa$ $\varepsilon_u = 0.15$
Steel of reinforcing bars	$Transverse\ reinforcement$: Ø8@100 $Longitudinal\ reinforcement$: 12Ø8	$Density = 7850\ kg/m3$ $E_s = 210000\ MPa, \nu_s = 0.3$ $f_y = 358\ MPa, f_u = 455\ MPa$ $\varepsilon_u = 0.11$
Stud connectors	$Number\ of\ stud$: 25 $Height = 90\ mm$ $Diameter = 16\ mm$	$Grade\ ML15$ $Density = 7850\ kg/m3$ $E_s = 210000\ MPa,\ \nu_s = 0.3$ $f_y = 245\ MPa, f_u = 365\ MPa$ $\varepsilon_u = 0.12$

The diameter of headed studs is 16 mm, and the shear connection degree η in this composite beam (FBST-1) was 50 %. Table 6.2 summarizes the geometrical characteristics and material properties of this composite beam.

The load-deflection curve of the FBST-1 composite beam obtained numerically is compared with that from experiment tests in Fig. 6.12. It can be seen that the results of both methods are relatively close to each other. Furthermore, in the FE simulation, the ultimate load capacity was 552.72 kN, while that of the experimental test was 550 kN. This means that there is a good agreement between the two methods for the ultimate load.

As for the slip distribution at the steel-concrete interface, the comparison between the two curves obtained experimentally and numerically is presented in Fig 6.13. The numerical curve showed that the results were slightly overestimated, where the difference between the numerical and the experimental results exceeds 1 mm.

On the other side, in the experimental tests, the failure mods of the composite beam FBST-1 were the concrete crushing, the bending of the composite beam where the bottom flange of the steel beam yielded in tension, and the deformation of headed studs, as shown in Fig. 6.14. This figure also shows the comparison of failure modes between numerical and experimental tests. From this comparison, it can be observed that, good correlation in the failure mods between the both methods. Therefore, it should be noted that the simulation results indicate that the developed finite element model is suitable for the experimental results.

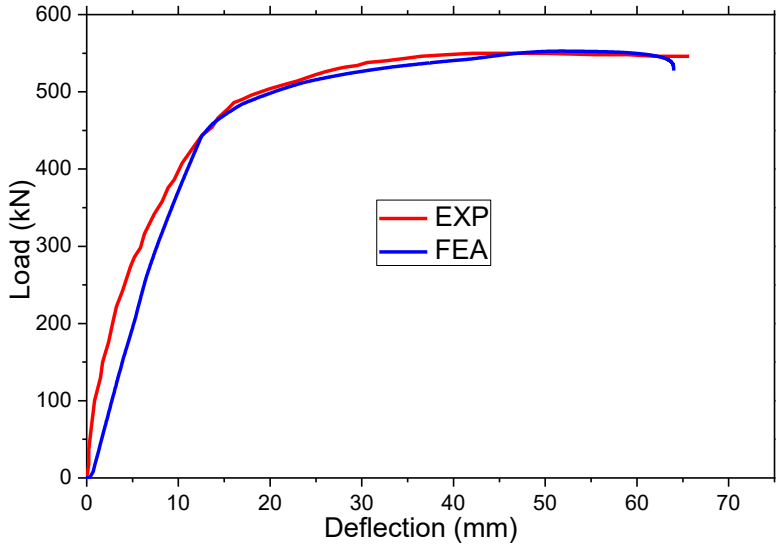

Figure 6.12: Load-deflection curves of FBST-1 specimen.

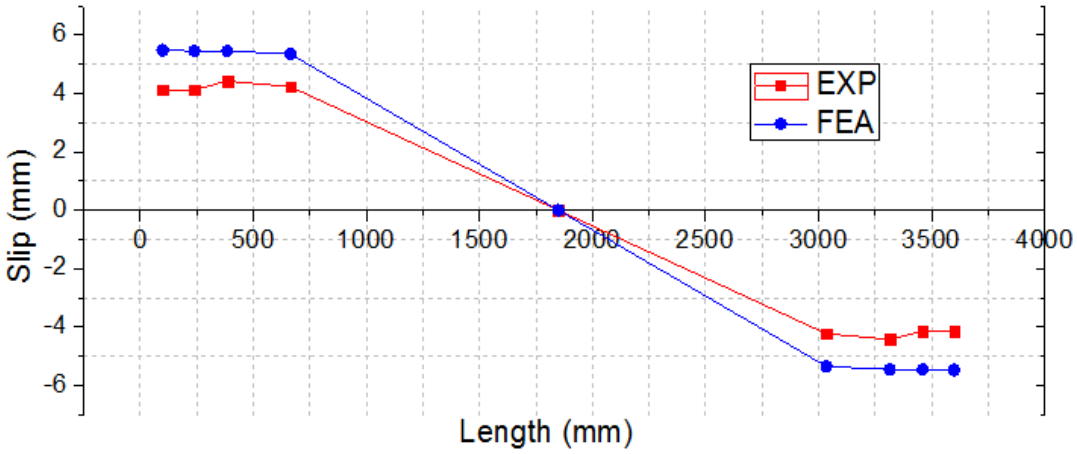

Figure 6.13: Slip distribution along the FBST-1 composite beam.

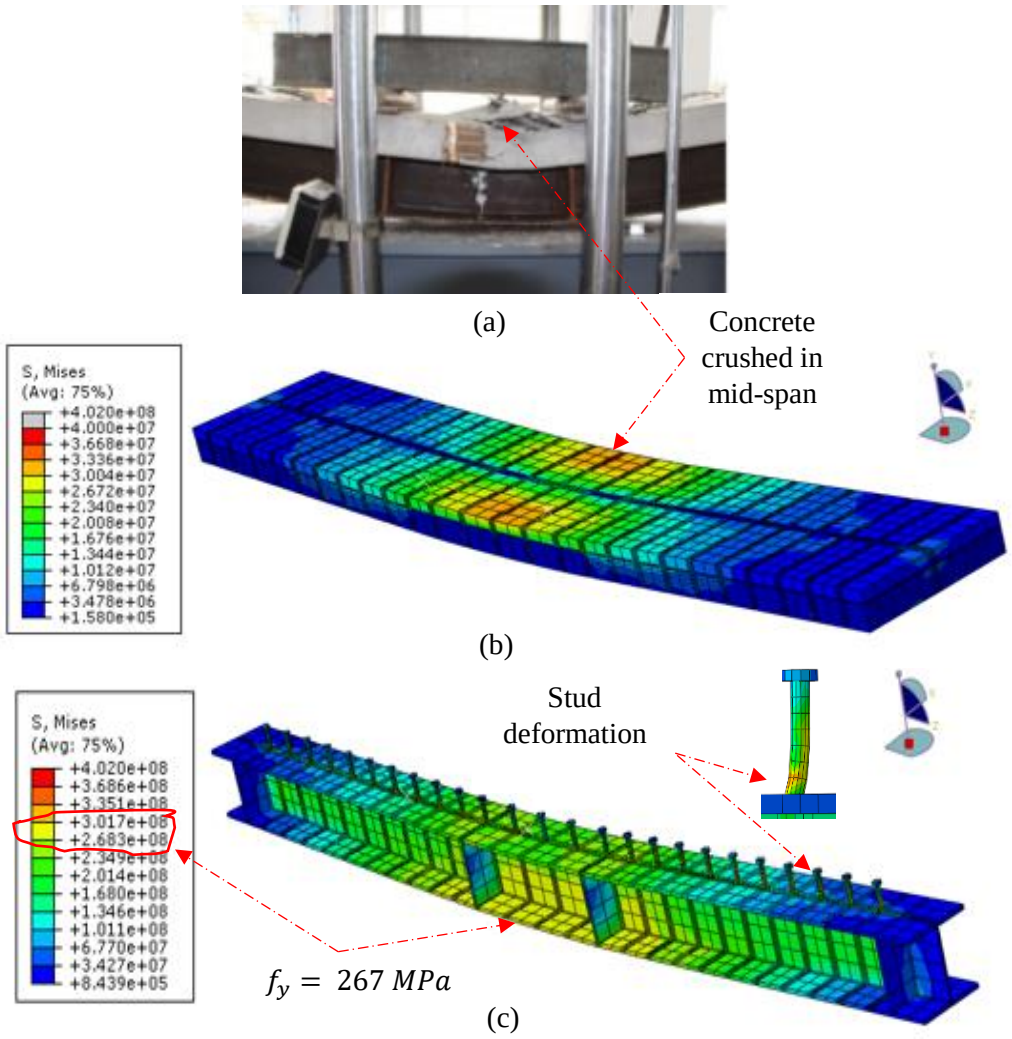

Figure. 6.14: Failure modes of FBST-1: (a) experimental tests [16]; b, c) FE simulation.

6.4- Composite beams results

After the validation of the developed FE model in the previous sections, this section presented the results of three different composite beams BCH1, BCH2, and BST1. These composite beams differ only in the type of connector. Where each of the channel shear connectors CH1, and CH2, as well as the stud connector ST1, were used in the composite beams BCH1, BCH2, and BST1, respectively. Except that the type of connector, the three composite beams have the same geometrical and materiel properties, as shown in Table 6.3.

Table 6.3: Details of composite beams BCH1, BCH2, and BST1.

Materials	geometrical characteristics	materials properties
Concrete Slab	$Width = 650\ mm$ $Thickness = 140\ mm$	$Density = 2500\ kg/m3$ $E_c = 2660\ MPa,\ \nu_c = 0.2$ $f_{ck} = 30\ MPa\ ,\ f_t = 3\ MPa$
Steel beam	$Cross\ section\ area = 5381mm^2$ $Total\ length = 4250\ mm$ $Span\ length = 4100\ mm$ $height = 300\ mm$ $Top\ flange = 10.7 \times 150\ mm$ $Bottom\ flange = 10.7 \times 150\ mm$ $Web = 7.1 \times 278.6\ mm$	$Density = 7850\ kg/m3$ $E_s = 210000\ MPa,\ \nu_s = 0.3$ $f_y = 275\ MPa,$ $f_u = 410\ MPa$ $\varepsilon_u = 0.27$
Steel of reinforcing Bars	$Transverse\ reinforcement$: Ø10@200 $Longitudinal\ reinforcement$: 12Ø10	$Density = 7850\ kg/m3$ $E_s = 200000\ MPa,\ \nu_s = 0.3$ $f_y = 392\ MPa, f_u = 656\ MPa$ $\varepsilon_u = 0.13$
Channel connectors	$Number\ of\ channel$: 10 $channel\ spacing$: 445 mm $Height = 100\ mm$ $Length = 75\ mm$	$Density = 7850\ kg/m3$ $E_s = 205000\ MPa,\ \nu_s = 0.3$ $f_y = 327\ MPa,\ f_u = 481\ MPa$ $\varepsilon_u = 0.27$
Stud connectors	$Number\ of\ stud$: 28 $Stud\ spacing$: 215 mm $Height = 60\ mm$ $Diameter = 13\ mm$	$Density = 7850\ kg/m3$ $E_s = 202000\ MPa,\ \nu_s = 0.3$ $f_y = 389\ MPa,\ f_u = 554\ MPa$ $\varepsilon_u = 0.12$

All composite beams were loaded in a four-point bending test scheme with a span length of 4100 mm. Based on the shear connection capacity of each connector obtained in the experimental push-out tests and the equation 1.20 (see chapter own), a full shear connection is used in each beam. In addition, the performance comparison between the three composite beams was performed according to the following factors: load-deflection relationship, slip at the steel-concrete interface, and the failure mode.

6.4.1- Load-deflection relationship

Figure 6. 15 shows the load-deflection curves of the three composite beams BCH1, BCH2, and BST1. It can be observed that a good correlation between the three curves in the elastic stage, but a slight divergence was in the plastic stage. The ultimate load capacity P_u, and the corresponding deflection value δ_d are summarized in Table 6.4. As mentioned earlier, the three composite beams have the same geometric and materiel properties, as well as with full connection degrees except that the type of connectors. Thus, any difference between the results of ultimate load and the corresponding deflection δ_d is due to the connection in the concrete-steel interface (i.e., type of connectors). However, the difference in the ultimate load capacity of the three specimens was not significant. Where, the BCH1 composite beam supported around 4 % and 3 % higher load than the BCH2 and BST1 composite beams, respectively. In contrast, the deflection δ_d of the composite beam BCH1 was almost 13% lower than that obtained for the BCH2 composite beam, while was 24 % lower than that obtained for the BST1 composite beam.

Table 6.4: Results of BCH1, BCH2, and BST1 composite beams.

Specimens	Ultimate load P_u (kN)	Corresponding deflection δ_d (mm)
BCH1	452.36	49.9
BCH2	432	57
BST1	439.06	62.12

6.4.2- Slip at the steel-concrete interface

It is necessary to determine the slip behavior at the steel-concrete interface in the composite beams. Therefore, the relative slip at the steel-concrete interface is taken as the difference of the displacement in the axial direction U_z of the beam between node A located on the bottom surface of the concrete slab and node B located on the top surface of the steel beam. Figure 6.16

shows de slip distribution in the steel-concrete interface along the Z direction and at the maximum deflection for the composite beams BCH1, BCH2, and BST1. This figure indicates that slip values are greatest near the supports and small at mid-span. It should be noted that the greatest slip value of each composite beam is lower than that obtained from the push-out test in the previous chapters. In addition, the highest slip value was that of BST1 by about 5.6 mm. By comparing with the experimental push test, it was found that the amount of slip was 68% of the ultimate slip supported by the headed stud connectors. For the composite beams BCH1 and BCH2, the highest slip values were 3.56 and 4.65 mm, which represent 35% and 38% of their ultimate slip, respectively.

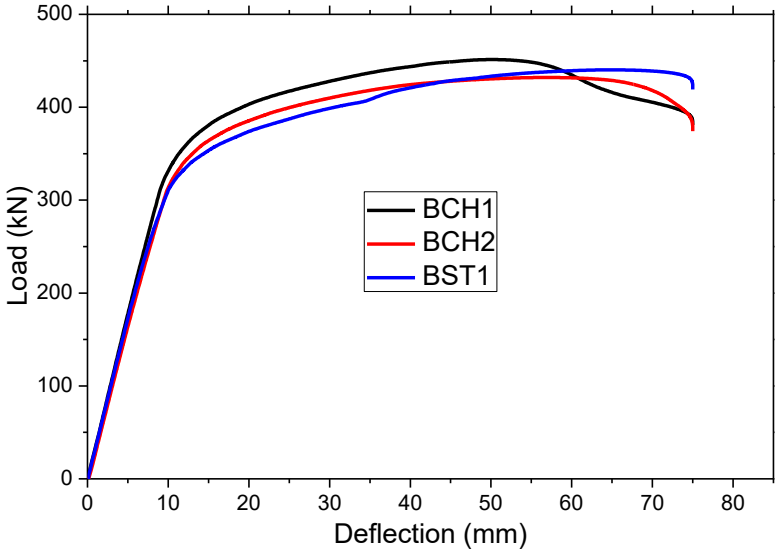

Figure 6.15: Load-deflection curves for composite beams BCH1, BCH2, and BST1.

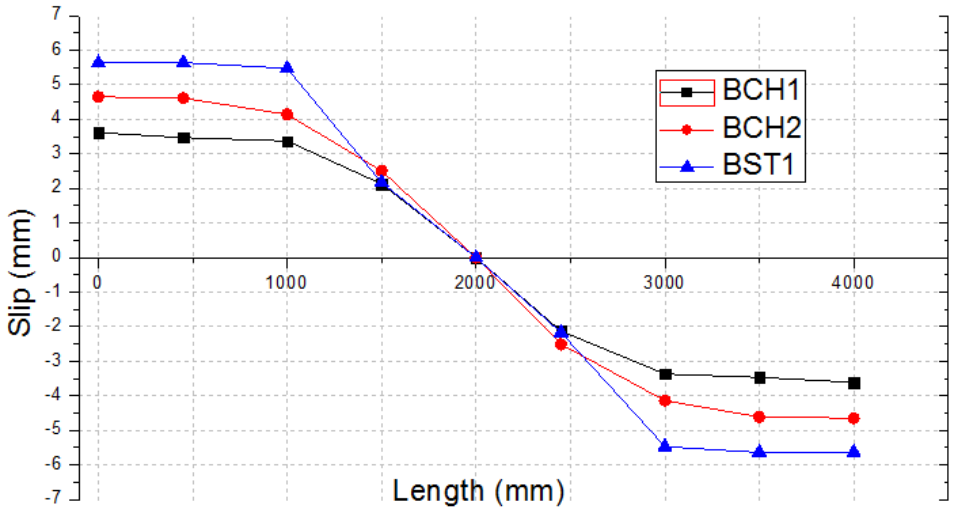

Figure 6.16: Slip distribution along the composite beams BCH1, BCH2, and BST1.

6.4.3-Failure mode

Each component of the three composite beams, BCH1, BCH2, and BST1, was visualized separately, which can help to identify the failure mode at the collapse load. These components are concrete slab, steel beam, shear connectors, and reinforcing bars.

a) Concrete slab: As mentioned earlier, the concrete compressive strength in the three specimens is 30 MPa. Figures 6.17 (a), (b), and (c) demonstrate the Mises stress distribution in the top and bottom concrete slab of each composite beam. For the BCH1 concrete slab (Fig 6.17 (a)), the stress distribution was in the top mid-span exactly where located the top supports, and the Stress contours give a value around 20 MPa, which means no failure can occur in this location. In contrast, Stress contours demonstrated a value over 30 MPa in front of the web and bottom flange of channels, as shown in the zoomed view of Fig 6.17 (a). This means that the concrete was crushed in this area (the grey section) due to the large compressive stress.

On the other hand, the Mises stress distribution in both sides (top and bottom) of the BCH2 concrete slab is demonstrated in Fig 6.17 (b). It can be observed that for the top concrete slab, the stress distribution was positioned in the mid-span, and Stress contours exhibited a value around 30 MPa at some point in this area. Therefore, there is a possibility of concrete crushing at these points. However, the gray section (i.e., more than 30 MPa in the stress contours) in the zoomed view of Fig 6.17 (b) shows that the concrete is crushed in front of the lower web of channels.

As for the BST1 concrete slab, Fig 6.17 (c) shows its Mises stress distribution. It can be seen that there is a possibility of concrete crashing in the top med-span where the stress distribution was around 30 MPa. In addition, except for the concrete that surrounds the three studs in the mid-span, the concrete crushing was in the front of the stud shanks due to the large compressive stress, as shown in the zoomed view of Fig 6.17 (c).

b) Steel beam and shear connectors: Figures 6.18 (a), (b), and (c) illustrate the Mises stress distribution in the steel beam and the shear connectors of the composite beams BCH1, BCH2, and BST1, respectively. It can be observed that, for the three steel beams, the Mises stress distribution was higher in the bottom mid-span of each steel beam and exceeded the yield strength f_y (275 MPa). Therefore, the fibers of the steel beams was yielded in tension in this location.

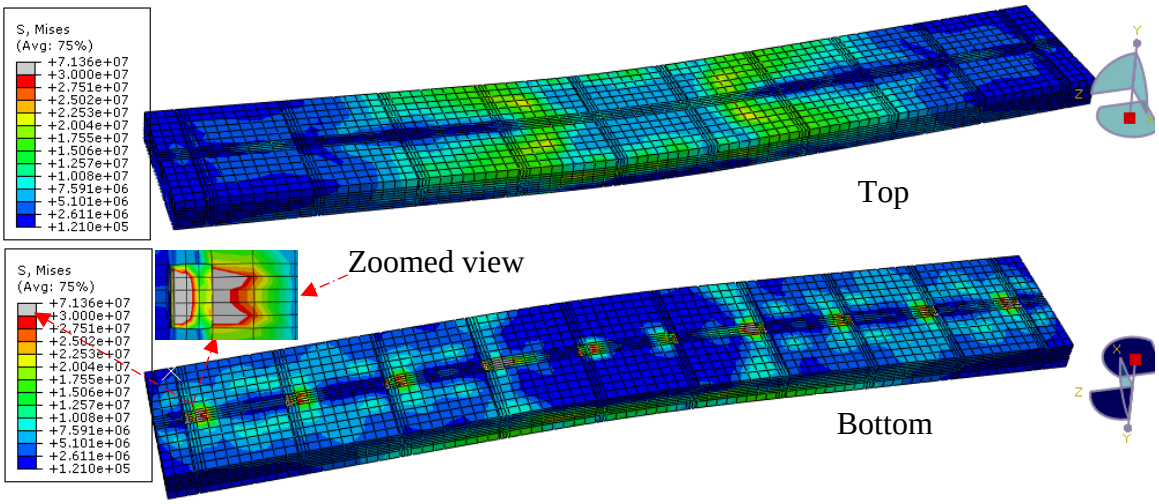

a) BCH1 concrete slab

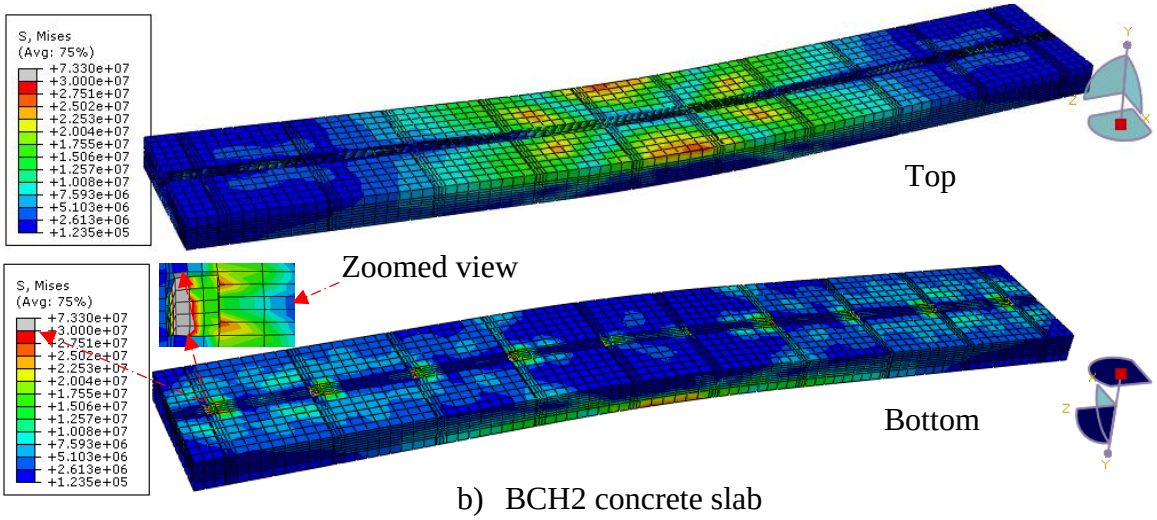

b) BCH2 concrete slab

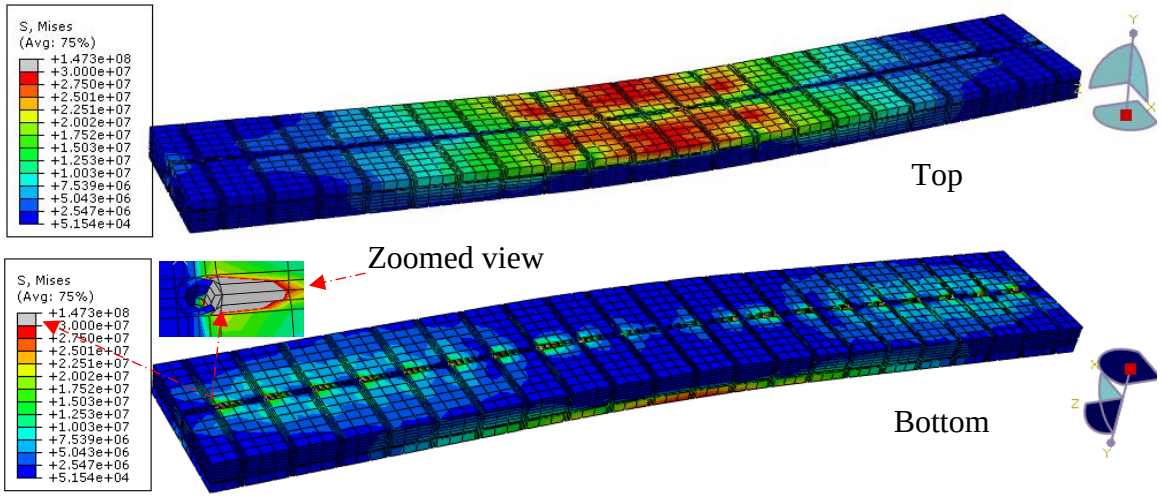

c) BST1 concrete slab

Figure 6.17: Mises stress distribution at the concrete slabs.

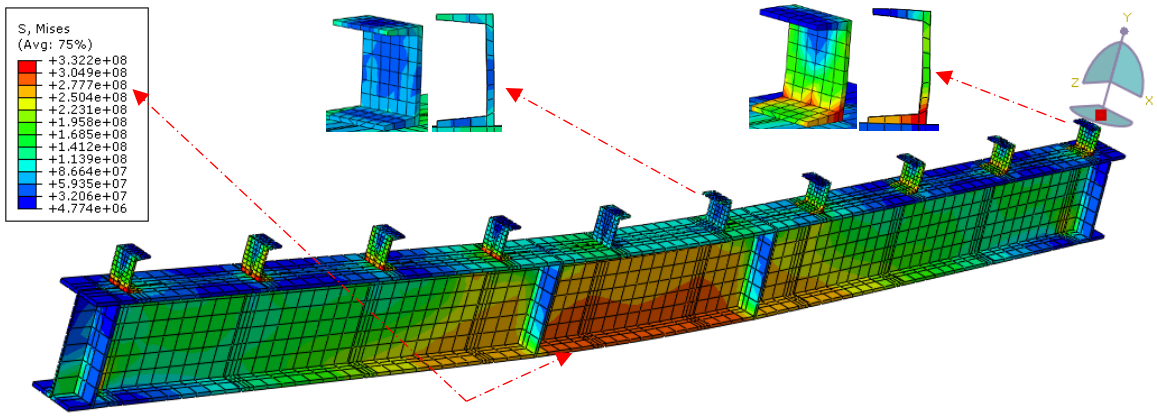

a) BCH1 steel beam with shear channels

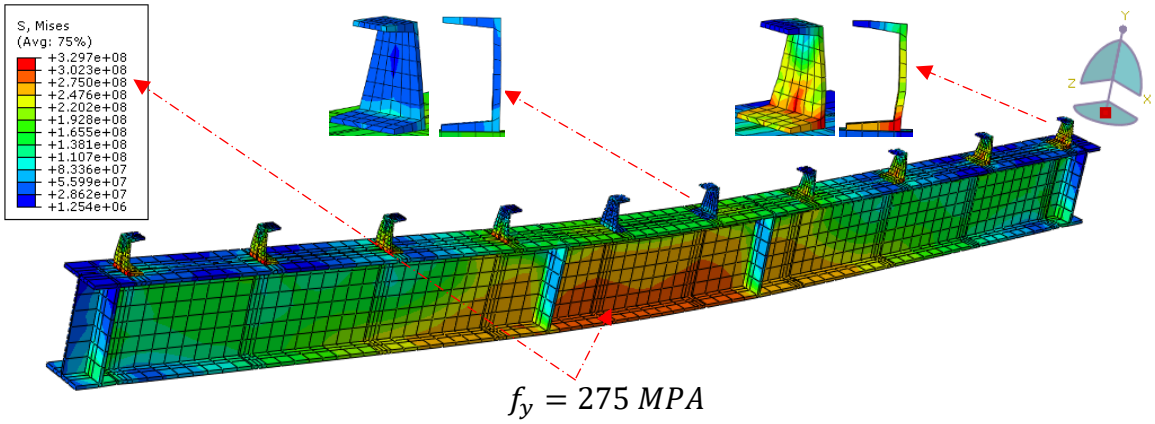

b) BCH2 steel beam with shear channels

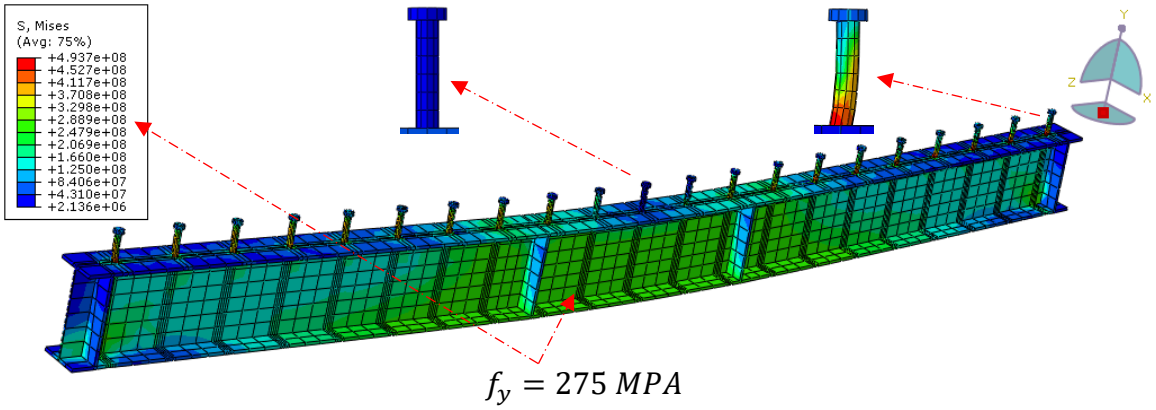

c) BST1 steel beam with headed studs

Figure 6.18: Mises stress distribution at steel beams and shear connectors.

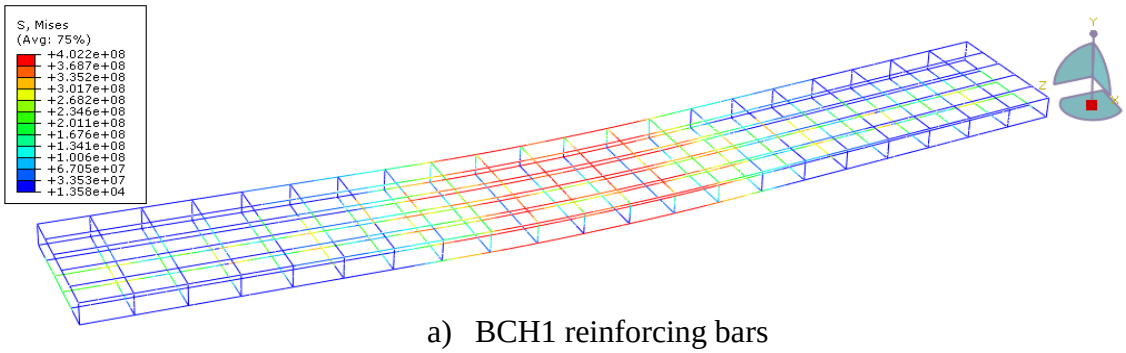

a) BCH1 reinforcing bars

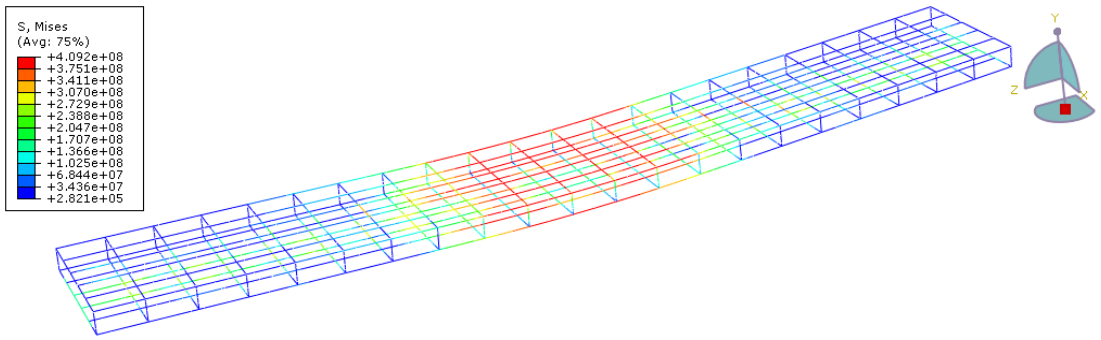

b) BCH2 reinforcing

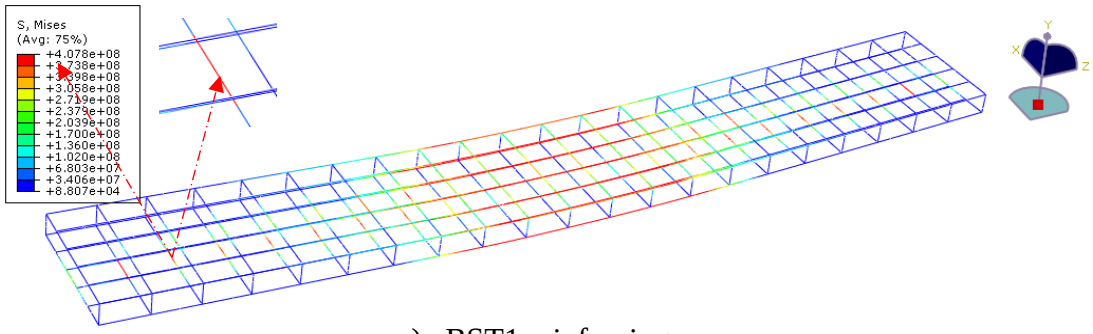

c) BST1 reinforcing

Figure 6.19: Mises stress distribution at the reinforcing bars.

In contrast, Mises stress distribution was higher above the bottom flange of shear channels and in the bottom of the stud shanks, as shown in the zoomed views of Fig 6.18 (a), (b), and (c). Stress contours shown in these figures give over 327 MPa and 411 MPa of stress for shear channels and stud connectors, respectively. Therefore, the bending deformation of connectors was observable in their lower parts. It can be noted that the edge connectors experienced greater bending deformation, while the mid-span connectors remained almost in their initial shape.

c) Reinforcing bars: Misses stress distribution at the reinforcing bars of the three specimens is demonstrated in Fig 6.19 (a), (b), and (c). From these figures, it can be seen that a concentration of the maximum stresses appeared at the mid-span of the reinforcing bars for the three specimens. In addition, the stress was greater also at the lower reinforcing bars located in front

of stud connectors for the BST1 specimen, as shown in Fig 6.19 (c). These maximum stresses are over the yield strength of the reinforcing bars, which is 392 MPa. Therefore, the yielding of reinforcing bars was where appeared the maximum stresses.

6.5- Parametric study

6.5.1- Effect of connection degree

As mentioned earlier, to achieve full/partial composite action, the shear connection capacity of each connector obtained in the experimental push-out tests and the equation 1.20 (see chapter own) are employed to calculate the different degrees of connection η. Five models with different degrees of the shear connection were analyzed to evaluate the influence of connection degree, as shown in Fig 6.20. The connection at the steel-concrete interface of the composite beams is achieved using the CH2 shaped shear channel as in the composite beam BCH2.

The shear channels number, the distance between them, and the ultimate load capacity for each beam are summarized in Table 6.5. However, Figure 6.21 presents the load-deflection curves of the five composite beams with different shear connection degrees. It can be seen that the composite beam with the degree of connection η= 0.8 carried almost the same ultimate load capacity as the composite beam with full connection. But, the ultimate load capacity decreased by about 7% and 11% when the degree of connection decreased to η= 0.6 and η= 0.4, respectively. Finally, the ultimate load capacity significantly decreased by around 40% when the composite beam was without connection (η= 0), and the deflection was the smallest as well.

On the other hand, the slip distribution at the steel-concrete interface of the composite beam for different degrees of connection and in the maximum deflection is presented in Fig 6.22. This figure shows that the slip values are maximum near the supports and weak in the mid-span. In addition, by comparison between the curves, it can be concluded that both curves of the composite beam with full and 80% (η= 0.8) connection degree reached almost the same slip values, and their maximum slip values were around 4.8 mm. In contrast, the slip values of the composite beam with 60% and 40% connection degree were greater than those with full and 80% connection degree, and their maximum slip values were about 6.17 and 7.1 mm, respectively. It can be noted that the maximum slip value, which was 7.1 mm, is less than that supported by the CH2 shape channel on the push-out tests. As for the composite beam without connection, their slip values were significantly greater and the maximum slip value, in this case, exceeds 12 mm.

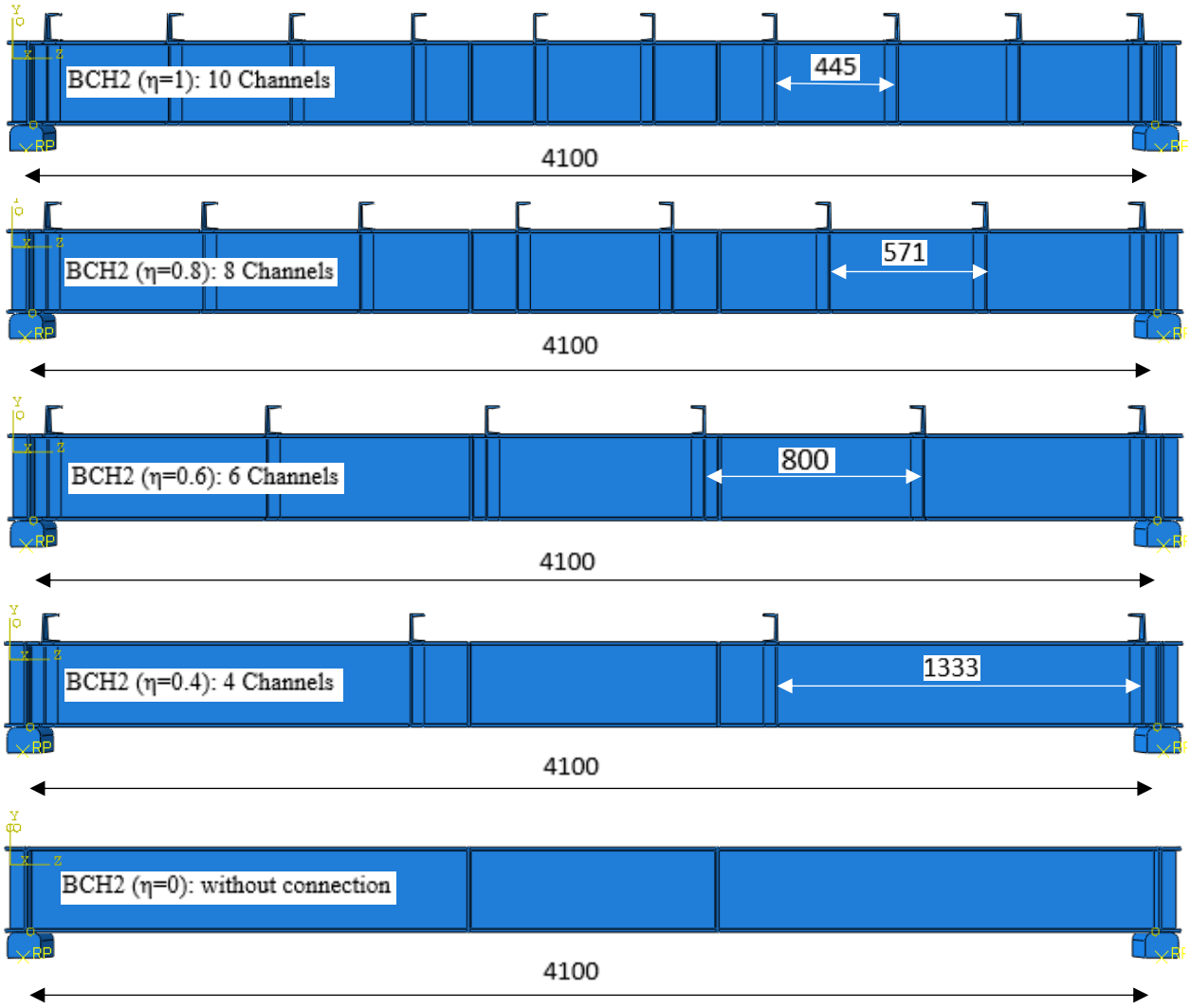

Figure 6.20: Geometric and connection degrees.

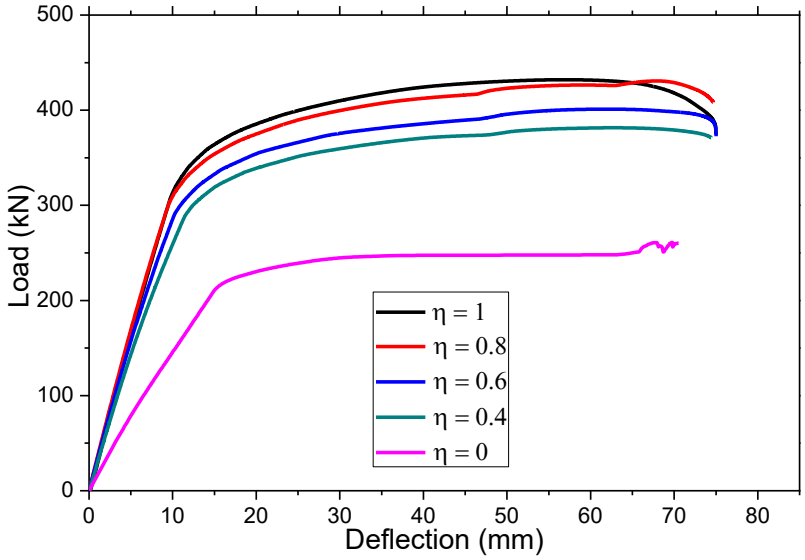

Figure 6.21: Load–deflection responses of the specimens with different shear connection degrees.

Table 6.5: Results of composite beam BCH2 with five different connection degrees.

Specimen	Concrete strength (MPa)	Connection degree η	Shear channels number (mm)	Shear channels distance	Ultimate load (kN)
BCH2	30	1	10	445	432.01
		0.8	8	571	430.73
		0.6	6	800	401.08
		0.4	4	1333	381.53
		0	0	-	260.94

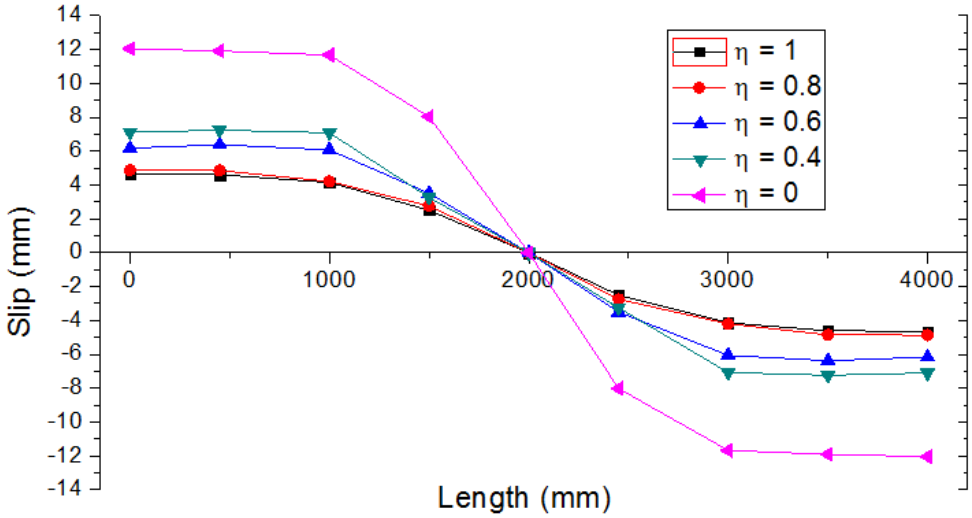

Figure 6.22: Slip distribution along the composite beam BCH2 with five different connection degrees.

6.5.2- Effect of concrete strength

To evaluate the influence of the concrete compressive strength on the performance of composite beam BCH2, three different strengths of concrete 20 MPa, 30 MPa, and 40 MPa were used. The load-deflection curves are illustrated in Fig. 6.23. Whereas, the results of ultimate load capacity and the deflection value δ_d, obtained are shown in Table 6.6. As in the sections above, the ultimate load capacity is defined according to the maximal value in the load-deflection curve, and the value δ_d is its corresponding deflection.

As indicated in Table 6.5, the ultimate load capacity increased with the increase of concrete strength from 20 to 40 MPa, where the increase in the compressive strength of concrete from 20 MPa to 30 MPa, provides an increase in the ultimate load capacity from 230.32 kN to

299.45 kN this is over 9%. Then, when the compressive strength of the concrete increased from 30 MPa to 40 MPa, the ultimate load capacity increased by only 6.5% to reach 460.24 kN.

On the other side, the effect of the concrete compressive strength on the deflection value δ_d is similar to its effect on the ultimate load capacity. In which, the composite beam with a concrete compressive strength of 20 MPa carried about 14% lower deflection than that with a 30 MPa concrete strength. While increasing the concrete compressive strength of this composite beam from 30 MPa to 40 MPa led to an increase by over 8 % of its deflection value δ_d.

Table 6.6: Results of composite beam BCH2 with three different compressive strengths.

Specimen	Concrete strength (MPa)	FE results	
		Ultimate load (kN)	Deflection $\delta_d(mm)$
BCH2	20	395.44	49.96
	30	432.01	57
	40	460.24	61.81

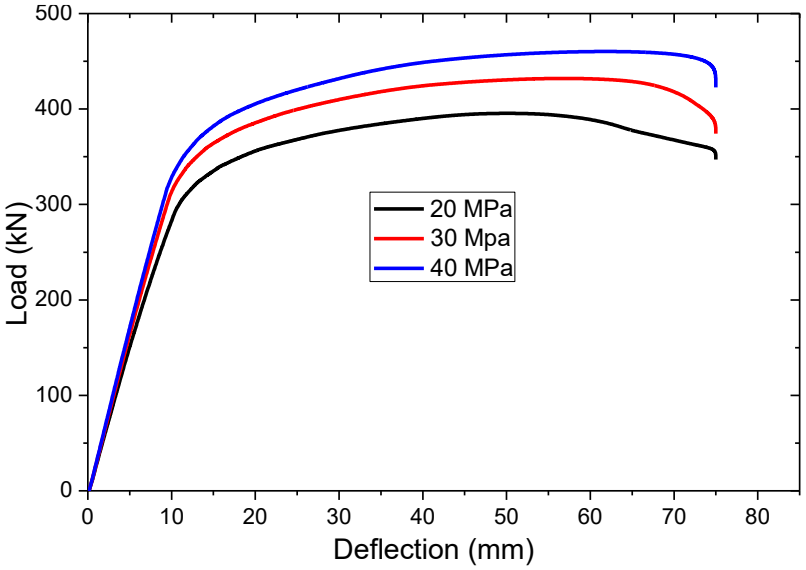

Figure 6.23: Effect of the concrete compressive strength.

6.5.3- Effect of the connectors' steel grade.

The BCH2 composite beam was used, as well, to investigate the influence of the connector's steel grade. As in the push-out test, the results of connectors' steel with a yield strength of 327 MPa, were compared against those of S235 steel grade. Figure 6.24 shows the load-slip curves,

while Table 6.7 is summarized the results of ultimate load P_u and the corresponding deflection δ_d. From these results, it can conclude that the decrease in the steel grade of CH2 shape connectors by about 28% does not affect the performance of the composite beam.

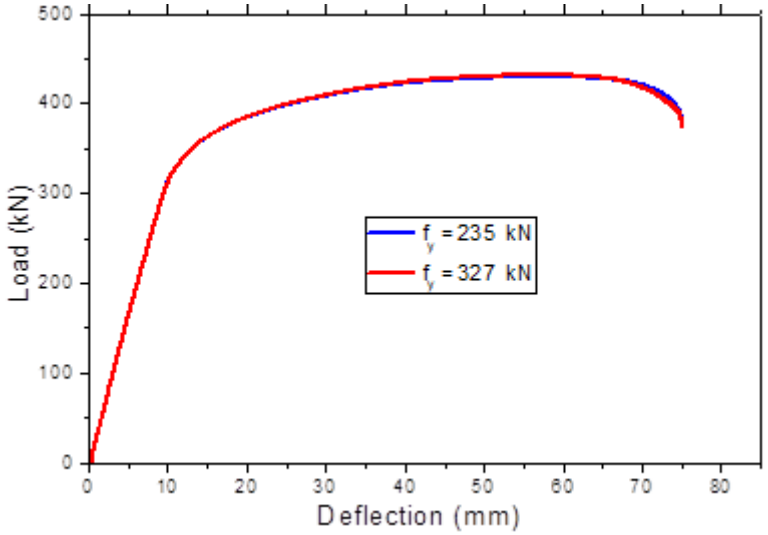

Figure 6.24: effect of the connectors' grade.

Table 6.7: Results of composite beam BCH2 with two different steel grade.

Specimens	Yield strength f_y(MPa)	Ultimate strength f_u(MPa)	Ultimate load P_u (kN)	Corresponding deflection δ_d (mm)
BCH2	235	360	430.13	57.32
	327	481	432	57

6.6- Conclusion

A 3D finite element model has been developed in this chapter for steel-concrete composite beams to investigate the connection performance of three types of shear connectors. The connectors investigated are headed stud connector ST1, ordinary channel connector shape CH1, and the new channel connector shape CH2. Furthermore, the effect of connection degree, concrete strength, and connectors' steel grade were studied. The following conclusions can be drawn from this study.

1) The developed FE model can obtain the load-deflection behavior and the slip at the steel-concrete interface of composite beams under the 3-point and 4-point bending tests. In addition, this developed FE model can successfully capture different types of failure

modes of composite beams, such as bending deformation and shear failure of connectors, concrete crushing failure, steel beam failure, and reinforcing bars failure.

2) The ultimate load capacity of the full-connection composite beam with the new channel connectors shape CH2 was slightly less than those with CH1 ordinary channels and ST1 headed studs. Meanwhile, the corresponding deflection δ_d of the BCH2 specimen was higher than that of the BCH1 specimen and lower than that of the BST1 specimen. Also, the slip values at the steel-concrete interface of the BCH2 specimen were between those of the two other specimens.
3) The main failure modes observed at the collapse load were the bending deformation of connectors and concrete crushing due to the large compressive stress at the mid-span and in front of the bottom of the connectors accompanied by the yielding of steel beam at the mid-span.
4) In general, the performance of the composite beam with the new channel shape CH2 is nearly similar to those of the other two composite beams.
5) Each of the connection degrees and the concrete strength significantly affects the overall behavior of the steel-concrete composite beam. Meanwhile, the connectors 'steel grade does not affect the behavior of composite beams.

Conclusions and Recommendations

Conclusions

New shapes of the shear channel and headed stud connectors were proposed and investigated in this thesis. The experimental investigation involved the testing of 20 push-out and 3 pull-out specimens under monotonic loading to evaluate the effect of various parameters. The push-out tests were carried out using a newly developed setup. In the second part of this thesis, the specimens that achieved the best performance in the first part were investigated numerically and compared with those from the experimental tests. Furthermore, the nonlinear behavior of some shear connectors in the steel-concrete composite beam is numerically studied. The following conclusions can be drawn from this investigation:

1. The new setup was useful and safe during all push-out tests. Many advantages were provided by using the new push-out setup such as; i) concentrating the load on the flange where the shear plane is located; hence, the eccentricity problem is avoided. ii) Ensuring the movement between the two elements (steel-concrete) in one direction only. iii) Reduce the specimen weight to half, thereby minimizing the cost and the time of specimen preparation.
2. The proposed new channel shear connector shapes CH2 and CH6 achieved better strength-ductility performance than the ordinary shape. In addition, these two shapes experienced a lower effect on the concrete slab and provided more space for the placement of reinforcing bars. Meanwhile, the CH2 shape costs less than 25% of the ordinary channel connector shape. Based on the pull-out results the reduction of the channel shear connector head in the two new shear channels (CH2 and CH6) does not impact its ability to prevent concrete slab uplift.
3. The new shape of the headed stud (ST3) has better deformation and better ductility than the ordinary stud shape. However, using the procedure of concrete slab clamping mechanism increased the ultimate strength by about 11% and slightly increased the ultimate slip (3%).
4. Requirements of Eurocode- 4 for an ideal plastic behavior of the shear connection is 6 mm slip. But previous researches discovered that in some cases of partial shear connection, propped construction, longer spans, and the unequal flanges of the steel section slip demand in the shear connection at the ultimate limit state is higher than this value. Therefore, the two new shapes of channel shear connectors (CH2, CH6) and the new stud shape ST3 can be beneficial for steel-concrete composite beams with the above cases.
5. In terms of bearing capacity, the empirical equation of channel shear connectors developed by (Pashan 2006) [31] agrees well with the test results. As for the headed studs, the results

of the empirical equation proposed by American National Standard ANSI/AISC 360-05 [29] are in accord with the test results.

6. The finite element model predicted the shear connection capacity, load-slip behavior, and failure modes of the push-out test. The results obtained from finite element analysis were validated against those of the experimental tests. It was observed that the results showed close agreement with experimental results in terms of shear connector capacity and failure modes. In addition, the parametric study showed that the concrete compressive strength significantly governed the ultimate load capacity of shear connectors. While the connector's steel grade does not have a significant effect on ultimate load capacity.
7. The behavior of the new channel shear connector shape CH2, which has economic benefits and good performance in the push-out tests was studied and compared with those of ordinary channel and stud connectors using a 3D finite element model of a simply-supported steel-concrete composite beam. The results showed that the performance of the composite beam with the new channel shape CH2 is mostly identical to those of the ordinary CH1 and ST1 connectors in terms of load-deflection performance. According to the Mises stress distribution, this new connector shape (CH2) provided a lower effect on the concrete slab. On the other hand, both connection degrees and the concrete strength significantly affects the overall behavior of the steel-concrete composite beam. Meanwhile, the steel grade of the connectors has no effect.

Recommendations and suggestions

a) Push out test

1. As a recommendation for future research, using a concrete slab clamping mechanism in the push-out test does not provide the correct results.
2. Using a single concrete slab provides many advantages.

b) Channel shear connector

Due to the economic advantage and the above results of the new channel connector shape CH2 the following recommendations are provided for future research to better understand its behavior:

1) Further experimental investigations on CH2 channel shape are required to investigate the effect of lower and higher concrete grades.
2) The effect of this new shape with various heights and lengths could be studied.
3) The effect of this new shape in metal deck composite slabs needs to be investigated.

4) The behavior of this new shape in steel-concrete composite beams could be experimentally investigated.
5) A 3D finite element composite beams model with a longer span, partial shear connection, and the unequal flanges of the steel section must be developed to investigate the higher slip effect of this shape.

c) Headed stud shear connector

Studying a large stud by modifying its shape is necessary for the possible practical application of large-headed stud connectors.

References

[1] F. Tout, "Experimental study of composite bonded structures: effect of creep, fatigue and durability," University Claude Bernard-Lyon I, 2014.

[2] D. J. Oehlers, *Composite steel and concrete structural members: fundamental behaviour*: Pergamon, 1995.

[3] D. Oehlers, D. J. Oehlers, and M. A. Bradford, *Elementary behaviour of composite steel and concrete structural members*: Elsevier, 1999.

[4] D. Oehlers and C. Coughlan, "The shear stiffness of stud shear connections in composite beams," *Journal of Constructional Steel Research,* vol. 6, pp. 273-284, 1986.

[5] I. M. Viest, "Full-scale tests of channel shear connectors and composite t-beams," University of Illinois at Urbana Champaign, College of Engineering …1951.

[6] S. Maleki and S. Bagheri, "Behavior of channel shear connectors, Part I: Experimental study," *Journal of Constructional Steel Research,* vol. 64, pp. 1333-1340, 2008.

[7] M. Shariati, N. Ramli Sulong, M. Arabnejad, and M. Mahoutian, "Shear resistance of channel shear connectors in plain, reinforced and lightweight concrete," *Scientific research and essays,* vol. 6, pp. 977-983, 2011.

[8] M. Shariati, N. R. Sulong, A. Shariati, and A. Kueh, "Comparative performance of channel and angle shear connectors in high strength concrete composites: An experimental study," *Construction and Building Materials,* vol. 120, pp. 382-392, 2016.

[9] M. Shariati, F. Tahmasbi, P. Mehrabi, A. Bahadori, and A. Toghroli, "Monotonic behavior of C and L shaped angle shear connectors within steel-concrete composite beams: an experimental investigation," *Steel Compos Struct,* vol. 35, pp. 237-247, 2020.

[10] Q. Zhao, Y. Du, Y. Peng, C. Xu, and G. Huang, "Shear Performance of Short Channel Connectors in a Steel-UHPC Composite Deck," *International Journal of Steel Structures,* vol. 20, pp. 300-310, 2020.

[11] J. Ollgaard, R. Slutter, and J. Fisher, "Shear strength of stud connectors in lightweight and normal weight concrete, AISC Eng'g Jr., April 1971 (71-10)," ed: Fritz Laboratory Reports. Paper, 2010.

[12] D. Oehlers and L. Foley, "The fatigue strength of stud shear connections in composite beams," *Proceedings of the Institution of Civil Engineers,* vol. 79, pp. 349-364, 1985.

[13] L. An and K. Cederwall, "Push-out tests on studs in high strength and normal strength concrete," *Journal of constructional steel research*, vol. 36, pp. 15-29, 1996.

[14] Q. Han, Y. Wang, J. Xu, and Y. Xing, "Static behavior of stud shear connectors in elastic concrete–steel composite beams," *Journal of Constructional Steel Research,* vol. 113, pp. 115-126, 2015.

[15] Y. Xing, Q. Han, J. Xu, Q. Guo, and Y. Wang, "Experimental and numerical study on static behavior of elastic concrete-steel composite beams," *Journal of Constructional Steel Research,* vol. 123, pp. 79-92, 2016.

[16] X. Xu, Y. Liu, and J. He, "Study on mechanical behavior of rubber-sleeved studs for steel and concrete composite structures," *Construction and Building Materials*, vol. 53, pp. 533-546, 2014.

[17] C. Xu and K. Sugiura, "Analytical investigation on failure development of group studs shear connector in push-out specimen under biaxial load action," *Engineering Failure Analysis*, vol. 37, pp. 75-85, 2014.

[18] V. Abaqus, "6.14-1. Abaqus/standard user's manual and Abaqus CAE manual," *Providence, RI, USA: Dassault Systemes Simulia Corp,* 2014.

[19] N. Loqman, N. A. Safiee, N. A. Bakar, and N. A. M. Nasir, "Structural Behavior of Steel-Concrete Composite Beam using Bolted Shear Connectors: A Review," in *MATEC Web of Conferences*, 2018, p. 06010.

[20] J. Bujnak, "Global analysis of steel-concrete composite beams-Analytical approach and nonlinear modelling," Blaise Pascal University, Clermont, 2007.

[21] K. Chung, "Composite beams and floor systems fully integrated with building services," Progress in Structural Engineering and Materials, vol. 4, pp. 169-178, 2002.

[22] R. Seracino, "Partial-interaction Behaviour of Composite Steel-concrete Bridge Beams Subjected to Fatigue Loading," University of Adelaide, Department of Civil and Environmental Engineering, 1999.

[23] R. Johnson, N. Molenstra, and EPPIB, "Partial shear connection in composite beams for buildings," *Proceedings of the Institution of Civil Engineers*, vol. 91, pp. 679-704, 1991.

[24] F. Leonhardt, W. Andrä, H. P. Andrä, and W. Harre, "Neues, vorteilhaftes Verbundmittel für Stahlverbund-Tragwerke mit hoher Dauerfestigkeit," *Beton-und Stahlbetonbau*, vol. 82, pp. 325-331, 1987.

[25] A. Mazoz, A. Benanane, and M. Titoum, "Push-out tests on a new shear connector of I-shape," *International journal of steel structures*, vol. 13, pp. 519-528, 2013.

[26] M. Crisinel, "Push-out tests of steel-concrete connections with Hilti connectors," 1983.

[27] E. C. f. Standardization, "Eurocode 4: Design of composite steel and concrete structures—Part 1.1: General rules and rules for buildings," ed, 2004.

[28] "GB 50017—2003. Design of steel structures [S]. (in Chinese)."

[29] ANSI-AISC, "Specification for Structural Steel Buildings," *An American National Standard*, 2005.

[30] C. S. Association, *Limit states design of steel structures*: Canadian Standards Association, 2001.

[31] A. Pashan, "Behaviour of channel shear connectors: push-out tests," University of Saskatchewan, 2006.

[32] E. Baran and C. Topkaya, "An experimental study on channel type shear connectors," *Journal of Constructional Steel Research*, vol. 74, pp. 108-117, 2012.

[33] EN, "1-1. Eurocode 2: Design of concrete structures–Part 1-1: General rules and rules for buildings," *European Committee for Standardization (CEN)*, 2004.

[34] E. DIN, "6892-1: 2017-02: Metallic materials-Tensile testing-Part 1: Method of test at room temperature (ISO 6892-1: 2016)," ed: Beuth Verlag, 2017.

[35] E. 3, "Design of steel structures," *Part 1-8: Design of joints*, 2005.

[36] d. a. LabVIEW: A software system for data acquisition, and instrument control.

[37] B. Maghaghi, M. Titoum, and A. Mazoz, "Experimental evaluation of new channel shear connector shapes," *International Journal of Steel Structures*, vol. 21, pp. 883-900, 2021.

[38] Z.-h. Zhu, L. Zhang, Y. Bai, F.-x. Ding, J. Liu, and Z. Zhou, "Mechanical performance of shear studs and application in steel-concrete composite beams," *Journal of Central South University*, vol. 23, pp. 2676-2687, 2016.

[39] A. Prakash, N. Anandavalli, C. Madheswaran, and N. Lakshmanan, "Modified push-out tests for determining shear strength and stiffness of HSS stud connector-experimental study," *International Journal of Composite Materials*, vol. 2, pp. 22-31, 2012.

[40] F. Tahmasbi, S. Maleki, M. Shariati, N. Ramli Sulong, and M. Tahir, "Shear capacity of C-shaped and L-shaped angle shear connectors," *PloS one*, vol. 11, p. e0156989, 2016.

[41] Y. Liu, Q. Zhang, Y. Bao, and Y. Bu, "Static and fatigue push-out tests of short headed shear studs embedded in Engineered Cementitious Composites (ECC)," *Engineering Structures*, vol. 182, pp. 29-38, 2019.

[42] J.-S. Kim, J. Kwark, C. Joh, S.-W. Yoo, and K.-C. Lee, "Headed stud shear connector for thin ultrahigh-performance concrete bridge deck," *Journal of Constructional Steel Research*, vol. 108, pp. 23-30, 2015.

[43] K. Naithani, V. Gupta, and A. Gadh, "Behaviour of shear connectors under dynamic loads," *Materials and structures*, vol. 21, pp. 359-363, 1988.

[44] C. Topkaya, J. A. Yura, and E. B. Williamson, "Composite shear stud strength at early concrete ages," *Journal of structural engineering*, vol. 130, pp. 952-960, 2004.

[45] D. Lowe, R. Das, and C. Clifton, "Characterization of the splitting behavior of steel-concrete composite beams with shear stud connection," *Procedia materials science,* vol. 3, pp. 2174-2179, 2014.

[46] P. Arıkoğlu, E. Baran, and C. Topkaya, "Behavior of channel connectors in steel-concrete composite beams with precast slabs," *Journal of Constructional Steel Research,* vol. 172, p. 106167, 2020.

[47] M. Shariati, A. Shariati, N. R. Sulong, M. Suhatril, and M. A. Khanouki, "Fatigue energy dissipation and failure analysis of angle shear connectors embedded in high strength concrete," *Engineering Failure Analysis,* vol. 41, pp. 124-134, 2014.

[48] G. Kwon, M. D. Engelhardt, and R. E. Klingner, "Parametric studies and preliminary design recommendations on the use of postinstalled shear connectors for strengthening noncomposite steel bridges," *Journal of Bridge Engineering,* vol. 17, pp. 310-317, 2012.

[49] N. Fanaie, F. G. Esfahani, and S. Soroushnia, "Analytical study of composite beams with different arrangements of channel shear connectors," *Steel and Composite Structures,* vol. 19, pp. 485-501, 2015.

[50] A. Toghroli, M. Mohammadhassani, M. Suhatril, M. Shariati, and Z. Ibrahim, "Prediction of shear capacity of channel shear connectors using the ANFIS model," *Steel Compos Struct,* vol. 17, pp. 623-639, 2014.

[51] A. Zona and G. Ranzi, "Shear connection slip demand in composite steel–concrete beams with solid slabs," *Journal of Constructional Steel Research,* vol. 102, pp. 266-281, 2014.

[52] X. Xu and Y. Liu, "Analytical prediction of the deformation behavior of headed studs in monotonic push-out tests," *Advances in Structural Engineering,* vol. 22, pp. 1711-1726, 2019.

[53] W. Xue, M. Ding, H. Wang, and Z. Luo, "Static behavior and theoretical model of stud shear connectors," *Journal of bridge engineering,* vol. 13, pp. 623-634, 2008.

[54] X. Xu and Y. Liu, "Analytical and numerical study of the shear stiffness of rubber-sleeved stud," *Journal of Constructional Steel Research,* vol. 123, pp. 68-78, 2016.

[55] Q. Han, Y. Wang, J. Xu, Y. Xing, and G. Yang, "Numerical analysis on shear stud in push-out test with crumb rubber concrete," *Journal of Constructional Steel Research,* vol. 130, pp. 148-158, 2017.

[56] M. Titoum, A. Mazoz, A. Benanane, and D. Ouinas, "Experimental study and finite element modelling of push-out tests on a new shear connector of I-shape," *Advanced Steel Construction,* vol. 12, pp. 487-506, 2016.

[57] T. Jankowiak and T. Lodygowski, "Identification of parameters of concrete damage plasticity constitutive model," *Foundations of civil and environmental engineering,* vol. 6, pp. 53-69, 2005.

[58] J. Qureshi and D. Lam, "Behaviour of headed shear stud in composite beams with profiled metal decking," *Advances in Structural Engineering,* vol. 15, pp. 1547-1558, 2012.

[59] A. Prakash, N. Anandavalli, C. Madheswaran, J. Rajasankar, and N. Lakshmanan, "Three dimensional FE model of stud connected steel-concrete composite girders subjected to monotonic loading," *International Journal of Mechanics and Applications,* vol. 1, pp. 1-11, 2011.

[60] M. Hafezolghorani, F. Hejazi, R. Vaghei, M. S. B. Jaafar, and K. Karimzade, "Simplified damage plasticity model for concrete," *Structural Engineering International,* vol. 27, pp. 68-78, 2017.

[61] Y. Luo, K. Hoki, K. Hayashi, and M. Nakashima, "Behavior and strength of headed stud–SFRCC shear connection. II: Strength evaluation," *Journal of Structural Engineering,* vol. 142, p. 04015113, 2016.

[62] J. Cao and X. Shao, "Finite element analysis of headed studs embedded in thin UHPC," *Journal of Constructional Steel Research,* vol. 161, pp. 355-368, 2019.

[63] G. Ranzi, M. Bradford, P. Ansourian, A. Filonov, K. Rasmussen, T. Hogan, *et al.*, "Full-scale tests on composite steel–concrete beams with steel trapezoidal decking," *Journal of Constructional Steel Research,* vol. 65, pp. 1490-1506, 2009.

[64] C. Amadio, C. Fedrigo, M. Fragiacomo, and L. Macorini, "Experimental evaluation of effective width in steel–concrete composite beams," *Journal of Constructional Steel Research*, vol. 60, pp. 199-220, 2004.

[65] S. Al-deen, G. Ranzi, and Z. Vrcelj, "Full-scale long-term and ultimate experiments of simply-supported composite beams with steel deck," *Journal of Constructional Steel Research*, vol. 67, pp. 1658-1676, 2011.

[66] D. Fa-xing, L. Jing, L. Xue-mei, Y. Zhi-wu, and L. Yong-suo, "Experimental investigation on hysteretic behavior of simply supported steel-concrete composite beam," *Journal of Constructional Steel Research*, vol. 144, pp. 153-165, 2018.

[67] F. Tahmasebinia, G. Ranzi, and A. Zona, "Beam tests of composite steel-concrete members: A three-dimensional finite element model," *International Journal of Steel Structures*, vol. 12, pp. 37-45, 2012.

[68] B. Wang, Q. Huang, X. Liu, and W. Li, "Experimental investigation of steel-concrete composite beams with different degrees of shear connection under monotonic and fatigue loads," *Advances in Structural Engineering*, vol. 21, pp. 227-240, 2018.

ANNEX A

Load-slip curves of some specimens from the LabVIEW program interface

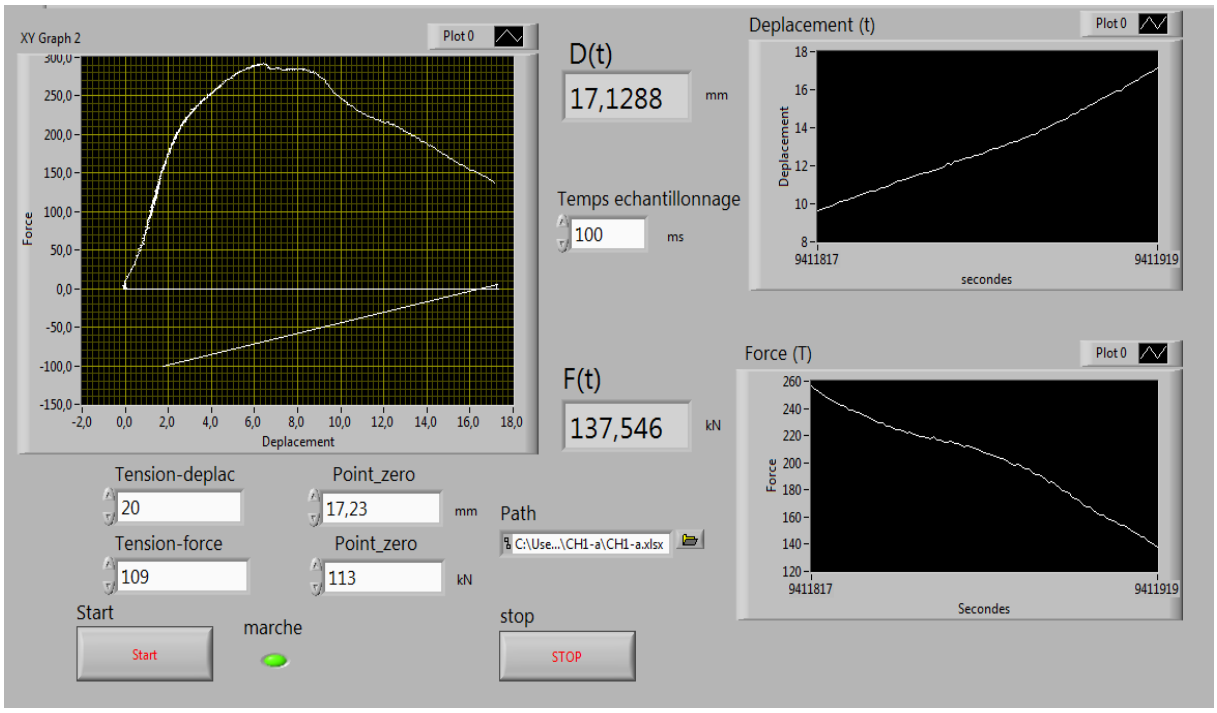

Figure A.1: CH1-a specimen.

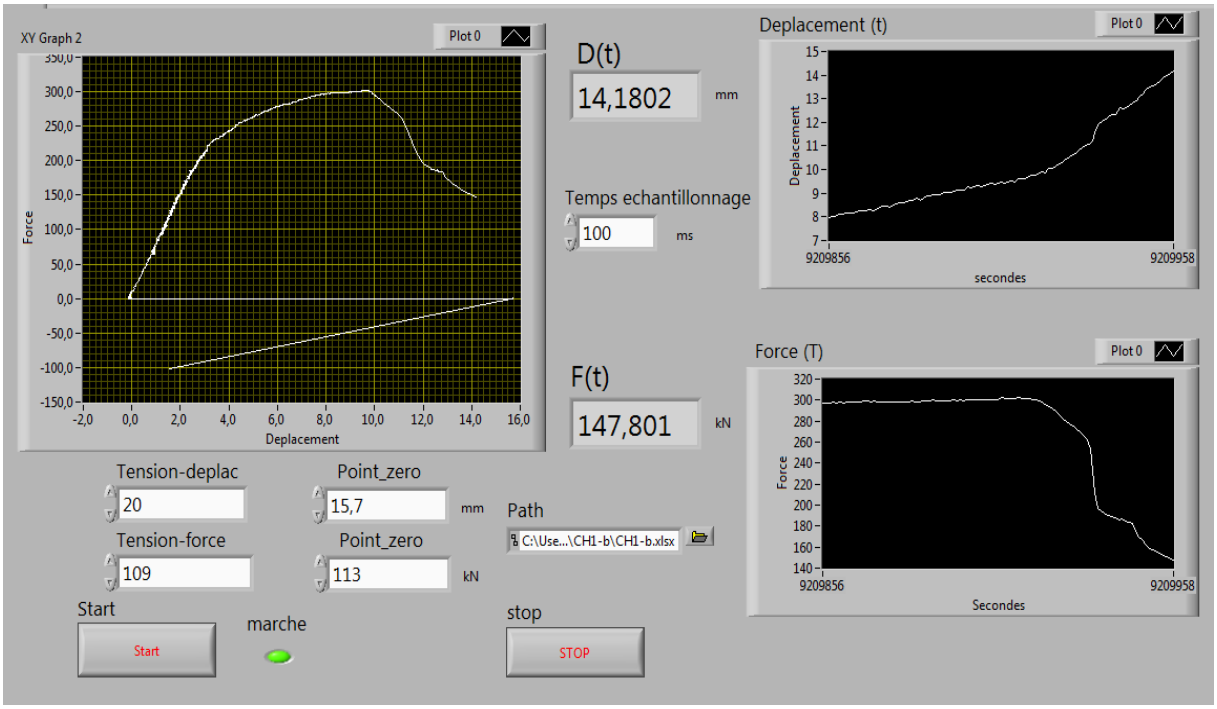

Figure A.2: CH1-b specimen.

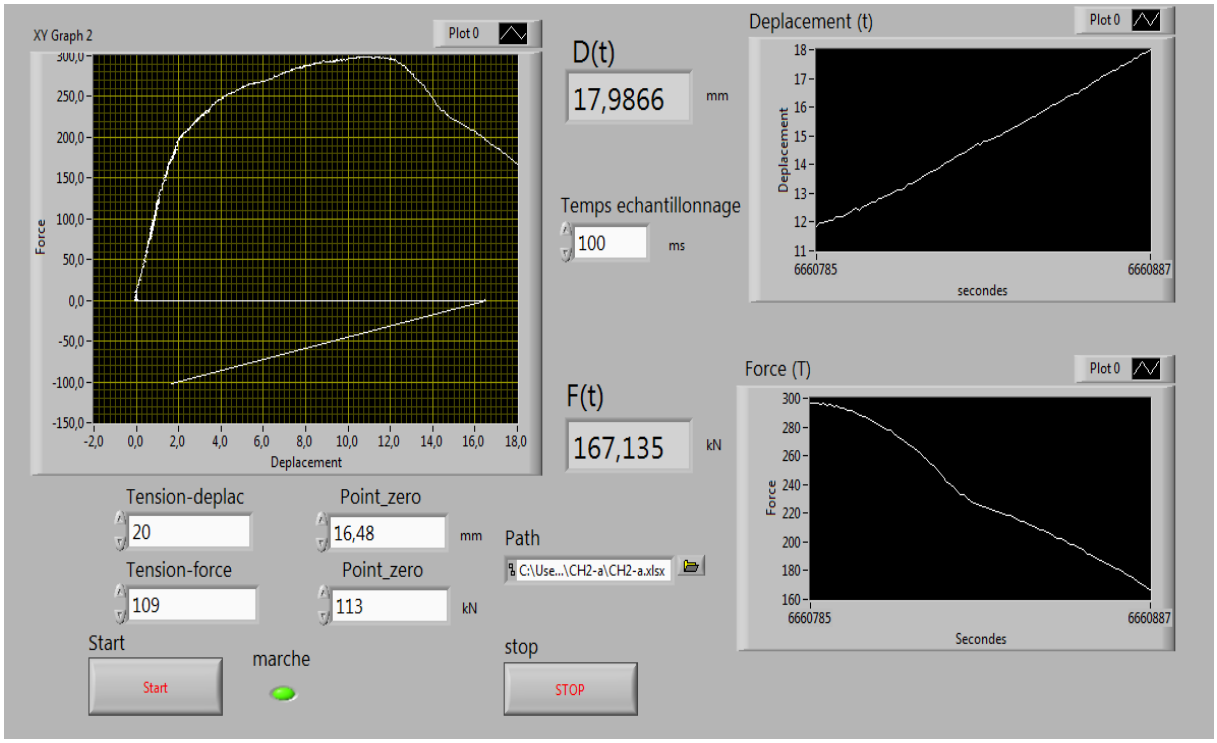

Figure A.3: CH2-a specimen.

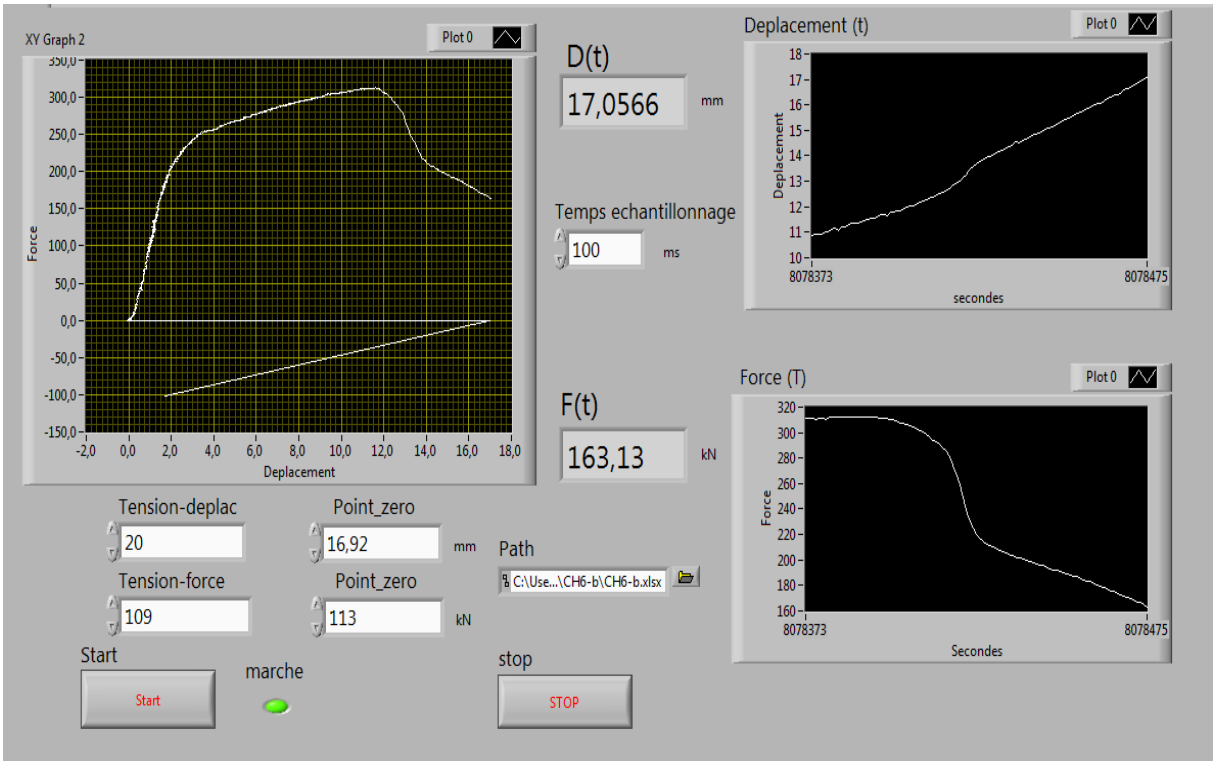

Figure A.4: CH6-b specimen.

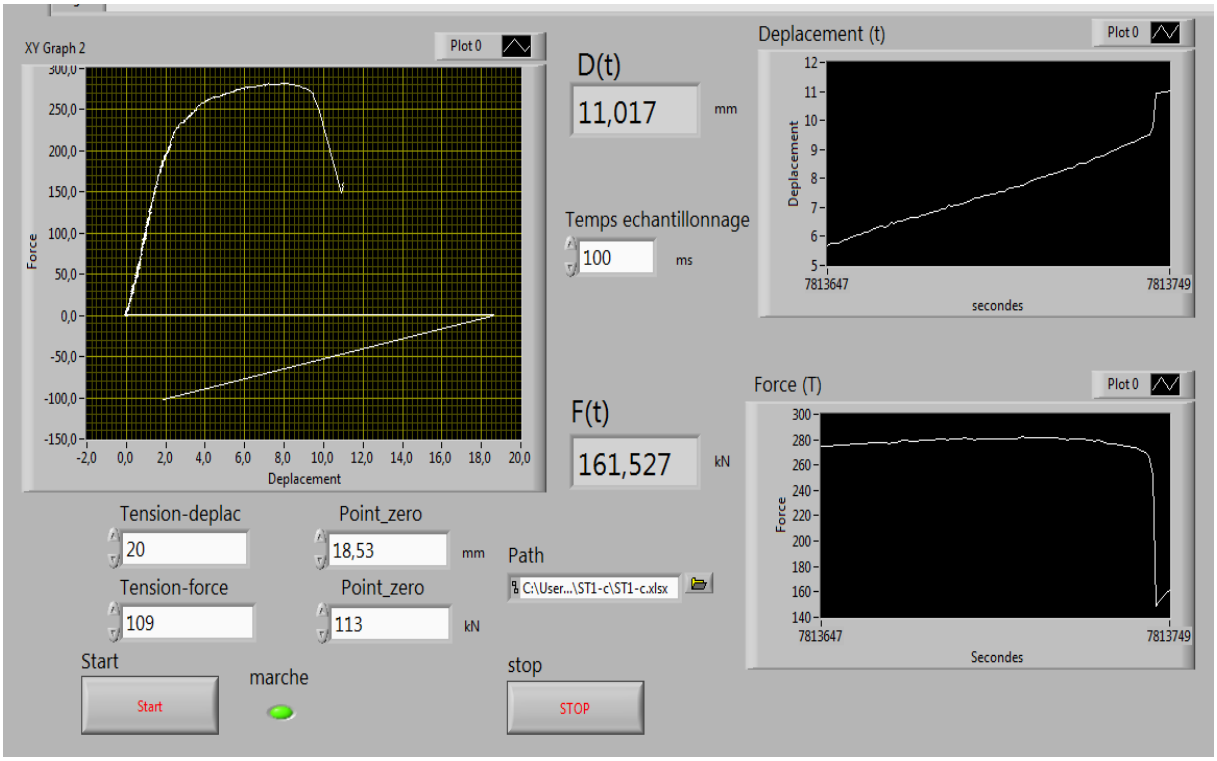

Figure A.5: ST1-c specimen.

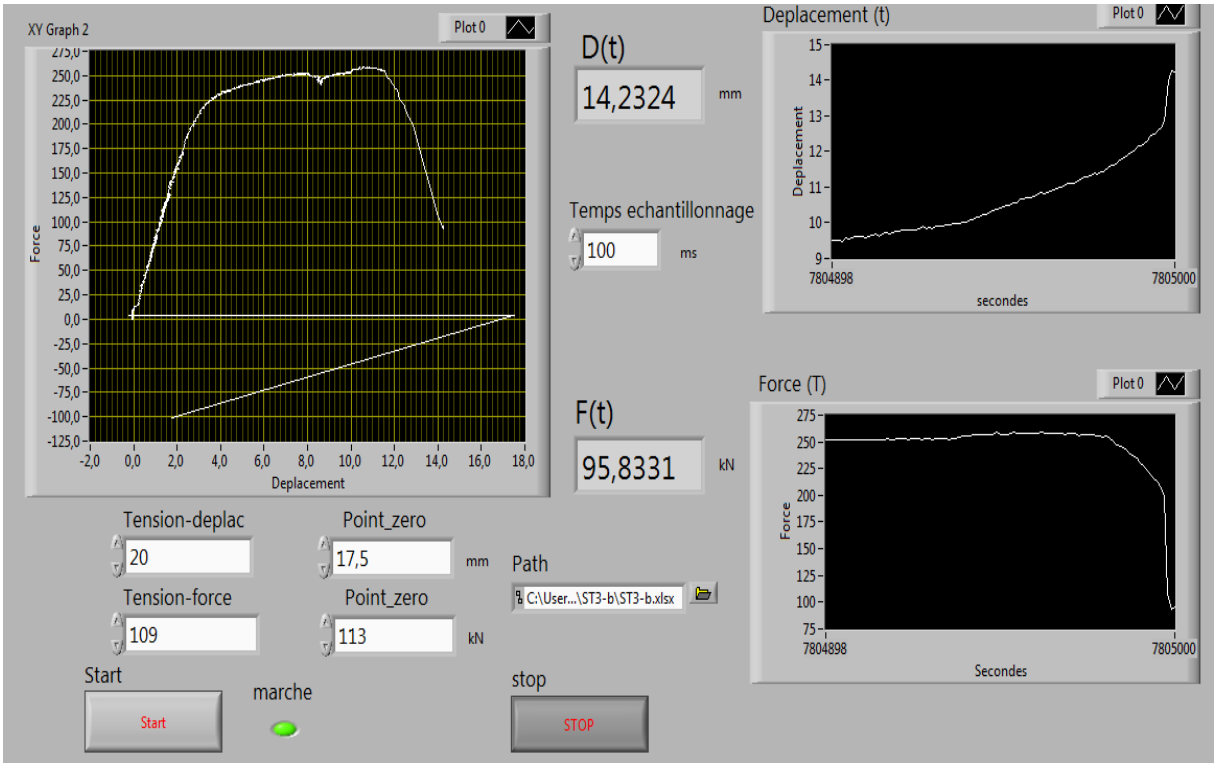

Figure A.6: ST3-b specimen.

ANNEX B

Experimental push-out results of CH1-a specimen

Slip (mm)	Load (kN)	Slip (mm)	Load (kN)	Slip (mm)	Load (kN)	Slip (mm)	Load (kN)
-0,041	0,283	-0,041	2,099	0,351	27,629	0,939	71,158
-0,002	0,550	-0,041	2,259	0,341	29,605	0,959	72,600
-0,070	0,496	-0,070	2,686	0,400	30,780	0,910	72,867
-0,031	0,283	-0,021	2,633	0,439	31,634	0,959	72,974
-0,021	0,763	-0,021	3,060	0,449	33,076	0,920	74,095
0,008	0,870	-0,031	3,220	0,439	34,145	0,949	74,790
-0,021	0,710	-0,011	3,274	0,459	35,266	0,969	75,484
-0,031	0,603	0,008	3,861	0,488	36,708	0,920	76,445
-0,041	0,656	-0,129	3,487	0,479	37,830	0,959	76,819
-0,011	0,763	0,028	3,914	0,498	39,005	0,978	77,781
-0,041	0,496	-0,080	3,914	0,537	40,126	1,106	78,315
-0,011	0,870	-0,041	4,288	0,567	41,622	0,978	79,596
-0,002	0,603	-0,011	4,769	0,518	42,530	1,018	79,329
-0,021	1,244	0,008	4,769	0,616	43,331	0,939	79,703
-0,002	0,656	0,008	5,036	0,577	44,292	1,027	80,825
-0,031	0,977	-0,021	5,784	0,635	46,375	0,969	80,771
-0,011	1,244	-0,051	5,891	0,606	46,963	1,018	81,199
-0,031	0,656	0,008	6,265	0,665	48,565	1,037	83,068
-0,051	0,924	-0,021	7,333	0,684	49,420	1,018	82,107
-0,011	1,191	-0,011	7,226	0,733	50,274	1,027	83,335
-0,021	1,137	-0,031	8,080	0,606	51,823	1,018	83,709
-0,021	1,030	-0,011	9,469	0,743	53,265	1,057	83,869
-0,031	1,137	0,018	9,790	0,733	54,334	1,027	85,098
-0,021	0,977	0,008	10,003	0,704	55,776	1,027	85,739
-0,041	1,351	0,008	11,178	0,812	56,844	1,037	85,311
-0,021	1,351	0,087	12,674	0,890	57,805	1,018	86,112
-0,031	1,511	0,057	12,887	0,812	59,247	1,086	86,860
-0,031	1,084	0,096	13,795	0,773	61,010	1,086	86,753
-0,002	1,671	0,067	15,504	0,782	61,277	1,106	87,501
-0,060	1,458	0,116	16,092	0,900	62,719	1,086	88,783
-0,051	1,618	0,145	17,587	0,871	62,879	1,047	87,928
-0,021	1,778	0,155	18,709	0,871	63,947	1,086	89,264
-0,011	1,938	0,194	19,884	0,802	64,855	1,047	89,264
-0,031	1,671	0,214	21,006	0,871	65,763	1,057	89,050
-0,051	1,938	0,253	21,753	0,880	66,191	1,096	90,866
-0,021	1,778	0,273	23,249	0,890	67,205	1,116	90,385
-0,002	2,312	0,253	23,890	0,900	68,167	1,086	90,813
-0,031	1,938	0,302	24,691	0,841	69,342	1,086	91,080

Slip (mm)	Load (kN)	Slip (mm)	Load (kN)	Slip (mm)	Load (kN)	Slip (mm)	Load (kN)
1,096	92,148	1,282	102,563	1,263	108,865	1,351	112,657
1,125	92,682	1,214	103,257	1,263	107,797	1,292	112,177
1,174	92,842	1,253	102,670	1,243	108,117	1,263	112,444
1,125	93,109	1,272	103,097	1,292	108,652	1,380	112,283
1,165	93,964	1,263	103,951	1,272	108,972	1,302	112,550
1,145	93,857	1,233	103,524	1,282	108,972	1,341	112,978
1,174	94,551	1,233	103,791	1,302	109,506	1,351	112,444
1,194	94,231	1,253	103,364	1,263	108,545	1,351	112,604
1,125	94,818	1,282	104,165	1,272	109,079	1,361	113,458
1,174	95,032	1,223	103,898	1,312	109,773	1,321	112,764
1,165	95,619	1,243	104,486	1,370	108,812	1,361	112,978
1,214	95,833	1,223	104,753	1,321	109,453	1,351	113,725
1,174	96,741	1,263	104,753	1,331	110,361	1,292	113,191
1,174	96,367	1,263	104,966	1,351	109,933	1,331	113,085
1,204	95,993	1,243	105,500	1,321	109,933	1,302	113,352
1,214	97,115	1,223	105,821	1,263	110,681	1,312	112,817
1,223	97,596	1,253	105,607	1,302	110,147	1,292	114,260
1,233	97,329	1,331	105,874	1,312	110,521	1,272	113,725
1,184	97,756	1,253	105,287	1,341	110,948	1,292	113,458
1,223	98,450	1,184	105,607	1,292	110,628	1,282	113,832
1,223	99,038	1,263	106,355	1,341	110,147	1,263	112,924
1,233	99,251	1,243	105,767	1,292	111,162	1,331	114,740
1,184	98,984	1,233	105,767	1,312	111,482	1,400	114,046
1,174	99,251	1,282	105,714	1,312	110,895	1,331	113,085
1,214	98,877	1,223	106,141	1,282	110,734	1,351	113,672
1,194	99,358	1,243	107,637	1,312	111,375	1,321	113,619
1,194	99,946	1,263	106,889	1,341	110,521	1,302	113,832
1,253	100,266	1,263	107,049	1,292	111,108	1,321	114,366
1,184	99,999	1,243	107,156	1,282	111,108	1,351	113,779
1,272	100,213	1,243	107,423	1,253	111,749	1,341	114,366
1,272	100,320	1,272	107,156	1,302	111,803	1,341	114,099
1,263	100,854	1,263	107,744	1,321	110,788	1,331	114,099
1,184	100,320	1,263	107,583	1,321	111,749	1,370	113,886
1,135	101,868	1,292	107,583	1,331	111,963	1,361	114,153
1,184	101,174	1,253	107,744	1,302	111,536	1,341	114,153
1,194	101,762	1,233	107,423	1,312	111,856	1,331	114,527
1,223	102,082	1,272	108,705	1,361	111,002	1,390	114,473
1,223	102,670	1,253	108,011	1,331	112,230	1,351	113,779
1,263	102,403	1,292	108,438	1,380	112,016	1,331	114,794
1,243	102,563	1,253	108,011	1,331	111,856	1,341	114,527

Slip (mm)	Load (kN)	Slip (mm)	Load (kN)	Slip (mm)	Load (kN)	Slip (mm)	Load (kN)
1,351	114,473	1,331	116,022	1,400	119,173	1,488	123,339
1,390	114,527	1,341	116,930	1,390	118,746	1,449	123,767
1,380	114,206	1,390	116,503	1,410	119,066	1,439	123,446
1,361	115,541	1,361	116,610	1,410	118,639	1,459	123,660
1,361	114,633	1,400	116,343	1,429	120,028	1,429	123,820
1,410	115,007	1,361	116,556	1,400	119,120	1,459	123,767
1,361	114,633	1,331	116,236	1,429	119,280	1,488	123,820
1,390	114,954	1,361	116,343	1,380	119,173	1,439	124,247
1,380	114,794	1,410	117,090	1,380	118,799	1,468	125,529
1,370	114,900	1,361	116,449	1,370	120,295	1,478	125,155
1,361	115,221	1,380	117,464	1,380	119,654	1,429	125,636
1,380	115,381	1,351	117,090	1,390	119,654	1,459	125,743
1,361	115,274	1,380	117,304	1,400	119,974	1,508	126,223
1,370	115,488	1,380	117,304	1,390	119,868	1,508	125,209
1,351	115,969	1,380	117,144	1,449	119,707	1,498	126,757
1,410	115,488	1,400	116,983	1,400	120,028	1,508	126,277
1,390	115,595	1,429	117,464	1,410	119,814	1,468	126,757
1,410	115,862	1,410	117,678	1,380	120,081	1,517	126,864
1,380	115,328	1,459	117,464	1,390	119,814	1,429	126,864
1,370	115,435	1,380	117,411	1,439	119,814	1,380	127,238
1,400	115,915	1,390	118,212	1,400	119,921	1,449	127,826
1,351	115,061	1,419	117,411	1,419	119,868	1,508	128,039
1,380	116,022	1,429	117,518	1,400	120,081	1,498	128,200
1,370	115,702	1,380	117,945	1,390	120,295	1,508	127,933
1,380	115,274	1,361	118,105	1,429	120,989	1,478	128,840
1,341	116,556	1,429	118,105	1,439	120,348	1,498	128,787
1,429	115,648	1,439	117,838	1,390	120,402	1,478	128,947
1,390	116,129	1,429	119,120	1,410	121,310	1,468	129,108
1,331	115,541	1,459	118,372	1,380	121,310	1,517	129,214
1,400	116,075	1,419	118,639	1,439	121,684	1,517	128,627
1,351	116,182	1,400	118,693	1,410	121,630	1,537	129,962
1,341	116,343	1,429	118,746	1,400	122,752	1,527	129,642
1,361	115,702	1,429	118,319	1,449	122,111	1,459	130,283
1,370	116,289	1,429	119,173	1,419	122,004	1,508	130,069
1,331	115,915	1,410	118,799	1,419	122,592	1,537	130,763
1,312	116,343	1,459	118,693	1,449	122,431	1,478	129,695
1,390	116,289	1,410	118,906	1,429	122,805	1,498	130,923
1,341	115,969	1,351	118,960	1,410	123,713	1,527	130,763
1,341	116,236	1,419	118,532	1,410	122,752	1,488	130,656
1,341	116,129	1,410	118,853	1,439	123,499	1,498	131,084

Slip (mm)	Load (kN)	Slip (mm)	Load (kN)	Slip (mm)	Load (kN)	Slip (mm)	Load (kN)
1,527	131,297	1,527	136,264	1,645	146,519	1,860	165,106
1,478	131,511	1,586	136,745	1,655	147,854	1,890	165,159
1,527	131,831	1,586	136,478	1,655	147,801	1,900	166,014
1,508	131,671	1,566	136,852	1,645	148,869	1,870	166,601
1,498	132,205	1,576	136,692	1,655	149,831	1,880	167,937
1,488	131,404	1,586	137,493	1,635	148,602	1,880	167,937
1,488	132,739	1,576	136,959	1,655	149,724	1,900	168,417
1,517	132,526	1,566	136,692	1,704	150,792	1,939	169,218
1,488	131,938	1,566	137,226	1,684	151,006	1,929	169,379
1,468	132,686	1,606	136,959	1,684	151,540	1,919	170,661
1,508	132,419	1,586	136,959	1,713	152,127	1,919	170,393
1,517	133,754	1,547	137,546	1,655	152,394	1,919	171,141
1,508	133,487	1,557	137,279	1,723	153,356	1,968	171,515
1,537	133,220	1,586	137,760	1,704	153,356	1,988	171,996
1,498	133,434	1,606	137,172	1,733	153,783	1,958	172,583
1,517	132,472	1,586	137,760	1,762	153,730	2,007	174,186
1,537	133,487	1,586	137,012	1,762	154,851	1,949	173,919
1,508	134,395	1,566	138,080	1,782	155,332	1,968	174,239
1,498	134,021	1,517	138,187	1,792	155,759	2,017	175,094
1,508	133,701	1,547	138,027	1,772	155,759	2,007	174,773
1,498	134,128	1,586	137,760	1,723	156,400	2,007	175,628
1,547	134,235	1,566	137,493	1,713	156,667	2,037	176,856
1,508	134,609	1,596	139,255	1,762	157,628	2,066	176,589
1,537	133,968	1,566	138,027	1,821	157,682	2,027	177,764
1,517	134,716	1,596	138,401	1,762	158,002	2,086	177,230
1,557	134,769	1,566	138,615	1,733	157,949	2,047	178,138
1,527	134,929	1,557	138,454	1,782	159,338	2,056	179,527
1,547	134,342	1,596	139,255	1,733	158,857	2,096	178,886
1,566	135,036	1,586	139,416	1,831	159,551	2,056	179,580
1,537	134,769	1,586	140,591	1,792	159,498	2,066	179,260
1,606	135,303	1,596	140,430	1,831	159,925	2,056	179,954
1,547	135,196	1,547	141,605	1,782	160,619	2,076	181,556
1,566	135,357	1,615	141,926	1,831	160,940	2,086	181,022
1,566	135,357	1,625	142,727	1,802	160,940	2,047	181,396
1,557	135,570	1,645	143,154	1,841	160,886	2,076	182,624
1,576	135,624	1,596	144,596	1,870	161,955	2,125	181,983
1,566	135,784	1,615	144,650	1,860	161,901	2,154	182,464
1,547	135,997	1,596	146,039	1,831	162,756	2,115	183,105
1,566	135,837	1,596	145,611	1,880	163,664	2,145	183,906
1,586	136,852	1,655	146,306	1,851	163,877	2,115	183,426

Slip (mm)	Load (kN)	Slip (mm)	Load (kN)	Slip (mm)	Load (kN)	Slip (mm)	Load (kN)
2,154	184,814	2,360	196,778	2,566	210,291	2,938	223,643
2,115	184,868	2,350	197,472	2,615	211,840	2,929	224,872
2,154	184,868	2,341	197,419	2,586	211,840	2,958	224,391
2,145	185,508	2,311	197,846	2,625	212,000	2,978	224,872
2,154	185,295	2,370	197,846	2,654	212,160	2,978	225,246
2,184	186,737	2,370	198,594	2,625	213,015	2,968	223,803
2,164	187,378	2,380	198,060	2,615	213,389	2,938	225,085
2,154	186,363	2,341	198,060	2,635	212,801	2,978	226,100
2,154	187,378	2,390	199,395	2,674	213,923	3,017	226,047
2,243	187,538	2,409	199,288	2,674	214,724	2,987	225,993
2,233	187,378	2,390	198,434	2,674	214,296	3,017	226,955
2,184	189,461	2,350	200,036	2,693	215,418	3,017	227,649
2,203	188,820	2,380	200,837	2,674	216,647	3,017	226,955
2,213	188,660	2,419	200,463	2,703	215,952	3,046	227,222
2,272	189,140	2,399	201,051	2,742	216,379	3,017	226,741
2,243	189,835	2,390	201,158	2,742	216,166	3,017	227,382
2,233	189,087	2,409	200,997	2,703	216,967	3,027	228,290
2,174	189,995	2,380	202,600	2,801	216,807	3,056	227,649
2,282	190,849	2,409	201,478	2,772	217,982	3,056	228,664
2,252	191,277	2,419	201,905	2,703	217,448	3,076	228,557
2,213	191,277	2,409	202,493	2,821	218,409	3,066	228,610
2,233	191,063	2,448	202,226	2,840	219,317	3,115	228,610
2,243	192,185	2,439	203,508	2,752	219,370	3,115	229,251
2,252	192,238	2,429	203,027	2,772	219,905	3,105	229,412
2,233	192,505	2,448	202,867	2,831	219,424	3,105	229,892
2,252	192,559	2,458	203,241	2,831	219,424	3,105	229,251
2,252	192,719	2,488	203,027	2,811	220,813	3,144	230,480
2,282	193,787	2,458	204,416	2,880	221,026	3,134	231,388
2,243	193,467	2,448	204,309	2,850	220,439	3,105	230,266
2,311	194,214	2,497	204,950	2,831	221,560	3,154	230,480
2,252	193,680	2,507	206,018	2,870	221,293	3,164	230,533
2,292	193,840	2,468	205,911	2,850	221,080	3,134	231,975
2,321	195,069	2,507	206,926	2,889	222,094	3,066	232,296
2,341	194,855	2,546	207,567	2,860	222,789	3,125	231,174
2,301	195,176	2,517	207,887	2,909	222,628	3,174	231,708
2,341	195,763	2,546	208,315	2,889	223,163	3,164	232,135
2,380	195,977	2,546	208,635	2,889	224,498	3,203	232,296
2,292	196,137	2,546	208,261	2,909	223,803	3,252	232,296
2,282	196,938	2,586	209,917	2,919	223,430	3,262	232,242
2,292	196,885	2,556	210,131	2,929	223,483	3,203	232,509

Slip (mm)	Load (kN)	Slip (mm)	Load (kN)	Slip (mm)	Load (kN)	Slip (mm)	Load (kN)
3,223	232,135	3,791	247,464	4,222	259,268	4,947	273,795
3,223	233,845	3,811	247,624	4,252	259,161	4,928	274,276
3,223	233,257	3,791	247,838	4,281	259,588	4,928	274,917
3,252	233,043	3,801	249,120	4,310	260,336	4,947	275,398
3,213	233,845	3,830	249,387	4,252	260,176	4,957	275,825
3,281	233,684	3,801	249,066	4,301	260,282	5,006	276,145
3,301	234,112	3,801	248,746	4,310	261,244	5,036	276,733
3,262	234,165	3,830	250,028	4,330	260,550	5,055	276,252
3,242	234,432	3,840	251,683	4,350	260,763	5,055	277,481
3,291	234,592	3,860	250,455	4,340	261,938	5,055	277,908
3,291	234,859	3,879	250,188	4,389	261,992	5,094	277,748
3,301	235,447	3,909	250,882	4,350	262,205	5,114	278,495
3,311	236,301	3,918	250,882	4,389	261,778	5,104	278,762
3,311	237,103	3,928	251,523	4,408	261,885	5,153	278,709
3,370	237,690	3,928	252,431	4,389	263,113	5,202	279,777
3,389	239,239	3,918	251,844	4,418	263,327	5,232	279,243
3,389	238,598	3,928	252,698	4,438	262,739	5,232	279,937
3,399	239,239	3,977	251,256	4,350	263,273	5,251	280,632
3,409	239,666	3,948	253,179	4,457	263,914	5,290	281,112
3,419	239,773	4,016	253,927	4,438	264,342	5,251	280,739
3,517	239,826	3,997	253,286	4,497	264,876	5,330	280,525
3,438	240,734	4,036	254,301	4,487	265,891	5,339	281,486
3,497	241,696	4,075	253,606	4,506	266,264	5,330	281,860
3,517	241,909	4,065	253,126	4,536	266,264	5,339	281,700
3,507	241,269	4,065	254,835	4,575	266,852	5,418	281,914
3,497	242,550	4,056	255,155	4,555	268,294	5,428	282,127
3,526	242,978	4,085	255,155	4,585	267,546	5,418	282,768
3,556	243,138	4,075	255,102	4,614	268,080	5,457	283,462
3,517	243,458	4,105	256,864	4,624	268,935	5,506	283,997
3,585	243,886	4,134	256,277	4,624	269,469	5,496	283,089
3,585	244,046	4,134	256,384	4,673	270,110	5,516	283,195
3,624	245,274	4,114	256,971	4,663	269,789	5,535	283,302
3,615	244,633	4,163	257,505	4,702	270,591	5,496	283,783
3,654	245,328	4,154	256,170	4,732	271,872	5,555	284,103
3,713	245,969	4,183	257,452	4,791	271,605	5,594	284,531
3,624	245,915	4,154	257,559	4,800	271,552	5,614	285,545
3,703	246,396	4,173	258,093	4,840	271,605	5,604	284,424
3,693	246,877	4,173	257,719	4,869	272,460	5,633	285,118
3,693	247,197	4,212	258,680	4,918	273,368	5,653	285,866
3,713	246,503	4,261	259,428	4,938	274,383	5,702	286,507

Slip (mm)	Load (kN)	Slip (mm)	Load (kN)	Slip (mm)	Load (kN)	Slip (mm)	Load (kN)
5,751	285,545	6,525	291,688	7,878	284,744	9,906	248,746
5,731	286,614	6,545	290,886	7,946	285,172	9,965	247,037
5,771	286,560	6,564	289,978	7,966	284,798	10,034	245,595
5,780	286,560	6,633	288,056	8,015	284,210	10,092	244,687
5,761	286,720	6,623	287,094	8,074	285,172	10,200	243,245
5,800	286,934	6,692	286,560	8,103	284,370	10,181	242,550
5,849	287,201	6,662	286,667	8,162	284,637	10,298	240,948
5,839	287,789	6,711	285,652	8,211	284,584	10,308	238,918
5,878	287,789	6,760	285,492	8,221	285,652	10,406	238,918
5,869	288,002	6,800	284,744	8,260	284,210	10,475	237,370
5,888	289,124	6,878	284,744	8,299	283,997	10,524	236,675
5,888	287,949	6,809	285,332	8,299	284,424	10,602	235,767
5,967	288,483	6,917	284,958	8,417	283,302	10,641	234,753
5,937	289,391	6,927	284,905	8,397	283,249	10,690	232,563
6,006	288,857	6,956	284,851	8,495	282,715	10,749	231,708
5,976	289,070	7,005	286,453	8,515	283,035	10,847	230,266
6,006	288,803	7,035	286,507	8,554	282,341	10,876	229,679
5,996	288,910	7,094	285,599	8,583	280,899	10,916	229,144
6,025	289,391	7,084	286,186	8,691	280,952	11,014	226,688
6,074	290,032	7,133	285,919	8,711	281,433	11,072	226,688
6,045	289,605	7,182	285,706	8,730	280,525	11,190	225,032
6,065	289,498	7,231	285,439	8,760	279,296	11,200	224,231
6,143	288,803	7,241	285,385	8,838	280,204	11,259	224,177
6,153	290,139	7,299	284,210	8,848	278,549	11,327	223,109
6,212	290,192	7,368	284,264	8,926	277,320	11,376	222,201
6,202	290,406	7,407	284,210	8,985	276,946	11,445	222,575
6,133	290,940	7,476	283,409	9,014	274,703	11,543	220,706
6,192	290,032	7,476	284,584	9,073	274,917	11,553	220,439
6,212	290,246	7,495	284,424	9,103	273,261	11,621	219,157
6,241	290,833	7,505	283,943	9,210	271,499	11,660	219,424
6,290	291,421	7,564	284,370	9,279	270,110	11,709	218,569
6,280	290,619	7,623	284,103	9,289	268,027	11,778	217,928
6,319	291,047	7,623	284,370	9,348	265,356	11,847	219,050
6,319	291,314	7,672	284,637	9,426	263,754	11,905	216,593
6,368	291,741	7,740	284,317	9,455	261,938	11,964	216,540
6,408	291,901	7,750	284,210	9,544	259,642	12,092	215,098
6,398	293,236	7,789	284,317	9,622	256,277	12,062	214,937
6,457	291,527	7,848	285,118	9,691	253,820	12,229	215,685
6,476	291,634	7,848	283,836	9,759	252,485	12,219	214,190
6,496	291,421	7,887	284,851	9,828	250,402	12,278	213,816

Slip (mm)	Load (kN)	Slip (mm)	Load (kN)
12,356	213,389	15,424	163,397
12,435	211,733	15,492	161,581
12,444	212,694	15,590	161,421
12,542	211,786	15,688	159,284
12,572	210,558	15,786	158,376
12,611	209,596	15,855	156,934
12,689	208,528	15,933	155,599
12,758	207,086	15,963	154,050
12,876	206,872	16,149	153,730
12,925	205,965	16,217	152,020
12,915	205,057	16,315	150,685
13,013	204,362	16,453	149,136
13,052	202,867	16,511	147,748
13,160	201,959	16,658	145,718
13,238	200,784	16,737	145,077
13,268	199,288	16,825	143,048
13,287	198,434	16,913	141,552
13,395	198,914	17,060	139,736
13,464	197,472	17,129	137,546
13,522	195,229		
13,620	195,122		
13,660	193,360		
13,718	191,437		
13,856	190,903		
13,924	189,674		
13,993	187,645		
14,101	185,402		
14,169	185,882		
14,297	183,426		
14,375	182,197		
14,434	179,740		
14,502	178,458		
14,649	177,390		
14,718	174,559		
14,806	173,758		
14,953	171,836		
14,983	169,272		
15,110	167,937		
15,218	167,189		
15,267	165,159		

ANNEX C

Additional pictures

Picture C1: Welding of the hydraulic press beam.

Picture C2: Drilling in the hydraulic press column.

Picture C3: Drilling of the T-shape steel section

Picture C4: Elimination of steel-concrete adhesion by oiling.

Picture C5: Push and pull - out specimens before casting.

Picture C6: Push and pull - out specimens after tests.